STRUCTURAL AND KINETIC COMPARISON OF ACETOLACTATE SYNTHASE AND ACETOHYDROXYACID SYNTHASE FROM *KLEBSIELLA PNEUMONIAE*

by

Alexander J. Latta

A Dissertation

Submitted to the Faculty of Purdue University

In Partial Fulfillment of the Requirements for the degree of

Doctor of Philosophy

Department of Chemistry and Chemical Biology

Indianapolis, Indiana

August 2019

THE PURDUE UNIVERSITY GRADUATE SCHOOL
STATEMENT OF COMMITTEE APPROVAL

Dr. Michael McLeish, Chair

Department of Chemistry and Chemical Biology

Dr. Andrew Mesecar

Department of Biochemistry

Dr. Sebastien Laulhe

Department of Chemistry and Chemical Biology

Dr. Lei Li

Department of Chemistry and Chemical Biology

Approved by:

Dr. Eric Long

Head of the Graduate Program

To my family

ACKNOWLEDGMENTS

Throughout the pursuit of my Ph.D., there are many people who have been crucial to my success in this endeavor. Each of these individuals deserves my thanks and gratitude. First, I would like to thank my advisor, Prof. Michael McLeish, for not only serving as my thesis advisor, but for also being a friend, offering advice in many situations, both academic and personal. I thank you for taking a personal interest in my professional development and allowing me the freedom and encouragement to pursue a professional internship during the course of my graduate studies. For your patience, guidance, and encouragement, I will always be grateful.

Additionally, I would like to thank Dr. Forest Andrews and Dr. Walter Novak for the introduction to the world of protein crystallography, and for the invaluable discussions and demonstrations on data collection, data processing, and structure solution. In the same vein, I would like to thank Prof. Chittaranjan Das and Prof. Quyen Hoang for allowing me to send protein crystals for data collection at Argonne National Laboratory. I would like to thank Dr. Robert Minto for unfettered use of his GC-MS instrument. I would also like to thank Dr. Malea Kneen for providing valuable feedback during the process of writing this thesis. I would like to thank all the researchers in the McLeish group for their comradery and thought-provoking scientific discussions.

Finally, I would like to thank my family, particularly my wife Melissa, for their continuous unwavering support and encouragement during this time.

TABLE OF CONTENTS

LIST OF TABLES

LIST OF FIGURES

LIST OF ABBREVIATIONS

2,3BD	2,3-butanedione
2,3PD	2,3-pentanedione
*Aa*ALS	*Aerobacter aerogenes* acetolactate synthase
AHAS	Acetohydroxyacid synthase
ALS	Acetolactate synthase
ALThDP	acetolactylthiamin diphosphate
BFDC	Benzoylformate decarboxylase
*Bs*ALS	*Bacillus subtilis* acetolactate synthase
CD	Circular dichroism
FAD	Flavin adenine dinucleotide
fHEThDP	fluorohydroxyethylthaimin diphosphate
HEPES	4-(2-hydroxyethyl)-1-piperazineethanesulfonic acid
HEThDP	hydroxyethylthiamin diphosphate
HPP	Hydroxypropiophenone
IPTG	Isopropylthio-β-galactoside
k_{cat}	Turnover number
K_m	Michaelis constant
*Kp*AHAS	*Klebsiella pneumoniae* acetolactate synthase
*Kp*ALS	*Klebsiella pneumoniae* acetohydroxyacid synthase
LB	Lysogeny broth
LThDP	Lactylthaimin diphosphate
MES	2-(*N*-morpholino)ethansulfonic acid
MOPS	3-(*N*-morpholino)propanesulfonic acid
Ni-NTA	Nickel-nitriloacetic
NMR	Nuclear magnetic resonance
PAC	Phenylacetyl carbinol
PAGE	Polyacrylamide gel electrophoresis
PCR	Polymerase chain reaction
PDB	Protein data bank

PDC	Pyruvate decarboxylase
PDH	Pyruvate dehydrogenase complex
PEG600	Polyethylene glycol average molecular weight 600 daltons
PEG8000	Polyethylene glycol average molecular weight 8000 daltons
PnDFP	Phosphonodifluoropyruvate
PnPyrDC	Phosphonopyruvate decarboxylase
RMSD	Root mean square deviation
*Sc*AHAS	*Saccharomyces cerevisiae* acetohydroxyacid synthase
SDS	Sodium dodecyl sulfate
ThDP	Thiamin diphosphate
UV	Ultraviolet

ABSTRACT

Author: Latta, Alexander, J.
Institution: Purdue University
Degree Received: August 2019
Title: Structural and Kinetic Comparison of Acetolactate Synthase and Acetohydroxyacid Synthase from *Klebsiella pneumoniae*
Committee Chair: Michael McLeish.

Acetolactate synthase (ALS) and acetohydroxyacid synthase (AHAS) are two thiamin diphosphate (ThDP)-dependent enzymes that catalyze the formation of acetolactate from two molecules of pyruvate. In addition to acetolactate, AHAS can catalyze the formation of acetohydroxybutyrate from pyruvate and α-ketobutyrate. When formed by AHAS, these compounds are important precursors to the essential amino acids valine and isoleucine. Conversely, ALS forms acetolactate as a precursor to 2,3-butanediol, a product formed in an alternative pathway to mixed acid fermentation.

While these enzymes catalyze the same reaction, they have been found to be quite different. Such differences include: biological function, pH optimum, cofactor requirements, reaction kinetics and quaternary structure. Importantly, AHAS has been identified as the target of the widely-used sulfonylurea and imidazolinone herbicides, which has led to many structural and kinetic studies on AHAS enzymes from plants, bacteria, and fungi. ALS, on the other hand, has only been identified in bacteria, and has largely not seen such extensive characterization. Finally, although some bacteria contain both enzymes, they have never been studied in detail from the same organism.

Here, the ALS and AHAS enzymes from *Klebsiella pneumoniae* were studied using steady-state kinetic analyses, X-ray crystallography, site-directed and site-saturation mutagenesis, and cell growth complementation assays to i) compare the kinetic parameters of each enzyme, ii) compare the active sites to probe their differences in substrate profile and iii) test the ability of ALS to function in place of AHAS *in vivo*.

CHAPTER 1. INTRODUCTION

1.1 Thiamin diphosphate

In the early 1900's, Neuberg and Karczag (1) made the initial discovery of a thiamin diphosphate (ThDP)-dependent enzyme, α-carboxylase, now known as pyruvate decarboxylase (PDC), when they observed that fermenting yeast culture was able to transform pyruvate from glycolysis into acetaldehyde. With no chemical information to refer to, the mechanism of acetaldehyde formation was the subject of some speculation. The earliest of the proposed mechanisms stemmed from the observation that primary amines catalyze the decarboxylation of α-ketoacids. Later called the Lagenbeck cycle (2), the mechanism proposed that the catalytic center of α-carboxylase was a primary amine and reaction would proceed through the formation of a Schiff base, *i.e.*, similar to the mechanism now known to be employed by pyridoxal phosphate-dependent enzymes (3).

The transformation of pyruvate to acetaldehyde in yeast was later found to be dependent on a cofactor called cocarboxylase (4), a compound of previously unknown function first described in 1931 by Auhagen (5). In the same study, Lohmann and Schuster (4) identified cocarboxylase as the diphosphate ester of thiamin, or vitamin B1. Fortunately, as there had been considerable interest in vitamin B1 due to its importance in diseases such as beriberi (6), its chemical structure had been published two years prior (7,8). The overall structure of thiamin (Figure 1.1 A) was reported to consist of a substituted pyrimidine ring connected to a thiazolium ring through a single methylene carbon. The thiazolium ring was found to contain two additional substitutions, a methyl group at C4, and an ethyl alcohol group at C5 (7,8). The structure of ThDP (Figure 1.1 B) was found to be similar to that of vitamin B1 with the only difference being the replacement of the alcohol group with a diphosphate group (4).

Immediately after the identification of cocarboxylase as ThDP, Melnick and Stern, who proposed that the cofactor functioned in an oxidation-reduction cycle, set out to investigate the catalytic center of ThDP (9). As the structures of thiamin showed the presence of a primary amine making the Lagenbeck cycle possible, they examined the reactivity of the 4' amino group found on the pyrimidine ring by treatment with ketene, a compound that readily acetylates primary amines. No evidence of the formation of *N*-acetylated thiamin was observed, leading to the

conclusion that the amine was not as reactive as other primary amines and, as such, could not be the reaction center as previously proposed (9). While this study supported their proposed oxidation-reduction cycle, they later published evidence showing that reduced thiamin was completely inactive, making catalysis via an oxidation-reduction cycle unlikely (10).

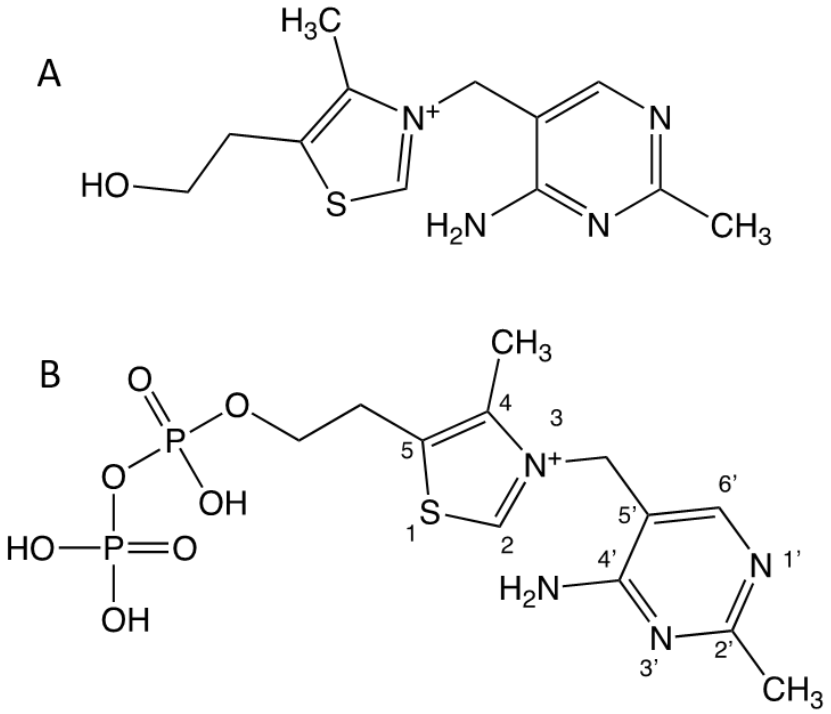

Figure 1.1: Chemical structures of A) thiamin, and B) thiamine diphosphate with the typical numbering scheme.

After Melnick and Stern showed that the catalytic center was not likely to be the primary amine, attention shifted to other groups in the cofactor. Not long after, it was found that thiazolium compounds, including thiamin, could catalyze the condensation of two molecules of benzaldehyde to form benzoin (3). The overall reaction was similar to the same reaction previously reported to be catalyzed by cyanide (11), and suggested the involvement of the thiazolium ring in catalysis.

Armed with this information, Ronald Breslow proposed that the connecting methylene carbon was the catalytic center of ThDP. He initially suggested that the first step of the reaction was deprotonation of the methylene carbon, forming a reactive carbanion (12). This was later disproved when it was revealed that the hydrogen atoms on the methylene carbon did not exchange

for deuterium in D_2O by ^1H NMR (13). Shortly after, using the same technique that disproved his original proposal, Breslow identified C2 as the active center of ThDP by showing that the C2 hydrogen was exchanged for deuterium at a relatively rapid rate (14).

Deprotonation of C2 results in the formation of the thiazolium ylid (Figure 1.2). It was shown that this zwitterionic species is structurally similar to the cyanide ion, and could act in a similar manner in the benzoin condensation (15). These observations led Breslow (16) to propose the first widely accepted mechanism involving thiamin as a catalyst for the benzoin condensation (Figure 1.3 A). He proposed that the reaction occurs involves five basic steps: i) deprotonation of C2 resulting a thiazolium ylid, ii) attack by the ylid on the carbonyl of benzaldehyde, iii) deprotonation of the hydroxybenzylthiazolium intermediate to form a resonance stabilized carbanion, now known as the Breslow intermediate (Figure 1.3 B), iv) attack of the Breslow intermediate on the carbonyl of a second benzaldehyde molecule, and v) release of the benzoin product and regeneration of the thiazolium ylid.

In the years since Breslow's original proposal, many mechanistic studies have been performed on both enzymatic and non-enzymatic systems, and the accepted mechanism of thiamin catalysis has remained basically the same; deprotonation of C2 followed by attack on a carbonyl of a substrate, usually a α-ketoacid, aldehyde, or α-hydroxyketone (3,17).

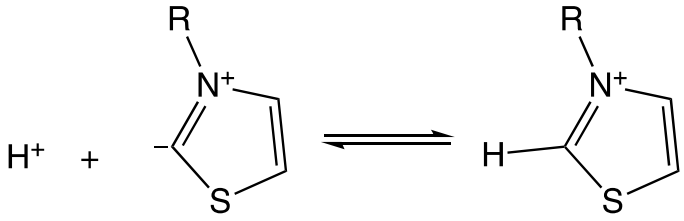

Figure 1.2: Deprotonation to form the thiazolium ylid.
Reproduced from Breslow (16).

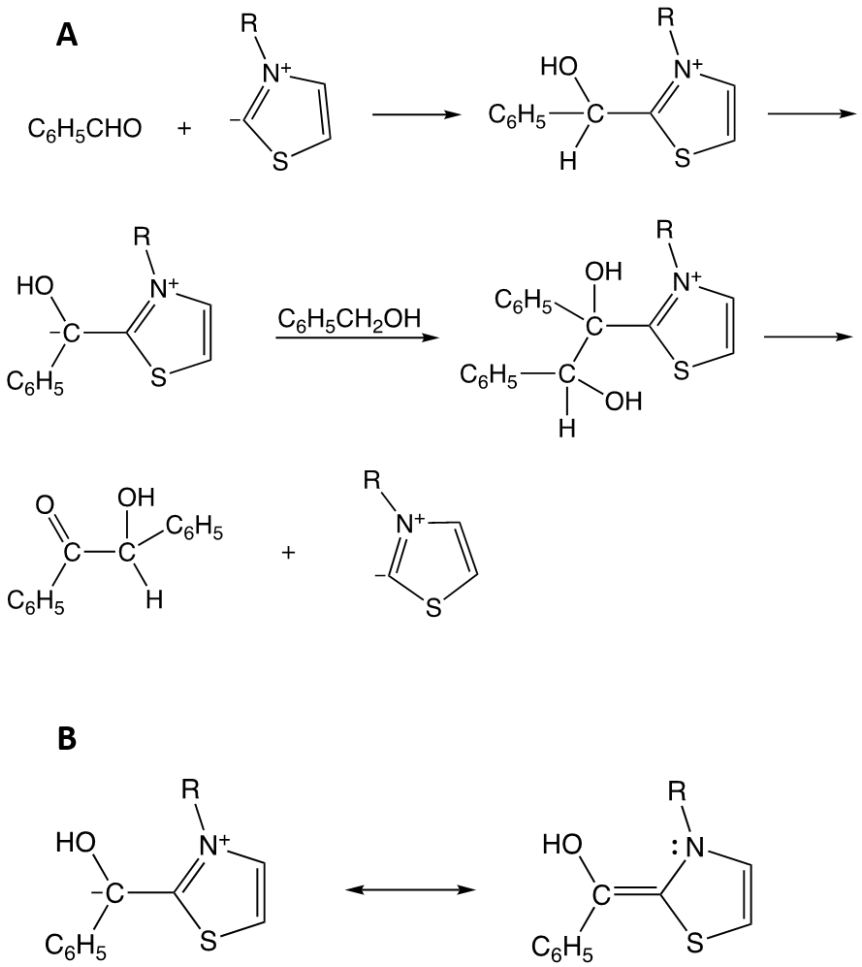

Figure 1.3: A) Reaction intermediates for the benzoin condensation by thiazolium salts, B) Breslow intermediate. Reproduced from Breslow (16).

1.2 Thiamin diphosphate-dependent enzymes

In the years since the discovery of α-carboxylase, studies have been performed on many other ThDP-dependent enzymes concurrently with those on the cofactor itself. Today, members of the ThDP-dependent superfamily have been identified belonging to 4 out of the 7 enzyme commission classifications. These include: oxidoreductases (1.X.X.X), transferases (2.X.X.X), hydrolases (3.X.X.X), and lyases (4.X.X.X). Indeed, enzymes in this superfamily catalyze a wide array of reactions including decarboxylations, carboligations, formation of carbon-nitrogen bonds, formation of carbon-oxygen bonds, and formation of carbon-sulfur bonds (18).

As seen in Figure 1.4, these enzymes function on a diverse range of substrates, forming even more diverse range of products. What is especially intriguing about this is that all

the reactions proceed through, in essence, the same reaction intermediate, even when forming different products from identical substrates.

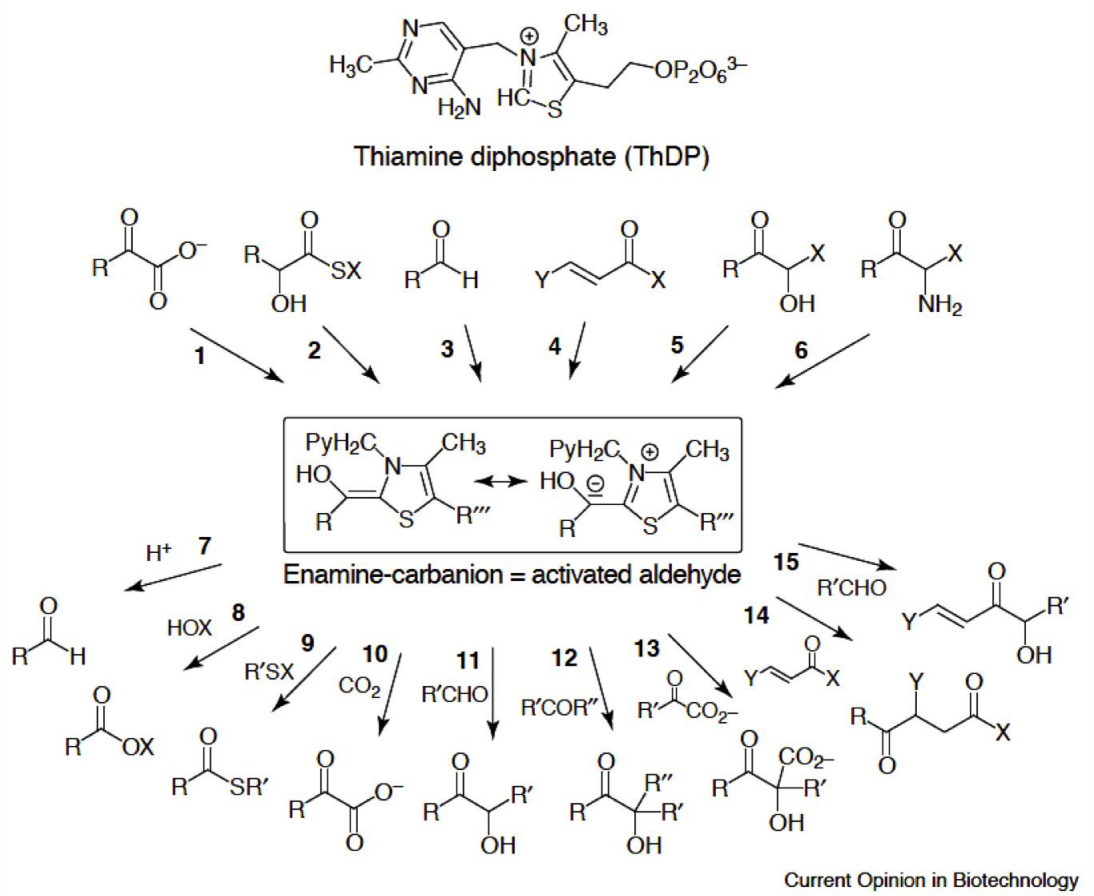

Figure 1.4: Reactions catalyzed by ThDP-dependent enzymes.
Reproduced from Pohl *et al.* (18).

1.2.1 General structural features of ThDP-dependent enzymes

Structurally, members of the ThDP-dependent family are quite similar. Each enzyme contains at least two domains, the pyrimidine-binding domain (Pyr), and the diphosphate-binding domain (PP). Barring one exception, sulfopyruvate decarboxylase (19), these domains are fused in one contiguous protein chain (20). In addition to the PP and Pyr domains, most enzymes in this family contain at least one more domain. In fact, sulfopyruvate decarboxylase (19) and phosphonopyruvate decarboxylase (21) are the only two known ThDP-dependent enzymes that do not contain an additional domain (22).

Many ThDP-dependent enzymes exist as either a dimer, or as a tetramer "dimer of dimers" in solution (Figure 1.5). With only two exceptions, pyruvate ferredoxin oxidoreductase (PFOR) (23) and d-xylulose-5-phosphate synthase (24), the active site is found at a dimer interface. The active site comprises residues from both the Pyr domain, and the PP domain. As the names imply, residues from the PP domain bind the diphosphate group of ThDP, while residues from the Pyr domain bind the pyrimidinyl group. By symmetry, two active sites are formed at each dimer interface (25).

Figure 1.6 shows the general architecture of the ThDP binding site. Even though the overall structure of the active sites is similar between members of this family, there are very few conserved residues among them. Only the diphosphate binding motif ($GDG(X)_{26\text{-}24}NN$) (26) is universally conserved. However, most also contain a glutamate residue located near N1' of the cofactor pyrimidine ring (27,28).

Inspection of the first X-ray crystal structures of ThDP-dependent enzymes, including PDC (29,30), pyruvate oxidase (31), and transketolase (TK) (32), revealed that the ThDP cofactor binds in a strained V-conformation (33). This conformation is conserved and has been observed in every cofactor bound structure of a ThDP-dependent enzyme to date. It was postulated that the V-conformation was held in place by a commonly observed hydrophobic residue in the active site, often leucine, isoleucine, or methionine (34). While mutation of this residue did result in reduction of reaction rate, it was shown that it is not due to loss of the V-conformation indicating that the hydrophobic residue is not essential for maintaining this conformation (35).

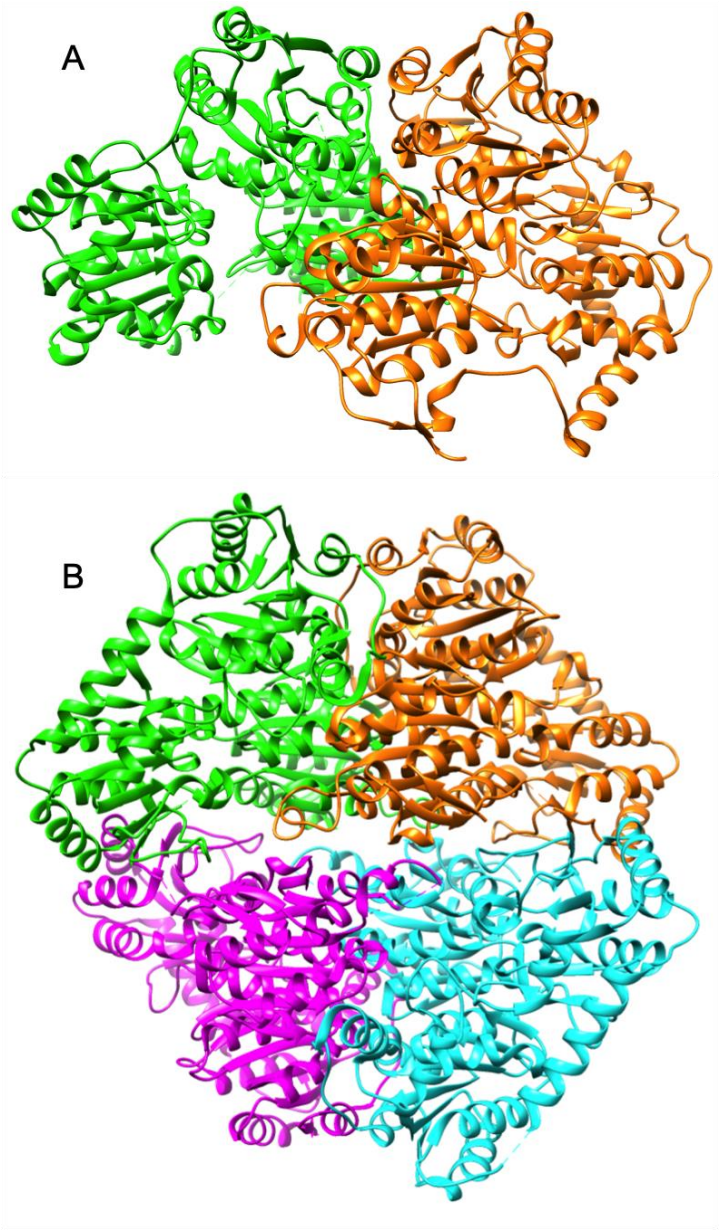

Figure 1.5: Typical A) dimeric (PDB ID: 5IMS) and B) tetrameric (PDB ID: 1OZF) structures of ThDP-dependent enzymes. Two active sites are formed at the interface of the green and orange monomers and the interface of the pink and blue monomers.

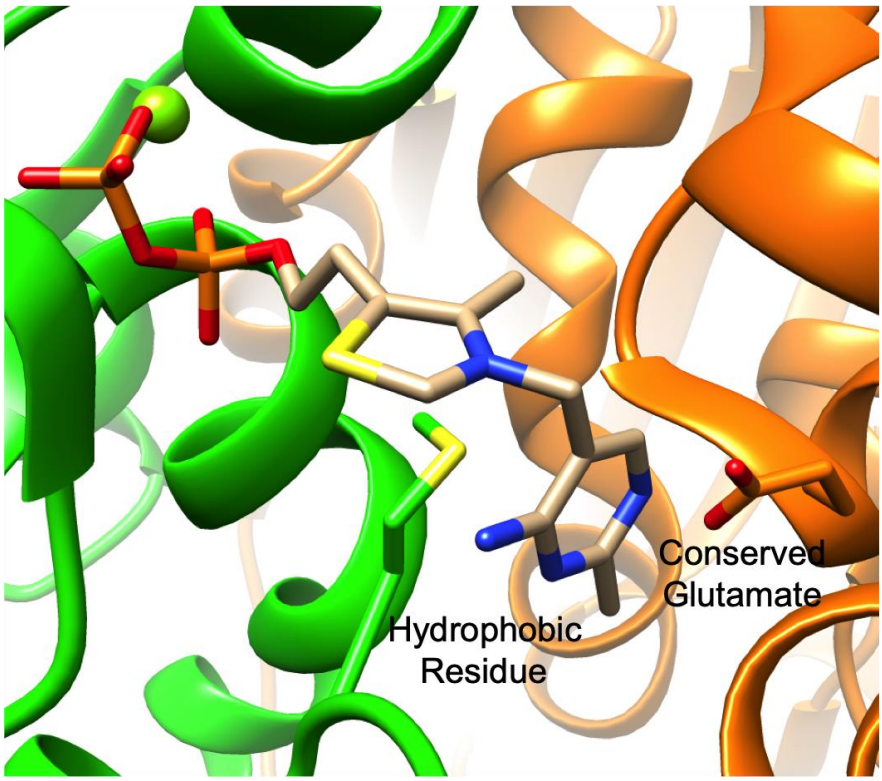

Figure 1.6: Typical ThDP binding site with bound ThDP. Residues from both the Pyr domain (orange) and the PP domain (green) form the ThDP binding pocket. The conserved hydrophobic residue and the conserved glutamate are also shown. Figure prepared in UCSF Chimera (36) using PDB ID: 5DX6.

1.2.2 Activation of enzyme-bound ThDP

Studies on these enzymes, as well as the ThDP cofactor, itself posed a major question about thiamin catalysis in enzymes. ThDP is a true catalyst, *i.e.*, it is able to catalyze reactions without the requirement of being bound to an enzyme. Therefore, what is the purpose of the enzyme if the cofactor can catalyze the reaction without it?

One basic answer to this question quickly became apparent; the protein contributes significant enhancement to the reaction rate. Kemp and O'Brien (37) demonstrated that the rate of decarboxylation catalyzed by PDC was much faster than what would be possible by the cofactor alone, even at very high ThDP concentrations. This was explained by the fact that, while H-D exchange on C2 was reasonably fast, the rate of protonation of the ylid was found to be much faster, bordering on the limits of diffusion control. This meant that, at equilibrium, the concentration of the reactive ylid in solution is extremely low, and therefore could not provide rate enhancements as great as those observed in the enzymatic reactions (37,38). Indeed, PDC was

shown to catalyze the decarboxylation of pyruvate as much as 10^4 times faster than thiamin alone (39).

The size of the rate enhancement led to many hypotheses on how the enzyme managed to increase the rate of transformation so drastically. Proposals included enzymatic stabilization of the ylid (37,40), rapid deprotonation of C2 (41), and a concerted model of deprotonation with simultaneous addition of the substrate to the cofactor (42,43). The debate continued until Kern *et al*. (44,45) provided evidence that showed that the rate of H-D exchange at C2 is sufficiently increased when the cofactor is bound to an enzyme to justify the measured enzymatic rates of catalysis. They went on to test a previously proposed mechanism through which the enzymes could accomplish this task. Based on earlier observations of the conserved glutamate residue that interacts with the 1' nitrogen of the pyrimidine ring, it was proposed that this residue somehow promotes deprotonation of C2 (33). In support of this, mutagenesis of the glutamate residue resulted significant reductions in both the rate of deprotonation at C2 and in overall reaction rate, indicating that the residue is indeed important for activation of the cofactor. To date, only one known ThDP-dependent enzyme, glyoxylate carboligase, lacks this otherwise conserved residue (27,28).

In the same study, the importance of the 4' amino group was also investigated. The introduction of 4'-desamino ThDP showed a similar decrease in both the rate of C2 deprotonation and overall reaction rate. Taken together, these results indicated that the conserved glutamate residue, the 1' nitrogen and the 4' amino group are all important for the reaction rate enhancement observed in ThDP-dependent enzymes (44).

The explanation of how these factors work in concert to promote deprotonation of C2 involved one other factor, the V-conformation of enzyme-bound ThDP. It was observed that this conformation places the 4' amino group in sufficiently close proximity to the C2 hydrogen to allow for proton abstraction. When considered in conjunction with the role of the conserved glutamate, the 1' nitrogen, and the 4' amino group, a more complete understanding of how the enzymes promote ThDP-dependent catalysis became clear. The conserved glutamate stabilizes the imino (IP) tautomeric form of ThDP. Concomitantly, the 4' amino group, now a 4' imino group, is positioned sufficiently close to close to C2 to allow for proton abstraction, resulting in the formation of the ThDP ylid (3,34,44,46).

Figure 1.7 shows the many states of enzyme-bound ThDP including a tricyclic dihydrothiachrome form. A version of this form of ThDP was first observed bound to an enzyme containing a trapped reaction intermediate where it was proposed to be directly involved in the catalytic mechanism (47). However, a similar tricyclic form of ThDP was later shown to act as a potential kinetic trap in at least some ThDP-dependent enzymes (48). A further analysis and discussion of this form of ThDP can be found in Chapter 4.

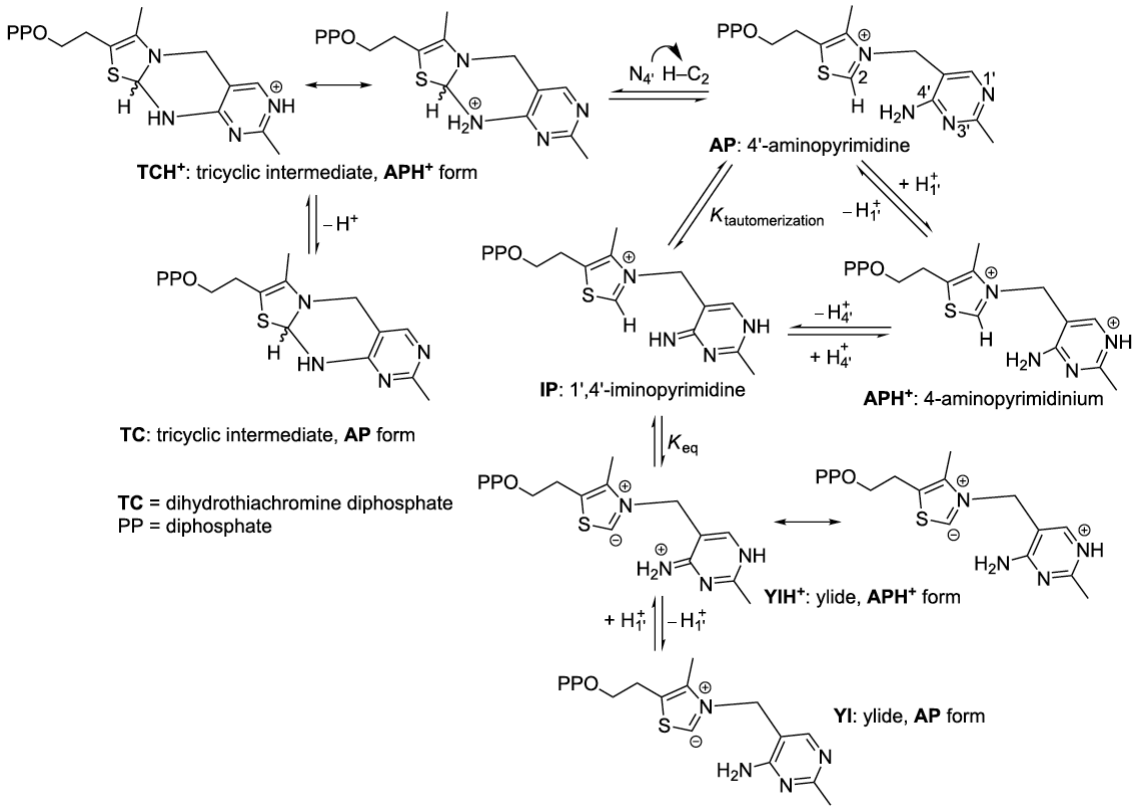

Figure 1.7: Formation of the ThDP ylid. Reproduced from Planas *et al.* (49).

1.2.3 Reactions of ThDP-dependent decarboxylases

The largest family of ThDP-dependent enzymes is the decarboxylase family (25), with the most well-studied of these, PDC, often referred to as the archetypal ThDP-dependent enzyme (50). As such, many of the following discussions will focus around studies performed on this enzyme.

1.2.3.1 Decarboxylation reactions

The simplest decarboxylases catalyze the decarboxylation of an α-ketoacid to form an aldehyde and carbon dioxide. A prime example of this is the reaction catalyzed by PDC, in which pyruvate is decarboxylated to provide acetaldehyde and carbon dioxide (Figure 1.8).

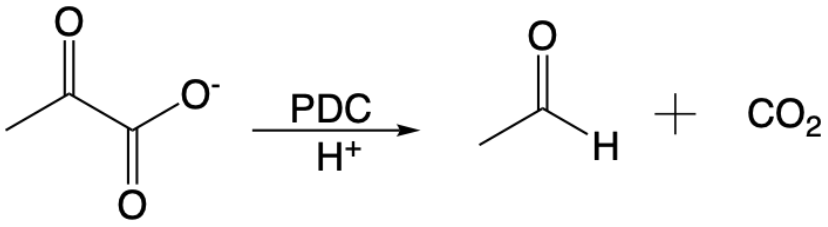

Figure 1.8: Decarboxylation reaction catalyzed by PDC.

Initially, reaction occurs through the same basic steps as the mechanism proposed by Breslow for the benzoin condensation (Figure 1.3 A). However, instead of attack on a second substrate by the Breslow intermediate, otherwise known as the carbanion/enamine or the "activated aldehyde", the intermediate is rapidly protonated (Figure 1.9). The basic steps include: i) attack on the pyruvate substrate by the ThDP ylid forming the first tetrahedral intermediate 2-α-lactylThDP (LThDP), ii) decarboxylation to form the activated aldehyde, iii) protonation of the activated aldehyde, forming the second tetrahedral intermediate, 2-α-hydroxyethylThDP (HEThDP), and iv) release of acetaldehyde and regeneration of the ThDP ylid (51).

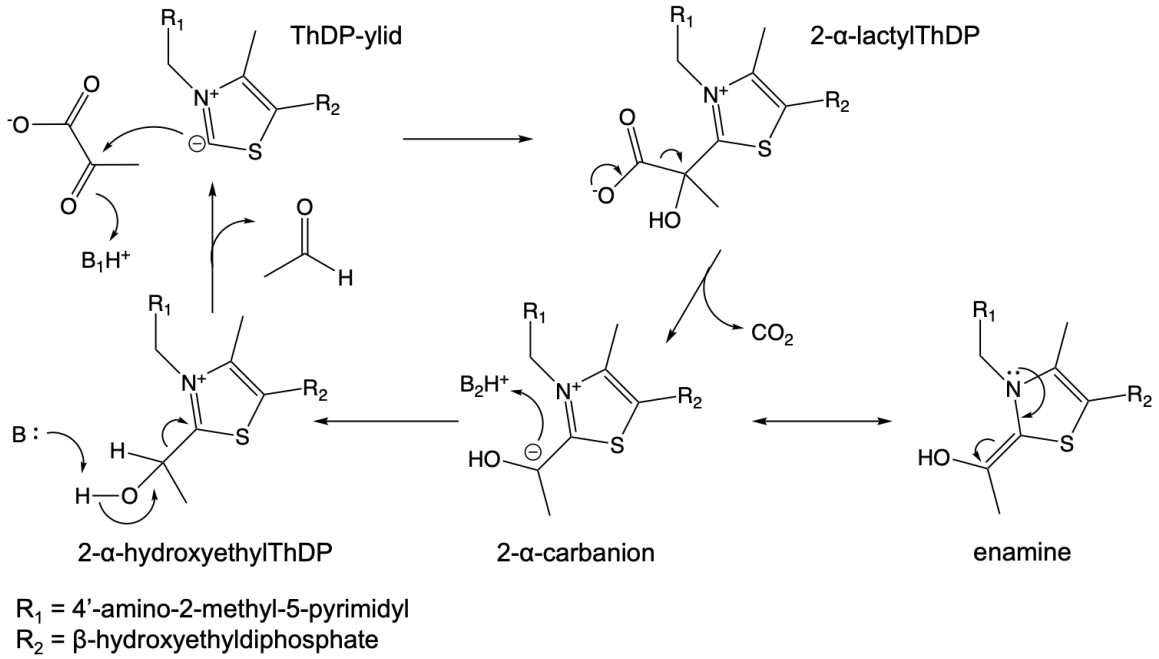

Figure 1.9: Consensus mechanism of acetaldehyde formation by PDC.

1.2.3.2 Carboligation reactions

Not all members of the decarboxylase family catalyze solely decarboxylation reactions. Many ThDP dependent decarboxylases are able to catalyze carbon-carbon bond formation as well. Typically, these occur through attack on a first α-ketoacid substrate, termed the donor substrate. However, instead of protonation, the enamine attacks a second substrate, termed the acceptor substrate (52). These carboligation reactions are directly analogous to the benzoin condensation previously discussed.

Most common among these reactions is the condensation of two α-ketoacids, one α-ketoacid and an aldehyde, or two aldehydes. For each of the substrate combinations listed, the product is a chiral α-hydroxyketone (52). These α-hydroxyketone products have found utility in synthesis applications including that of antifungal compounds (53), and vitamin E (54). The oldest reported, and perhaps the most well known of these transformations is the use of PDC to form (*R*)-phenylacetyl carbinol ((*R*)-PAC). The transformation is the result of condensation of pyruvate with benzaldehyde (Figure 1.10), and was originally discovered by adding both glucose and benzaldehyde to fermenting yeast cultures (55). In fact, this transformation is the subject of the first known patent for green chemistry.

(*R*)-PAC is an important compound in pharmaceutical synthesis as it can be easily converted to ephedrine through reductive amination using methylamine (55), or to phenylpropanolamine, another common pharmaceutical compound, by reaction with hydroxylamine followed by treatment with lithium aluminum hydride (56).

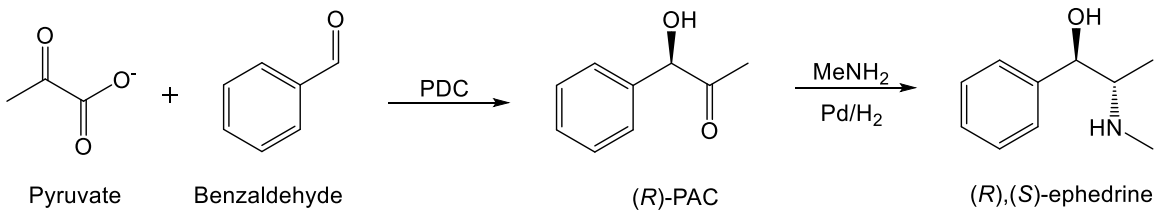

Figure 1.10: Synthesis of ephedrine using PDC to form (*R*)-PAC.

Over time, interest in these carboligation reactions has grown (52) and many other reactions have been reported. Discovery and modification of ThDP-dependent decarboxylases such as phenylpyruvate decarboxylase (57-59), benzoylformate decarboxylase (BFDC) (60-62), as well as the identification and utilization of pyruvate decarboxylases from new sources (63-68), has brought about a large expansion of synthetic possibilities. Some of this improvement is obvious, in that these new enzymes accept different substrates, or can be engineered to do that.

A different approach has been to develop catalysts with altered stereospecificity. For example, the synthesis of ephedrine described above used *S. cerevisiae* PDC to convert a mixture of pyruvate (or acetaldehyde) and benzaldehyde into (*R*)-PAC. More recently, a combination of site-directed and random mutagenesis converted the PDC from *Acetobacter pasteurianus*, *Ap*PDC, into a variant that would catalyze the formation of (*S*)-PAC in >97% enantiomeric excess (ee) (67,68). These two reactions used pyruvate (or acetaldehyde) as the donor and benzaldehyde as the acceptor. Under the same reaction conditions, BFDC uses benzoylformate (or benzaldehyde) as the donor and acetaldehyde as the acceptor to provide (*S*)-2-hydroxypropiophenone ((*S*)-HPP) in good ee (52), whereas ThDP-dependent decarboxylase, KdcA, provides >90% (*R*)-HPP (69). If benzaldehyde was used as both donor and acceptor, BFDC affords (*R*)-benzoin as the sole product (52). *Ap*PDC proved to be an adaptable enzyme as variants were prepared that catalyzed formation of (*S*)-benzoin (70). Taken together, these enzymes or variants, all of which are formally decarboxylases, have the ability to form all regio- and stereoisomers from a mixture of acetaldehyde and benzaldehyde (Figure 1.11).

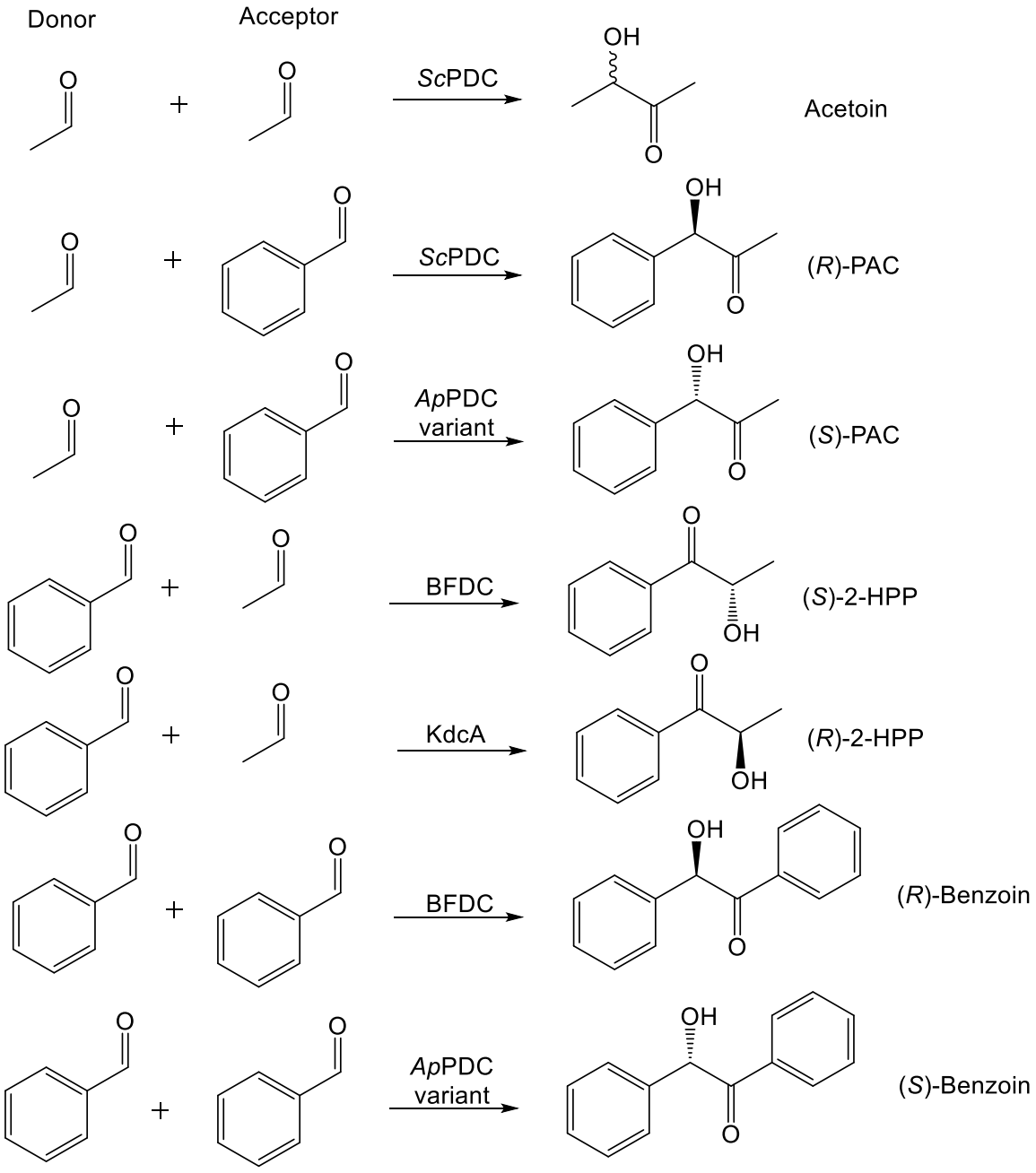

Figure 1.11: Formation of PAC, HPP, and benzoin from acetaldehyde and benzaldehyde by ThDP-dependent decarboxylases.

1.2.3.3 Pyruvate-utilizing ThDP-dependent decarboxylases

It should be noted that the carboligation reactions described in the previous section have all been catalyzed by ThDP-dependent enzymes whose principal function is decarboxylation. However, for many members of this family, decarboxylation is only the first part of the reaction

they catalyze. As an example of this diversity, it has been shown that there are at least 6 different enzymes that form unique products using only pyruvate as the donor substrate (18). These enzymes catalyze the formation of carbon-hydrogen bonds, carbon-carbon bonds, carbon-oxygen bonds, and carbon-sulfur bonds (Figure 1.12). Interestingly, the reactions all go through the identical intermediates up to the formation of the carbanion/enamine. It is at this point that the reactions diverge and lead to a range of products.

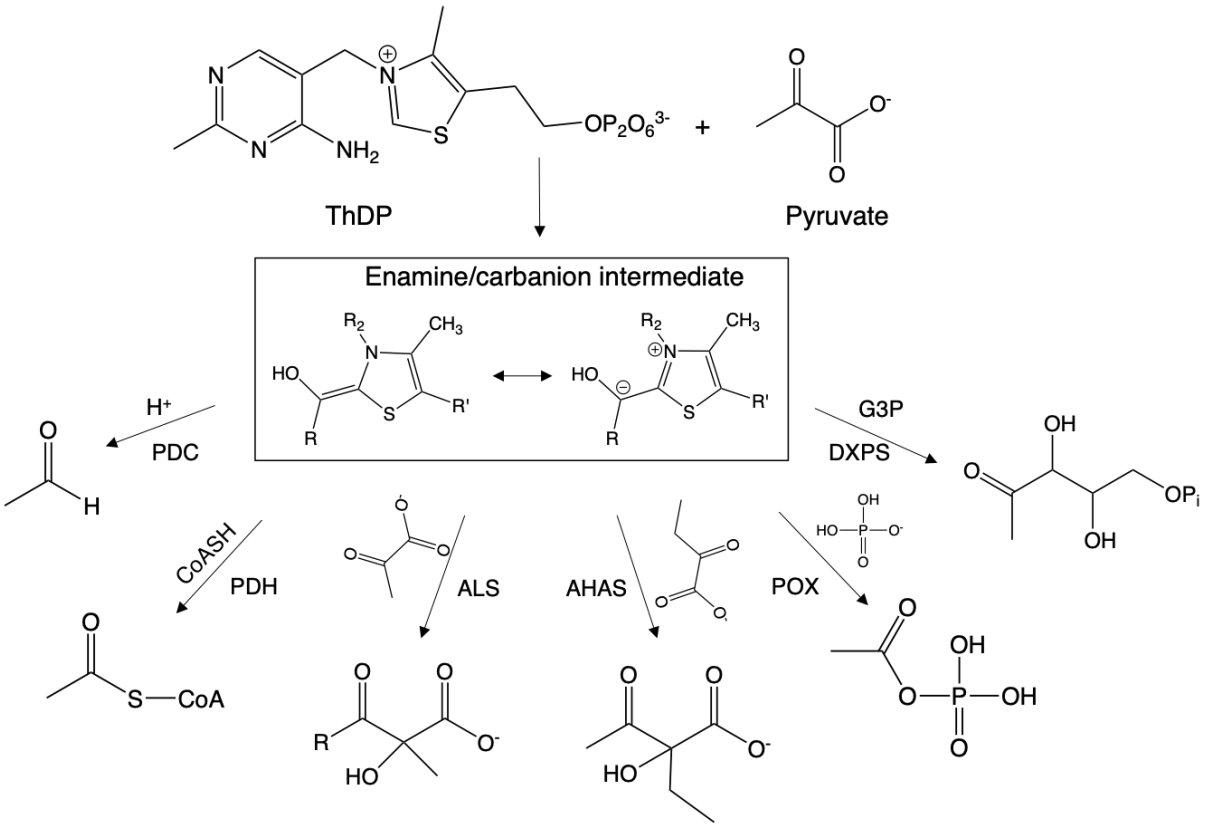

Figure 1.12: Reactions catalyzed by pyruvate-utilizing ThDP-dependent decarboxylases. Abbreviations used: PDC, pyruvate decarboxylase; PDH, pyruvate dehydrogenase complex; ALS, acetolactate synthase; AHAS, acetohydroxyacid synthase; POX, pyruvate oxidase; DXPS, deoxyxylulose-5-phosphate synthase.

1.3 Acetolactate synthase and acetohydroxyacid synthase

For some members of the ThDP-dependent decarboxylase family, carboligation is their primary function. Two examples of these are acetolactate synthase (ALS), and acetohydroxyacid synthase (AHAS). These enzymes catalyze the formation of (*S*)-acetolactate from two molecules

of pyruvate. Additionally, AHAS readily catalyzes the formation of (*S*)-acetohydroxybutyrate (Figure 1.13) from one molecule of pyruvate and one molecule of α-ketobutyrate (47,71-74).

Although these enzymes catalyze the same reaction, they are quite different. In addition to having distinct physiological roles, these differences include reaction kinetics, substrate profile, structure, and cofactor requirements.

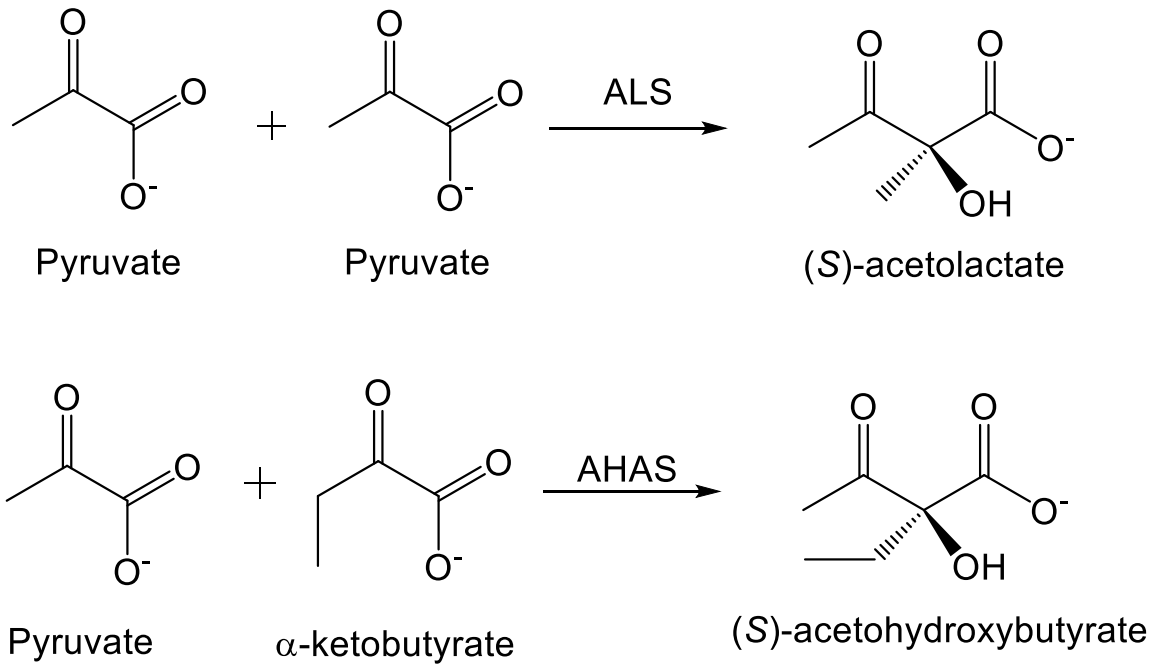

Figure 1.13: Reactions catalyzed by ALS and AHAS *in vivo*.

AHAS catalyzes the first step of valine and isoleucine biosynthesis through the formation of (*S*)-acetolactate and (*S*)-acetohydroxybutyrate, respectively (71,72). The biosynthetic pathway for isoleucine and valine is discussed in detail in Chapter 5. Conversely, ALS catalyzes the formation of (*S*)-acetolactate in the first step of the 2,3-butanediol pathway (Figure 1.14).

The biosynthesis of isoleucine and valine is an anabolic pathway, and the purpose it serves is clear; these compounds are required for protein synthesis. Accordingly, AHAS is highly expressed during the exponential phase of cell culture growth (75). Conversely, synthesis of 2,3-butanediol is part of a catabolic pathway, and its purpose is less clear. However, there are two main proposals: i) it is an alternative to mixed acid fermentation by forming a less acidic product, and ii) regulation of cellular NAD^+/NADH ratios upon the exhaustion of a carbon source (76). Support

for both is provided in that expression of ALS has been shown only in stationary phase cultures undergoing anaerobic mixed acid fermentation (75).

The involvement of AHAS in anabolism and ALS in catabolism led to many references to them in the literature as the "anabolic ALS" and the "catabolic ALS". Other times, both enzymes were simply referred to as ALS. To prevent confusion, the terms AHAS and ALS were adopted and will be the standard terminology used throughout this dissertation.

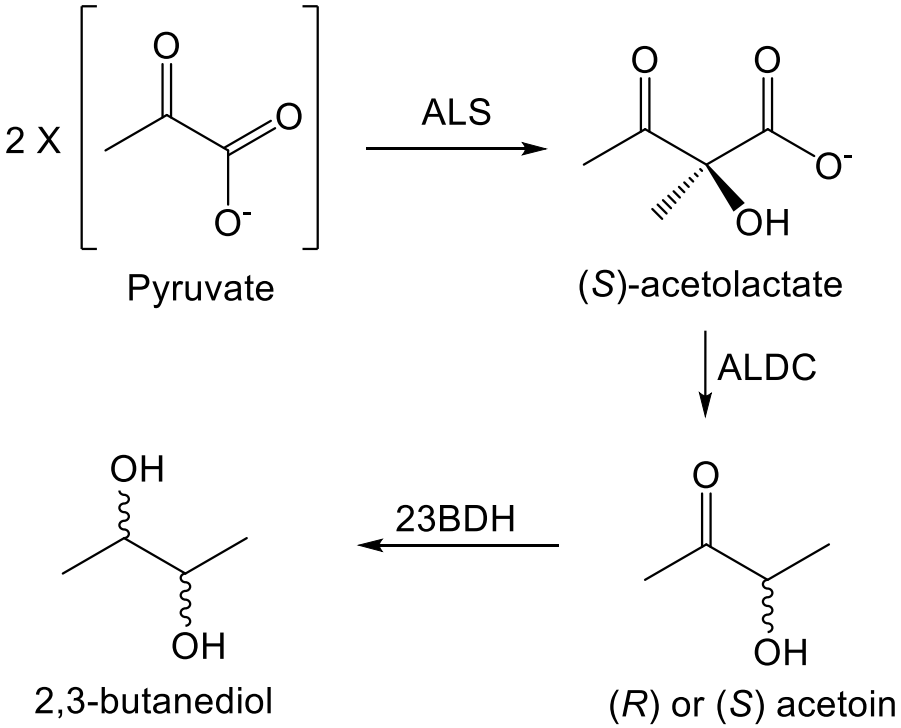

Figure 1.14: Formation of 2,3-butanediol by enzymes on the *bud* operon.
ALDC: acetolactate decarboxylase, 23BDH: 2,3-butanediol dehydrogenase.

Despite the differences between them, both ALS and AHAS are thought to catalyze the formation of acetolactate through the same mechanism. The reaction (Figure 1.15) comprises four main steps, the first two of which are identical to the reaction catalyzed by PDC: i) attack by the ThDP ylid on the α-carbonyl carbon on pyruvate (donor substrate) forming LThDP, ii) decarboxylation of LThDP forming the activated aldehyde, iii) attack by the activated aldehyde on the acceptor substrate forming the second tetrahedral intermediate, acetolactylThDP (ALThDP), and iv) release of the acetolactate product and regeneration of the ThDP ylid. In AHAS, α-ketobutyrate can be used as the acceptor substrate to provide acetohydroxybutyrate. While early

evidence for the mechanism of acetaldehyde formation in PDC was provided by synthesizing proposed intermediates and testing their reactivity (77), observation of individual reaction intermediates by NMR provided evidence for the mechanism of formation of acetolactate in AHAS (78-80).

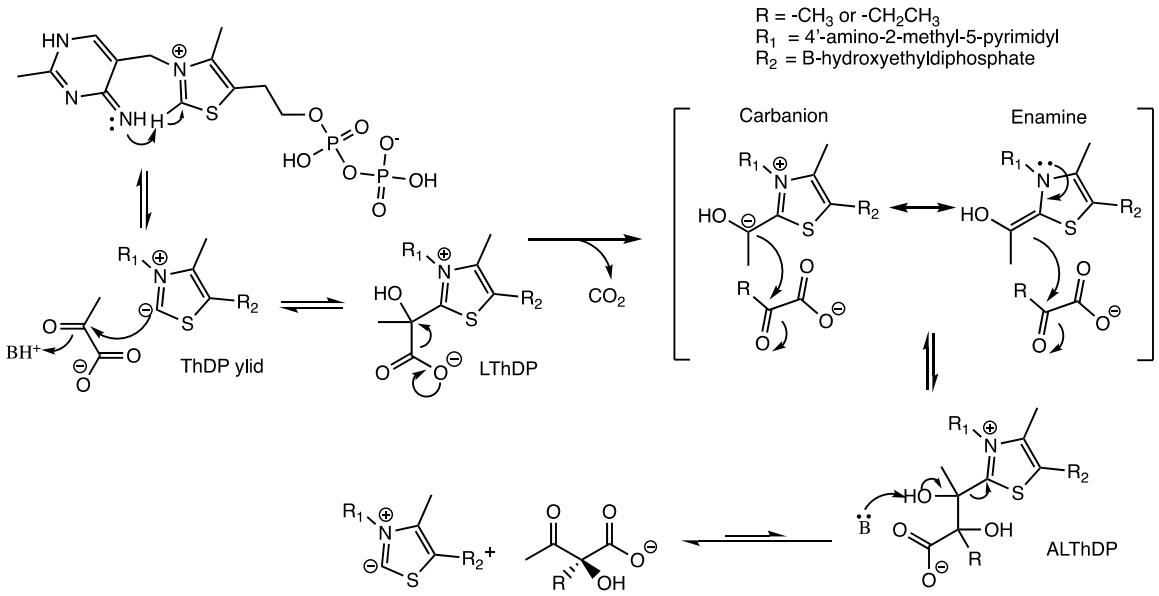

Figure 1.15: Mechanism of acetolactate and acetohydroxybutyrate formation by AHAS and ALS.

Notwithstanding the ability of AHAS to readily form acetohydroxybutyrate, one of the most interesting differences between these enzymes is that AHAS binds FAD (81), while ALS does not (82,83). Initially, the role of FAD in AHAS was thought to be structural (81,84). Recently, however, a new mechanism of acetolactate formation by the AHAS from *Saccharomyces cerevisiae* (*Sc*AHAS) was proposed, which suggests a role for FAD in which it is directly involved in the reaction mechanism (85). The new mechanism potentially sheds light on the previous observations that reduced FAD is required for AHAS activity (85-89), as the first step of the reaction directly involves fully reduced FAD. Finally, the proposed mechanism potentially provides insight into the mechanism through which popular sulfonylurea and imidazolinone herbicides show time-dependent inactivation of AHAS (90,91). This new reaction mechanism and the inactivation of AHAS by these herbicides are discussed in detail in Chapter 5.

1.4 Summary of research covered in this dissertation

The main focus of the work presented in this dissertation is on determining the differences between two similar enzymes, ALS and AHAS, from the same organism, *Klebsiella pneumoniae*. In Chapter 3, both enzymes were kinetically characterized. Of primary interest were: kinetic profile, substrate specificity, and product distribution. In Chapter 4, three X-ray crystal structures were solved after crystals were soaked with 3 different compounds, and the effect each has on the enzyme structure is discussed. Additionally, a mutagenesis study prompted by both structural and kinetic observations to investigate a unique feature of ALS is also described. Finally, in Chapter 5, a mutagenesis study was performed and a growth complementation assay was implemented to determine the ability of ALS to function in place of AHAS *in vivo*.

References

1. Neuberg, C., and Karczag, L. (1911) Die gärung der brenztraubensäure und oxalessigsäure als vorlesungsversuch. *Berichte der deutschen chemischen Gesellschaft* **44**, 2477-2479
2. Langenbeck, W. (1932) Fermentproblem und organische katalyse. *Angew. Chem. Int. Ed.* **45**, 97-99
3. Kluger, R., and Tittmann, K. (2008) Thiamin diphosphate catalysis: Enzymic and nonenzymic covalent intermediates. *Chem. Rev.* **108**, 1797-1833
4. Lohmann, K., and Schuster, P. (1937) Untersuchungen uber die cocarboxylase. *Biochem Z* **294**, 188-193
5. Peters, R. A., and O'Brien, J. R. (1938) The vitamin-B group. *Annu. Rev. Biochem.* **7**, 305-324
6. Peters, R. A. (1938) The physiology and biochemistry of vitamin B1. *Trans. R. Soc. Trop. Med. Hyg.* **31**, 483-492
7. Williams, R. R. (1935) Structure of vitamin B. *J. Am. Chem. Soc.* **57**, 229-230
8. Williams, R. R. (1936) Structure of vitamin B1. *J. Am. Chem. Soc.* **58**, 1063-1064
9. Stern, K. G., and Melnick, J. L. (1939) On the mechanism of cocarboxylase action *J. Biol. Chem.* **131**, 597-613
10. Stern, K. G., and Melnick, J. L. (1940) On the mechanism of cocarboxylase action ; A reinvestigation. *J. Biol. Chem.* **135**, 365-369

11. Lapworth, A. (1903) XCVI.—Reactions involving the addition of hydrogen cyanide to carbon compounds. *J. Chem. Soc. Trans.* **83**, 995-1005
12. Breslow, R. (1956) The mechanism of thiamine action. *Chem and Ind* **BIF Review**, 28
13. Fry, K., Ingraham, L. L., and Westheimer, F. H. (1957) The thiamin-pyruvate reaction. *J. Am. Chem. Soc.* **79**, 5225-5227
14. Breslow, R. (1957) Rapid deuterium exchange in thiazolium salts. *J. Am. Chem. Soc.* **79**, 1762-1763
15. Breslow, R. (1957) Mechanism of thiamine action: participation of a thiazolium zwitterion. *Chem and Ind*, 893
16. Breslow, R. (1958) On the mechanism of thiamine action. IV. Evidence from studies on model systems. *J. Am. Chem. Soc.* **80**, 3719-3726
17. Kluger, R. (1987) Thiamin diphosphate: a mechanistic update on enzymic and nonenzymic catalysis of decarboxylation. *Chem. Rev.* **87**, 863-876
18. Pohl, M., Sprenger, G. A., and Müller, M. (2004) A new perspective on thiamine catalysis. *Curr. Opin. Biotechnol.* **15**, 335-342
19. Graupner, M., Xu, H., and White, R. H. (2000) Identification of the gene encoding sulfopyruvate decarboxylase, an enzyme involved in biosynthesis of coenzyme M. *J. Bacteriol.* **182**, 4862-4867
20. Todd, A. E., Orengo, C. A., and Thornton, J. M. (2001) Evolution of function in protein superfamilies, from a structural perspective. *J. Mol. Biol.* **307**, 1113-1143
21. Zhang, G., Dai, J., Lu, Z., and Dunaway-Mariano, D. (2003) The phosphonopyruvate decarboxylase from *Bacteroides fragilis*. *J. Biol. Chem.* **278**, 41302-41308
22. Costelloe, S. J., Ward, J. M., and Dalby, P. A. (2008) Evolutionary analysis of the TPP-dependent enzyme family. *J. Mol. Evol.* **66**, 36-49
23. Chabrière, E., Vernède, X., Guigliarelli, B., Charon, M.-H., Hatchikian, E. C., and Fontecilla-Camps, J. C. (2001) Crystal structure of the free radical intermediate of pyruvate:ferredoxin oxidoreductase. *Science* **294**, 2559-2563
24. Xiang, S., Usunow, G., Lange, G., Busch, M., and Tong, L. (2007) Crystal structure of 1-deoxy-d-xylulose 5-phosphate Synthase, a Crucial Enzyme for Isoprenoids Biosynthesis. *J. Biol. Chem.* **282**, 2676-2682

25. Duggleby, R. G. (2006) Domain relationships in thiamine diphosphate-dependent enzymes. *Acc. Chem. Res.* **39**, 550-557

26. Hawkins, C. F., Borges, A., and Perham, R. N. (1989) A common structural motif in thiamin pyrophosphate-binding enzymes. *FEBS Lett.* **255**, 77-82

27. Kaplun, A., Binshtein, E., Vyazmensky, M., Steinmetz, A., Barak, Z., Chipman, D. M., Tittmann, K., and Shaanan, B. (2008) Glyoxylate carboligase lacks the canonical active site glutamate of thiamine-dependent enzymes. *Nat. Chem. Biol.* **4**, 113-118

28. Nemeria, N., Binshtein, E., Patel, H., Balakrishnan, A., Vered, I., Shaanan, B., Barak, Z. e., Chipman, D., and Jordan, F. (2012) Glyoxylate carboligase: a unique thiamin diphosphate-dependent enzyme that can cycle between the 4'-aminopyrimidinium and 1',4'-iminopyrimidine tautomeric forms in the absence of the conserved glutamate. *Biochemistry* **51**, 7940-7952

29. Dyda, F., Furey, W., Swaminathan, S., Sax, M., Farrenkopf, B., and Jordan, F. (1993) Catalytic centers in the thiamin diphosphate dependent enzyme pyruvate decarboxylase at 2.4 Å resolution. *Biochemistry* **32**, 6165-6170

30. Arjunan, P., Umland, T., Dyda, F., Swaminathan, S., Furey, W., Sax, M., Farrenkopf, B., Gao, Y., Zhang, D., and Jordan, F. (1996) Crystal structure of the thiamin diphosphate-dependent enzyme pyruvate decarboxylase from the yeast *Saccharomyces cerevisiae* at 2.3 Å resolution. *J. Mol. Biol.* **256**, 590-600

31. Muller, Y. A., and Schulz, G. E. (1993) Structure of the thiamine- and flavin-dependent enzyme pyruvate oxidase. *Science* **259**, 965-967

32. Lindqvist, L., Schneider, G., Ermler, U., and Sundstrom, M. (1992) Three-dimensional structure of transketolase, a thiamine diphosphate enzyme at 2.5 Å resolution. *EMBO J.* **11**, 2373-2379

33. Muller, Y. A., Lindqvist, Y., Furey, W., Schulz, G. E., Jordan, F., and Schneider, G. (1993) A thiamin diphosphate binding fold revealed by comparison of the crystal structure of transketolase, pyruvate oxidase and pyuvate decarboxylase. *Structure* **1**, 95-103

34. Guo, F., Zhang, D., Kahyaoglu, A., Farid, R. S., and Jordan, F. (1998) Is a hydrophobic amino acid required to maintain the reactive V conformation of thiamin at the active center of thiamin diphosphate-requiring enzymes? Experimental and computational studies of isoleucine 415 of yeast pyruvate decarboxylase. *Biochemistry* **37**, 13379-13391

35. Andrews, F. H., Tom, A. R., Gunderman, P. R., Novak, W. R. P., and McLeish, M. J. (2013) A bulky hydrophobic residue is not required to maintain the V-conformation of enzyme-bound thiamin diphosphate. *Biochemistry* **52**, 3028-3030

36. Pettersen, E. F., Goddard, T. D., Huang, C. C., Couch, G. S., Greenblatt, D. M., Meng, E. C., and Ferrin, T. E. (2004) UCSF Chimera - A visualization system for exploratory research and analysis. *J. Comput. Chem.* **25**, 1605-1612

37. Kemp, D. S., and O'Brien, J. T. (1970) Base catalysis of thiazolium salt hydrogen exchange and its implications for enzymic thiamine cofactor catalysis. *J. Am. Chem. Soc.* **92**, 2554-2555

38. Kemp, D. S., and Paul, K. (1970) Decarboxylation of benzisoxazole-3-carboxylic acids. Catalysis by extraction of possible relevance to the problem of enzymic mechanism. *J. Am. Chem. Soc.* **92**, 2553-2554

39. Washabaugh, M. W., and Jencks, W. P. (1988) Thiazolium C(2)-proton exchange: structure-reactivity correlations and the pKa of thiamin C(2)-H revisited. *Biochemistry* **27**, 5044-5053

40. Crosby, J., Stone, R., and Lienhard, G. E. (1970) Mechanisms of thiamine-catalyzed reactions. Decarboxylation of 2-(1-carboxy-1-hydroxyethyl)-3,4-dimethylthiazolium chloride. *J. Am. Chem. Soc.* **92**, 2891-2900

41. Schellenberger, A. (1967) Structure and mechanism of action of the active center of yeast pyruvate decarboxylase. *Angew. Chem. Int. Ed.* **6**, 1024-1035

42. Crane, E. J., Vaccaro, J. A., and Washabaugh, M. W. (1993) Single-turnover studies of brewer's yeast pyruvate decarboxylase: C(2)-proton transfer from thiamin diphosphate. *J. Am. Chem. Soc.* **115**, 8912-8917

43. Harris, T. K., and Washabaugh, M. W. (1995) Solvent-derived protons in catalysis by brewers' yeast pyruvate decarboxylase. *Biochemistry* **34**, 14001-14011

44. Kern, D., Kern, G., Neef, H., Tittmann, K., Killenberg-Jabs, M., Wikner, C., Schneider, G., and Hübner, G. (1997) How thiamin diphosphate is activated in enzymes. *Science* **275**, 67-70

45. Hübner, G., Tittmann, K., Killenberg-Jabs, M., Schaffner, J., Spinka, M., Neef, H., Kern, D., Kern, G., Schneider, G., Wikner, C., and Ghisla, S. (1998) Activation of thiamin diphosphate in enzymes. *Biochem. Biophys. Acta* **1385**, 221-228

46. Nemeria, N., Chakraborty, S., Baykal, A., Korotchkina, L. G., Patel, M. S., and Jordan, F. (2007) The 1′,4′-iminopyrimidine tautomer of thiamin diphosphate is poised for catalysis in asymmetric active centers on enzymes. *Proc. Natl. Acad. Sci. U. S. A.* **104**, 78-82

47. Pang, S. S., Duggleby, R. G., Schowen, R. L., and Guddat, L. W. (2004) The crystal structures of *Klebsiella pneumoniae* acetolactate synthase with enzyme-bound cofactor and with an unusual intermediate. *J. Biol. Chem.* **279**, 2242-2253

48. Planas, F., Sheng, X., McLeish, M. J., and Himo, F. (2018) A theoretical study of the benzoylformate decarboxylase reaction mechanism. *Front. Chem.* **6**

49. Planas, F., McLeish, M. J., and Himo, F. (2019) Computational characterization of enzyme-bound thiamin diphosphate reveals a surprisingly stable tricyclic state: implications for catalysis. *Beilstein J. Org. Chem.* **15**, 145-159

50. Andrews, F. H., and McLeish, M. J. (2012) Substrate specificity in thiamin diphosphate-dependent decarboxylases. *Bioorg. Chem.* **43**, 26-36

51. Jordan, F. (2003) Current mechanistic understanding of thiamin diphosphate-dependent enzymatic reactions. *Nat Prod Rep* **20**, 184-201

52. Iding, H., Siegert, P., Mesch, K., and Pohl, M. (1998) Application of a-keto acid decarboxylases in biotransformations. *Biochem. Biophys. Acta* **1385**, 307-322

53. Gala, D., DiBenedetto, D. J., Clark, J. E., Murphy, B. L., Schumacher, D. P., and Steinman, M. (1996) Preparations of antifungal Sch 42427/MS 9164: preparative chromatographic resolution, and total asymmetric synthesis via enzymic preparation of chiral α-hydroxy arylketones. *Tetrahedron Lett.* **37**, 611-614

54. Fuganti, C., and Grasselli, P. (1982) Synthesis of the C14 chromanyl moiety of natural α-tocopherol (vitamin E) *J. Chem. Soc. Chem. Comm.* **4**, 205-206

55. Hildebrandt, G., and Klavehn, W. (1930) Verhafen zur herstellung von 1-1-phenyl-2-methylaminopropan-1-ol. in *German Patent no 548-459*

56. Gazaliev, A. N., Zhurinov, M. Z., Fazylov, S. D., and Balitskii, S. N. (1989) Isolation, analysis, and synthesis of ephedrine and its derivatives. *Chem. Nat. Compd.* **25**, 261-271

57. Barrowman, M. M., and Fewson, C. A. (1985) Phenylglyoxylate decarboxylase and phenylpyruvate decarboxylase from *Acinetobacter calcoaceticus*. *Curr. Microbiol.* **12**, 235-239

58. Guo, Z., Goswami, A., Mirfakhrae, K. D., and Patel, R. N. (1999) Asymmetric acyloin condensation catalyzed by phenylpyruvate decarboxylase. *Tetrahedron: Asymmetry* **10**, 4667-4675

59. Guo, Z., Goswami, A., Nanduri, V. B., and Patel, R. N. (2001) Asymmetric acyloin condensation catalysed by phenylpyruvate decarboxylase. Part 2: Substrate specificity and purification of the enzyme. *Tetrahedron: Asymmetry* **12**, 571-577

60. Hegeman, G. D. (1970) Benzoylformate decarboxylase (*Pseudomonas putida*). *Methods Enzymol.* **17**, 674-678

61. Dünnwald, T., Demir, A. S., Siegert, P., Pohl, M., and Müller, M. (2000) Enantioselective synthesis of *(S)*-2-hydroxypropanone derivatives by benzoylformate decarboxylase catalyzed C-C bond formation. *Eur J Org Chem* **2000**, 2161-2170

62. Lingen, B., Grötzinger, J., Kolter, D., Kula, M.-R., and Pohl, M. (2002) Improving the carboligase activity of benzoylformate decarboxylase from *Pseudomonas putida* by a combination of directed evolution and site-directed mutagenesis. *Prot Eng* **15**, 585-593

63. Lie, M. A., Celik, L., Jorgensen, K. A., and Schiott, B. (2005) Cofactor activation and substrate binding in pyruvate decarboxylase. Insights into the reaction mechanism from molecular dynamics simulations. *Biochemistry* **44**, 14792-14806

64. Kutter, S., Wille, G., Relle, S., Weiss, M. S., Hübner, G., and König, S. (2006) The crystal structure of pyruvate decarboxylase from *Kluyveromyces lactis*. Implications for the substrate activation mechanism of this enzyme. *FEBS J* **273**, 4199-4209

65. Höhne, M., Kühl, S., Robins, K., and Bornscheuer, U. T. (2008) Efficient Asymmetric Synthesis of Chiral Amines by Combining Transaminase and Pyruvate Decarboxylase. *ChemBioChem* **9**, 363-365

66. Meyer, D., Walter, L., Kolter, G., Pohl, M., Müller, M., and Tittmann, K. (2011) Conversion of pyruvate decarboxylase into an enantioselective carboligase with biosynthetic potential. *J Am Chem Soc* **133**, 3609-3616

67. Rother, D., Kolter, G., Gerhards, T., Berthold, C. L., Gauchenova, E., Knoll, M., Pleiss, J., Müller, M., Schneider, G., and Pohl, M. (2011) *S*-Selective mixed carboligation by structure-based design of the pyruvate decarboxylase from *Acetobacter pasteurianus*. *ChemCatChem* **3**, 1587-1596

68. Sehl, T., Bock, S., Marx, L., Maugeri, Z., Walter, L., Westphal, R., Vogel, C., Menyes, U., Erhardt, M., Muller, M., Pohl, M., and Rother, D. (2017) Asymmetric synthesis of (S)-phenylacetylcarbinol - closing a gap in C-C bond formation. *Green Chem* **19**, 380-384

69. Gocke, D., Nguyen, C. L., Pohl, M., Stillger, T., Walter, L., and Müller, M. (2007) Branched-chain keto acid decarboxylase from *Lactococcus lactis* (KdcA), a valuable thiamine diphosphate-dependent enzyme for assymmetric C-C bond formation. *Adv. Synth. Catal.* **349**, 1425-1435.

70. Westphal, R., Vogel, C., Schmitz, C., Pleiss, J., Muller, M., Pohl, M., and Rother, D. (2014) A Tailor-Made Chimeric Thiamine Diphosphate Dependent Enzyme for the Direct Asymmetric Synthesis of (S)-Benzoins. *Angew. Chem. Int. Ed.* **53**, 9376-9379

71. Umbarger, H. E., and Brown, B. (1958) Isoleucine and valine metabolism in *Escherichia coli* : VIII. The formation of acetolactate. *J. Biol. Chem.* **233**, 1156-1160

72. Leavitt, R. I., and Umbarger, H. E. (1961) Isoleucine and valine metabolism in *Escherichia coli*. X. The enzymatic formation of acetohydroxybutyrate. *J. Biol. Chem.* **236**, 2486-2491

73. Störmer, F. C. (1968) The pH 6 acetolactate-forming enzyme from *Aerobacter aerogenes*. I. Kinetic studies. *J. Biol. Chem.* **243**, 3735-3739

74. Steinmetz, A., Vyazmensky, M., Meyer, D., Barak, Z. e., Golbik, R., Chipman, D. M., and Tittmann, K. (2010) Valine 375 and phenylalanine 109 confer affinity and specificity for pyruvate as donor substrate in acetohydroxy acid synthase isozyme II from *Escherichia coli*. *Biochemistry* **49**, 5188-5199

75. Halpern, Y. S., and Umbarger, H. E. (1959) Evidence for two distinct enzyme systems forming acetolactate in *Aerobacter aerogenes*. *J. Biol. Chem.* **234**, 3067-3071

76. Johansen, L., Bryn, K., and Störmer, F. C. (1975) Physiological and biochemical role of the butanediol pathway in *Aerobacter (Enterobacter) aerogenes*. *J. Bacteriol.* **123**, 1124-1130

77. Kluger, R., Chin, J., and Smyth, T. (1981) Thiamin-catalyzed decarboxylation of pyruvate. Synthesis and reactivity analysis of the central, elusive intermediate, α-lactylthiamin. *J. Am. Chem. Soc.* **103**, 994-888

78. Tittmann, K., Golbik, R., Uhlemann, K., Khailova, L., Patel, M., Jordan, F., Chipman, D., Duggleby, R., Hübner, G., and Schneider, G. (2003) How thiamine works in enzymes. in *Thiamine*, CRC Press. pp

79. Tittmann, K., Golbik, R., Uhlemann, K., Khailova, L., Schneider, G., Patel, M., Jordan, F., Chipman, D. M., Duggleby, R. G., and Hübner, G. (2003) NMR analysis of covalent intermediates in thiamin diphosphate enzymes. *Biochemistry* **42**, 7885-7891

80. Tittmann, K., Vyazmensky, M., Hübner, G., Barak, Z. e., and Chipman, D. M. (2005) The carboligation reaction of acetohydroxyacid synthase II: Steady-state intermediate distributions in wild type and mutants by NMR. *Proc. Natl. Acad. Sci. U. S. A.* **102**, 553-558

81. Størmer, F. C., and Umbarger, H. E. (1964) The requirement for flavine adenine dinucleotide in the formation of acetolactate by *Salmonella typhimurium* extracts. *Biochem. Biophys. Res. Commun.* **17**, 587-592

82. Störmer, F. C. (1968) The pH 6 acetolactate-forming enzyme from *Aerobacter aerogenes*. II. Evidence that it is not a flavoprotein. *J. Biol. Chem.* **243**, 3740-3741

83. Holtzclaw, W. D., and Chapman, L. F. (1975) Degradative acetolactate synthase of *Bacillus subtilis*: purification and properties. *J. Bacteriol.* **121**, 917-922

84. Duggleby, R. G., and Pang, S. S. (2000) Acetohydroxyacid Synthase. *J. Biochem. Mol. Biol.* **33**, 1-36

85. Lonhienne, T., Garcia, M. D., Noble, C., Harmer, J., Fraser, J. A., Williams, C. M., and Guddat, L. W. (2017) High resolution crystal structures of the acetohydroxyacid synthase-pyruvate complex provide new insights into its catalytic mechanism. *ChemistrySelect* **2**, 11981-11988

86. Tittmann, K., Schroder, K., Golbik, R., McCourt, J., Kaplun, A., Duggleby, R. G., Barak, Z., Chipman, D. M., and Hubner, G. (2004) Electron transfer in acetohydroxy acid synthase as a side reaction of catalysis. Implications for the reactivity and partitioning of the carbanion/enamine form of (alpha-hydroxyethyl)thiamin diphosphate in a "nonredox" flavoenzyme. *Biochemistry* **43**, 8652-8661

87. Lonhienne, T., Nouwens, A., Williams, C. M., Fraser, J. A., Lee, Y. T., West, N. P., and Guddat, L. W. (2016) Commercial herbicides can trigger the oxidative inactivation of acetohydroxyacid synthase. *Angew. Chem. Int. Ed.* **55**, 4247-4251

88. Lonhienne, T., Garcia, M. D., and Guddat, L. W. (2017) The role of a FAD cofactor in the regulation of acetohydroxyacid synthase by redox signaling molecules. *J. Biol. Chem.* **292**, 5101-5109

89. Lonhienne, T., Garcia, M. D., Pierens, G., Mobli, M., Nouwens, A., and Guddat, L. W. (2018) Structural insights into the mechanism of inhibition of AHAS by herbicides. *Proc. Natl. Acad. Sci. U. S. A.* **115**, E1945-E1954

90. LaRossa, R. A., and Schloss, J. V. (1984) The sulfonylurea herbicide sulfometuron methyl is an extremely potent and selective inhibitor of acetolactate synthase in *Salmonella typhimurium*. *J. Biol. Chem.* **259**, 8753-8757

91. Chang, A. K., and Duggleby, R. G. (1997) Expression, purification and characterization of Arabidopsis thaliana acetohydroxyacid synthase. *Biochem. J.* **327 (Pt 1)**, 161-169

CHAPTER 2. MATERIALS AND METHODS

2.1 Materials

NADH, IPTG, yeast alcohol dehydrogenase (YADH), 2-keto acids, and diketones were purchased from Sigma-Aldrich (St. Louis, MO, USA). Nickel-nitrilotriacetic acid (Ni-NTA) agarose resin was purchased from Qiagen (Valencia, CA, USA). Buffers and other reagents were purchased from either Sigma-Aldrich or Fisher Scientific (Pittsburg, PA, USA) and were of the highest commercially available grade.

Genomic DNA from *K. pneumoniae* str 7561 was purchased from the ATCC (Manassas, VA, USA). *E. coli* strains MI168, MI253, MI262, and FD1062 were obtained from the Coli Genetic Stock Center (New Haven, CT, USA). The plasmid vectors pET28a, pCRBlunt and pBAD-Myc/HisA, and *E. coli* strains TOP10 and BL21(DE3) were available from laboratory stocks. Restriction enzymes were purchased from New England Biolabs (Ipswich, MA, USA). *Pfu* Ultra was purchased from Stratagene (San Diego, CA, USA). All primers were designed according to the QuikChange protocol (Agilent Technologies, Santa Clara, CA, USA) and synthesized by Integrated DNA technologies (Coralville, IA, USA). DNA sequencing was carried out at the University of Michigan Sequencing Core Facility (Ann Arbor, MI, USA).

Crystal screening kits, crystallization trays, and silanized coverslips were purchased from Hampton Research (Aliso Viejo, CA, USA). Flow valves for diketone extraction were purchased from Cole-Parmer (Vernon Hills, IL, USA), and multiwell plates for cell growth assays were purchased from USA Scientific (Ocala, FL, USA).

2.2 Construction of expression vectors

2.2.1 Cloning and construction of expression vector pET28a*Kp*ALS-HisN

Plasmid pTL8 carrying the *bud*B gene was a kind gift from Prof. Hwan-You Chang (Institute of Molecular Medicine, National Tsing Hua University, Hsinchu City, TW). Construction of the pET28a*Kp*ALS-HisN expression vector was done by Prof. Michael McLeish, and was available for use in the laboratory.

2.2.2 Construction of expression vector pBAD*Kp*ALS*-HisN

An internal restriction site for NcoI was removed from the pET28a*Kp*ALS-HisN expression vector by PCR mutagenesis. The silent mutation resulted in expression vector pET28a*Kp*ALS*-HisN. This vector was then digested with Nco1 and the gene encoding *Kp*ALS was ligated into pBAD/Myc-HisA that had been previously digested with Nco1 resulting in the pBAD*Kp*ALS*-HisN expression vector.

2.2.3 Cloning and construction of expression vector pBAD*Kp*IlvGM-Nde

The gene encoding for *Kp*AHAS was amplified from *K. pneumoniae* str. 7561 gDNA (ATCC BAA-2146D-5) by PCR. Restriction sites for NdeI and HindIII were engineered at the N-terminus and C-terminus, respectively. The PCR product was ligated into the pCRBLUNT vector resulting in pCRB*Kp*IlvGM. Mutagenesis was then performed on the pCRB*Kp*IlvGM plasmid to remove an NdeI site internal to the *ilv*GM gene resulting in pCRB*Kp*IlvGM-Nde. Concomitantly, PCR mutagenesis was performed on expression vector pBAD-Myc/HisA to remove an extraneous NdeI site in the vector resulting in pBAD (-NdeI). Following this, PCR mutagenesis was used to introduce an Nde1 restriction site in place of the Nco1 and KpnI restriction sites in the multiple cloning site of the pBAD (-NdeI) vector resulting in pBAD/Nde. The pCRB*Kp*IlvGM-Nde and pBAD/Nde vectors were digested with NdeI and HindIII, and the *Kp*IlvGM-Nde fragment was ligated into the digested pBAD/Nde vector resulting in the pBAD*Kp*IlvGM-Nde expression vector.

2.2.4 Construction of expression vector pET28a*Kp*IlvGM-Nde

The pBAD*Kp*IlvGM-Nde vector was digested with NdeI and HindIII. The *Kp*IlvGM-Nde fragment was then ligated into the pET28a vector that was previously digested with NdeI and HindIII, resulting in the pET28a*Kp*IlvGM-Nde expression vector.

2.2.5 Site-directed mutagenesis of *Kp*ALS

Mutagenesis was performed on either the pET28a*Kp*ALS*-HisN or the pBAD*Kp*ALS*-HisN expression vectors. Site-directed mutagenesis was performed according to the QuikChange mutagenesis protocol (Agilent) using *Pfu* polymerase. Primers used in mutagenesis are listed in the chapters in which the mutants are discussed. Restriction enzyme DpnI was used to digest

template DNA prior to transformation into chemically competent One Shot TOP 10 chemically competent cells. Each plasmid was sequenced over the entire *Kp*ALS gene after mutagenesis to confirm that only desired mutations were introduced during PCR.

2.3 Protein expression and purification

2.3.1 Expression of recombinant proteins

Following transformation of the appropriate vector into *E. coli* strain BL21(DE3), over-expression of 6x-histidine tagged recombinant *Kp*ALS and *Kp*AHAS was carried out in either LB media or auto-induction media. In LB, production of the recombinant protein was induced by addition of 1 mM IPTG to the culture during the exponential growth phase. Following induction, cultures were grown at room temperature for 18-20 hours. Alternatively, for expression in auto-induction media, cultures were grown at 30 °C for 48 hours with rapid (275 rpm) shaking. In both cases cells were harvested by centrifugation and resuspended in 40 mL of Buffer A (50 mM sodium phosphate pH 7.0 or 8.0 containing 300 mM NaCl, and 10 mM imidazole). Resuspended cells were then stored at -80 °C until further use.

2.3.2 Purification of recombinant proteins

All purification steps were conducted at 4 °C. Frozen cells were thawed and incubated on ice with lysozyme (200 µg/mL) and DNase (5 µg/mL) for 30 minutes to lyse the cells. Cells were further lysed by sonication (2 x 90 s bursts at 30% duty cycle with a 90 s rest period between bursts) using a Branson Sonifier 450 sonicator (Danbury, CT, USA). Cellular debris was removed by two 30-minute centrifugation steps at 20,000g. Cell free extract (CFE) was loaded onto a Ni-NTA agarose column pre-equilibrated with Buffer A using a Biologic LC system (Bio-Rad, Hercules, CA, USA). The column was then washed with 10 column volumes of Buffer A and 5 column volumes of Buffer B (50 mM sodium phosphate pH 7.0 or 8.0, 300 mM NaCl, 20 mM imidazole). Protein was eluted with 5 column volumes of Buffer C (50 mM sodium phosphate pH 7.0 or 8.0, 300 mM NaCl, 250 mM imidazole). Fractions (5 mL) were collected from both the wash and elution steps. Initially the absorbance at 280 nm was used to determine which fractions contained protein and the result was confirmed by SDS-PAGE. Fractions containing protein were combined and concentrated to 3 mL using centrifugation filters with a 50k Da molecular weight

cutoff (Amicon Ultra, EMD Millipore, Burlington, MA, USA). Elution buffer was then exchanged for ALS (50 mM potassium phosphate, pH 7.0, 1 mM $MgCl_2$, 0.5 mM ThDP, 10% glycerol) or AHAS (50 mM potassium phosphate, pH 8.0, 1 mM $MgCl_2$, 0.5 mM ThDP, 2 μM FAD, 10% glycerol) storage buffer using an Econo-Pac DG10 desalting column (Bio-Rad). Purity was assessed by SDS-PAGE and protein concentration was determined either by absorbance at 280 nm or by Bradford Assay using BSA as a standard (1). Molar extinction coefficients were calculated using the EXPASY ProtParam tool (2).

2.4 Kinetic characterization studies

2.4.1 Steady-state analysis of *Kp*ALS

Purified *Kp*ALS variants were kinetically characterized using circular dichroism (CD) spectropolarimetry on a Jasco J-810 spectropolarimeter. Formation of (*S*)-acetolactate was followed at 310 nm at which (*S*)-acetolactate has a molar ellipticity (θ) of 3000 deg×cm^2/dmol (3). A typical reaction mixture contained buffer (100 mM sodium acetate, potassium phosphate, or MES pH 6.0), 1 mM $MgCl_2$, 0.5 mM ThDP, and pyruvate (1-125 mM) in a final volume of 1 mL. Reactions were carried out at 30 °C over a 5-minute period and reactions were initiated by the addition of enzyme. Assays were carried out in triplicate and the steady-state kinetic parameters were determined by fitting the initial rate data to the Michaelis-Menten equation (Equation 2.1), or the Hill equation (Equation 2.2) using the Enzyme Kinetics package in SigmaPlot 12.5 (Systat Software, Inc.).

Equation 2.1: $v = \frac{V_{max}[S]}{K_m + [S]}$

Equation 2.2: $v = \frac{V_{max}[S]^n}{S_{05}^n + [S]^n}$

2.4.2 Steady-state analysis of *Kp*AHAS

A Jasco J-810 spectropolarimeter was used to obtatin steady-state kinetic data for *Kp*AHAS. The formation of (*S*)-acetolactate (θ = 3000 deg×cm^2/dmol) and (*S*)-propiohydroxybutyrate (θ = 2640 deg×cm^2/dmol) was measured at 310 nm and 300 nm, respectively (3). A typical reaction mixture contained buffer (100 mM potassium phosphate, potassium phosphate and acetate, or HEPES pH 8.0), 1 mM $MgCl_2$, 0.5 mM ThDP, 2 μM FAD,

and varying concentrations of pyruvate or α-ketobutyrate in a total volume of 1 mL. Reactions were carried out at 30 °C and were initiated by addition of *Kp*AHAS. Assays were carried out in triplicate and the steady-state kinetic parameters were determined by fitting the initial rate data to the Michaelis-Menten equation (Equation 2.1).

2.4.3 Assay of decarboxylation activity

The decarboxylase activity of *Kp*ALS and *Kp*AHAS was determined using a coupled assay in which acetaldehyde formation was measured by following the disappearance of NADH at 340 nm (ε = 6220 $L \times mol^{-1} \times cm^{-1}$) (4) on a Varian Cary 50 UV/Vis spectrophotometer (Agilent). The assay contained pyruvate, 200 μM NADH, 80 U YADH, 100 mM sodium acetate buffer pH 6.0, 0.5 mM ThDP, and 1 mM $MgCl_2$ in a final volume of 1 mL. The reactions were carried out at 30 °C and were initiated by addition of enzyme.

2.4.4 Inhibition of *Kp*ALS by β-fluoropyruvate

Studies on inhibition of *Kp*ALS by β-fluoropyruvate were performed using the standard CD assay in which formation of (*S*)-acetolactate was followed at 310 nm. Each reaction contained 100 mM sodium acetate pH 6.0, 0.5 mM ThDP, 1 mM $MgCl_2$, and pyruvate (5-50 mM) and β-fluoropyruvate (0-125 μM). Reactions were carried out at 30 °C and were initiated by addition of *Kp*ALS. Assays were carried out in triplicate and the steady-state kinetic parameters and inhibition constants were determined by fitting the initial rate data to the equations for competitive (Equation 2.3), uncompetitive (Equation 2.4), non-competitive (Equation 2.5), and mixed (Equation 2.6) inhibition. The type of inhibition was determined by the best fit to the data.

Equation 2.3: $$v = \frac{V_{max}[S]}{K_m\left(1+\frac{[I]}{K_i}\right)+[S]}$$

Equation 2.4: $$v = \frac{V_{max}[S]}{K_m+\left(1+\frac{[I]}{K_i}\right)[S]}$$

Equation 2.5: $$v = \frac{V_{max}[S]}{K_m\left(1+\frac{[I]}{K_i}\right)+\left(1+\frac{[I]}{K_i}\right)[S]}$$

Equation 2.6: $$v = \frac{V_{max}[S]}{K_m\left(1+\frac{[I]}{K_i}\right)+\left(1+\frac{[I]}{K_i'}\right)[S]}$$ where $K_i \neq K_i'$

2.4.5 Inhibition of *Kp*AHAS by β-fluoropyruvate

Studies on inhibition of *Kp*ALS by β-fluoropyruvate were performed using the standard CD assay in which formation of (*S*)-acetolactate was followed at 310 nm. Each reaction contained 100 mM potassium phosphate pH 8.0, 0.5 mM ThDP, 1 mM $MgCl_2$, 2 μM FAD, pyruvate (1-10 mM) and β-fluoropyruvate (0-125 μM). Reactions were carried out at 30 °C and were initiated by addition of *Kp*AHAS. Assays were carried out in triplicate and the steady-state kinetic parameters and inhibition constants were determined by fitting the initial rate data to the equations for competitive (Equation 2.3), uncompetitive (Equation 2.4), non-competitive (Equation 2.5), and mixed (Equation 2.6) inhibition. The type of inhibition was determined by the best fit to the data.

2.4.6 Inhibition of *Kp*ALS by chlorsulfuron

Studies on inhibition of *Kp*ALS by chlorsulfuron were performed using the CD assay (see Section 2.4.1). Each reaction was made to a final volume of 1 mL and contained 100 mM sodium acetate pH 6.0, 0.5 mM ThDP, 1 mM $MgCl_2$, and varying concentrations of pyruvate (3-30 mM) and chlorsulfuron (0, 400 nM). The stock solution of chlorsulfuron was dissolved in DMSO to aid in solubility and stability. Assays were carried out in triplicate and the steady-state kinetic parameters and inhibition constants were determined by fitting the initial rate data to the equations for competitive (Equation 2.3), uncompetitive (Equation 2.4), non-competitive (Equation 2.5), and mixed (Equation 2.6) inhibition. The type of inhibition was determined by the best fit to the data.

2.4.7 Inhibition of *Kp*AHAS by chlorsulfuron

Studies on inhibition of *Kp*AHAS by chlorsulfuron were performed similarly to those performed on *Kp*ALS. Each reaction contained 100 mM potassium phosphate, 0.5 mM ThDP, 1 mM $MgCl_2$, 2 μM FAD, and varying concentrations of pyruvate (1-12 mM) and chlorsulfuron (0, 400 nM). Assays were carried out in triplicate and the steady-state kinetic parameters and inhibition constants were determined by fitting the initial rate data to the equations for competitive (Equation 2.3), uncompetitive (Equation 2.4), non-competitive (Equation 2.5), and mixed (Equation 2.6) inhibition. The type of inhibition was determined by the best fit to the data.

2.5 Analysis of product distribution by *Kp*AHAS

2.5.1 Enzymatic reactions and formation of diketones

Reactions and conversion of products to diketones was performed as described in the previously reported procedure (5). Reactions contained 100 mM potassium phosphate pH 8.0, 0.5 mM ThDP, 1 mM $MgCl_2$, 2 μM FAD, and varying amounts of pyruvate and α-ketobutyrate in a final volume of 4 mL. Reactions were carried out at 30 ℃, initiated by addition of *Kp*AHAS and were allowed to continue for 5 minutes before quenching with H_3PO_4 to a pH of 4.0. A solution (5 mL) containing $FeCl_3$ and $FeSO_4$ was added to the quenched reaction mixture to a final Fe^{2+} and Fe^{3+} concentration of 150 μM. The mixture was then heated to 80 ℃ for 10 minutes to convert the enzymatic reaction products, acetolactate and acetohydroxybutyrate, into 2,3-butanedione and 2,3-pentanedione, respectively.

2.5.2 Extraction of diketones for analysis

Following conversion of acetohydroxyacids to diketones, the solutions were cooled on ice for 10 minutes to prevent loss of volatile diketones. Once cooled, the reactions were transferred to an "air distillation" apparatus (see Chapter 3, Figure 3.6). The solutions were then heated to 60 °C while air flowed at a rate of 100 mL/minute through the reaction mixtures into a second tube containing 2 mL of ice-cold methanol. The air distillation was carried out for 25 minutes to ensure efficient capture of diketone products. Following distillation, acetoin was added to the methanol/diketone mixture to a final concentration of 1 mM to act as an internal standard for GC-MS analysis.

2.5.3 Analysis of extracted diketones by GC-MS

Diketone products were separated by gas chromatography using a 30 m × 250 μm × 0.25 μm capillary column with a VF-23ms stationary phase (Agilent). Samples (1 μL) were injected using an Agilent 7693 autosampler. The inlet temperature was held at 250 ℃ and samples were injected using a 3:1 split ratio. Helium flow through the column was held at 1.89 mL/minute. The starting column oven temperature was held at 40 ℃ held for 2 minutes. Oven temperature was then increased at a rate of 30 ℃/min to a final temperature of 90 ℃ and held for 2 minutes. The total run time for the separation was 5.4 minutes. Detection of compounds eluting

from the column was performed by mass spectrometry using an Agilent Technologies 5975C inert MSD with triple axis detector set to scan a mass range of 40 to 120 M/Z. Retention times for 2,3-butanedione, 2,3-pentanedione, 3,4-hexanedione, and acetoin were found to be 2.7 minutes, 3.4 minutes, 4.0 minutes, and 4.8 minutes, respectively. The column heating method was developed using standards of 2,3-butanedione, 2,3-pentanedione, 3,4-hexandione, and acetoin (Sigma). Peaks were integrated using the ChemStation software, and peak areas were used to determine the quantity of each compound in the sample. Peak areas corresponding to 2,3-butanedione, 2,3-pentanedione, and 3,4-hexanedione were normalized by division by the acetoin peak area in each sample to account for injection volume errors. Standard curves were constructed using a range of concentrations (0.05 mM – 1.0 mM) of each analyte. Each sample was analyzed at least three times and peak areas were reported as the average of the measurements. Where applicable, steady state kinetic parameters were determined by fitting the initial rate data to the Michaelis-Menten equation (Equation 2.1), or the Hill equation (Equation 2.2).

2.6 Conversion of *Kp*ALS into a functional AHAS enzyme

2.6.1 Mutagenesis of pBAD*Kp*ALS*-HisN

Site-saturation and site-directed mutagenesis was performed as previously reported (6) using the QuikChange site-directed mutagenesis protocol (Invitrogen). Site saturation variants were constructed using pBAD*Kp*ALS*-HisN as the template. Degenerate primers were used to encode for all 20 amino acids at selected sites. The mix of mutated plasmids was transformed into One Shot TOP10 chemically competent cells and plated on LB/agarose for colony growth. Following overnight growth, colonies were mixed on the LB/agarose plate using 1 mL of LB media. The culture was brought to a volume of 3 mL then grown overnight at 37 °C. Plasmid DNA was isolated using a Zyppy Plasmid Mini-Prep kit (Zymo Research) then immediately transformed into *E. coli* strain MI262 (7) and cells were grown overnight on LB/agarose for growth complementation studies. In some cases the isolated plasmid DNA mixture was stored at -20 °C.

2.6.2 Growth complementation assay

Growth complementation studies were performed as described by Sikdar and Kim (8). Plasmids containing engineered *Kp*ALS variants as well as the control plasmids,

pBAD*Kp*ALS*-HisN and pBAD*Kp*IlvGM-Nde, were transformed into *E. coli* MI262 cells and plated on LB agar containing ampicillin (7). The resultant colonies were picked and individually placed into 200 µL of LB media in 96-well plates. The plates were incubated while shaking at 37 °C overnight. A Biotek ELx808 IU plate reader was used to monitor cell growth at 595 nm taking 1 reading per hour. A small amount (<5 µL) of cell culture from overnight growth was transferred into the corresponding wells in a fresh 96-well plate containing M9 minimal media (6.8 g/L sodium phosphate dibasic, 5 g/L potassium phosphate monobasic, 0.5 g/L NaCl, 1 g/L NH_4Cl, 2 mM $MgSO_4$, 0.1 mM $CaCl_2$, 0.4% glucose, pH 7.4) supplemented with 0.2 mM thiamine-HCl, and 25 µg/mL each of 18 standard amino acids with the exception of valine and isoleucine. The minimal growth media was supplemented with valine or isoleucine as required. The plate containing the inoculated cultures was incubated for 24-48 hours at 37 °C and a reading at 595 nm was taken every 15 minutes. A sample was taken from any wells showing growth in the M9 minimal media, grown overnight in 3 mL of LB media, and plasmid DNA was isolated using a Zyppy Plasmid Mini-Prep kit. Purified plasmid DNA was then sent for DNA sequencing.

2.7 Solution and analysis of *Kp*ALS crystal structures

2.7.1 Crystallization of *Kp*ALS

Crystals of *Kp*ALS were grown using the hanging drop diffusion method using conditions reported by Pang *et al.* (9,10). Storage buffer was exchanged for crystallization buffer (50 mM potassium phosphate pH 7.0, 1 mM ThDP, 1 mM $MgCl_2$, 1 mM DTT) using an Econo-Pac DG10 desalting column (Bio-Rad). The well solution consisted of 0.1 M sodium HEPES pH 7.5, 5-10% PEG8000 (w/v), and 3-12% ethylene glycol (v/v). Equal volumes of well solution and enzyme (10 mg/mL) were pipetted onto a silanized glass cover slip and mixed. Crystallization trays were incubated at 4 °C and well-formed crystals appeared after 5-7 days.

2.7.2 Ligand soaking experiments

Crystals grown in the absence of ligand were used in soaking experiments with pyruvate, β-fluoropyruvate, and phosphonodifluoropyruvate. The experiments involving pyruvate and β-fluoropyruvate were performed at the Advanced Photon Source at the Argonne National Laboratory (Argonne IL, USA).

For soaking with pyruvate, the crystals were placed in well solution supplemented with 100 mM pyruvate and 30% (v/v) PEG600 as a cryoprotectant and allowed to incubate at 4 °C for 5-10 seconds before being flash frozen in liquid nitrogen. In the β-fluoropyruvate experiments, Crystals were placed in well solution containing 50 mM β-fluoropyruvate and 30 % (v/v) PEG600 as a cryprotectant and allowed to incubate at 4 °C for up to 5 minutes before being flash frozen.

Soaking with phosphonodifluoropyruvate was accomplished by adding 20 mM phosphonodifluoropyruvate to drops containing formed *Kp*ALS crystals. The crystals were then incubated at 4 °C for an additional 2 weeks before being transferred to well solution containing 30% (v/v) PEG600 as a cryprotectant and subsequently flash frozen.

2.7.3 X-ray data collection and processing

Diffraction data collection was carried out at 100 K at the GM/CA-CAT sector 23 beamline ID-B at the Advanced Photon Source at the Argonne National Lab (Argonne IL, USA). All data sets were indexed, scaled, and merged in the I_{121} space group using MOSFLM, Pointless, Aimless, and cTruncate in iMosflm (11).

2.7.4 Structure solutions and refinements

Molecular replacement was performed using phaser (12) in PHENIX (13). The search model was that of a previously published structure of *Kp*ALS (PDB ID: 10ZF) with bound ligands and water molecules removed. No further modification of the search model was necessary to obtain suitable molecular replacement solutions for each data set. Simulated annealing was performed using phenix.refine, and refinement was performed in both phenix.refine and Refmac (14,15). After each round of refinement, electron density was manually inspected and model building was performed in Coot (16). Refinement was carried out until the crystallographic and free R factors could no longer be improved, and model validity was checked using MolProbity (17,18). Images of protein structures were generated using PyMOL (19) or UCSF Chimera (20).

References

1. Bradford, M. M. (1976) A rapid and sensitive method for the quantitation of microgram quantities of protein utilizing the principle of protein-dye binding. *Anal. Biochem.* **72**, 248-254
2. Gasteiger, E., Hoogland, C., Gattiker, A., Duvaud, S. e., Wilkins, M., Appel, R., and Bairoch, A. (2005) Protein identification and analysis tools on the ExPASy server. in *The Proteomic Protocols Handbook* (Walker, J. M. ed.), Humana Press. pp 571-607
3. Vinogradov, M., Kaplun, A., Vyazmensky, M., Engel, S., Golbik, R., Tittmann, K., Uhlemann, K., Meshalkina, L., Barak, Z. e., Hübner, G., and Chipman, D. M. (2005) Monitoring the acetohydroxy acid synthase reaction and related carboligations by circular dichroism spectroscopy. *Anal. Biochem.* **342**, 126-133
4. McComb, R. B., Bond, L. W., Burnett, R. W., Keech, R. C., and Bowers, G. N. (1976) *Determination of the molar absorptivity of NADH*,
5. Gollop, N., Barak, Z. e., and Chipman, D. M. (1987) A method for simultaneous determination of the two possible products of acetohydroxy acid synthase. *Anal. Biochem.* **160**, 323-331
6. Yep, A., Kenyon, G. L., and McLeish, M. J. (2008) Saturation mutagenesis of putative catalytic residues of benzoylformate decarboxylase provides a challenge to the accepted mechanism. *Proc. Natl. Acad. Sci. U. S. A.* **105**, 5733-5738
7. Guardiola, J., De Felice, M., and Iaccarino, M. (1974) Mutant of *Escherichia coli* K-12 missing acetolactate synthase activity. *J. Bacteriol.* **120**, 536-538
8. Sikdar, M. S. I., and Kim, J. S. (2010) Expression of a gene encoding acetolactate synthase from rice complements two *ilv*H mutants in *Escherichia coli*. *Aust. J. Crop Sci.* **4**, 430-436
9. Pang, S. S., Guddat, L. W., and Duggleby, R. G. (2002) Crystallization of the FAD-independent acetolactate synthase of *Klebsiella pneumoniae*. *Acta Crystallogr. D Biol. Crystallogr.* **58**, 1237-1239
10. Pang, S. S., Duggleby, R. G., Schowen, R. L., and Guddat, L. W. (2004) The crystal structures of *Klebsiella pneumoniae* acetolactate synthase with enzyme-bound cofactor and with an unusual intermediate. *J. Biol. Chem.* **279**, 2242-2253

11. Battye, T. G. G., Kontogiannis, L., Johnson, O., Powell, H. R., and Leslie, A. G. W. (2011) IMosflm: a new graphical interface for diffraction-image processing with MOSFLM *Acta Cryst. D*, 271-281
12. Mccoy, A. J., Grosse-Kunstleve, R. W., Adams, P. D., Winn, M. D., Storoni, L. C., and Read, R. J. (2007) Phaser crystallographic software. *J. Appl. Crystallogr.* **40**, 658-674
13. Adams, P. D., Afonine, P. V., Bunkoczi, G., Chen, V. B., Davis, I. W., Echols, N., Headd, J. J., Hung, L. W., Kapral, G. J., Grosse-Kunstleve, R. W., McCoy, A. J., Moriarty, N. W., Oeffner, R., Read, R. J., Richardson, D. C., Richardson, J. S., Terwilliger, T. C., and Zwart, P. H. (2010) PHENIX: a comprehensive Python-based system for macromolecular structure solution. *Acta Crystallogr. D Biol. Crystallogr.* **66**, 213-221
14. Bailey, S. (1994) The CCP4 suite - Programs for protein crystallography. *Acta Crystallogr. D Biol. Crystallogr.* **50**, 760-763
15. Potterton, E., Briggs, P., Turkenburg, M., and Dodson, E. (2003) A graphical user interface to the CCP4 program suite. *Acta Crystallogr. D Biol. Crystallogr.* **59**, 1131-1137
16. Emsley, P., and Cowtan, K. (2004) Coot: model-building tools for molecular graphics. *Acta Crystallogr. D Biol. Crystallogr.* **60**, 2126-2132
17. Davis, I. W., Leaver-Fay, A., Chen, V. B., Block, J. N., Kapral, G. J., Wang, X., Murray, L. W., Arendall, W. B., 3rd, Snoeyink, J., Richardson, J. S., and Richardson, D. C. (2007) MolProbity: all-atom contacts and structure validation for proteins and nucleic acids. *Nucleic Acids Res.* **35**, W375-383
18. Chen, V. B., Arendall, W. B., 3rd, Headd, J. J., Keedy, D. A., Immormino, R. M., Kapral, G. J., Murray, L. W., Richardson, J. S., and Richardson, D. C. (2010) MolProbity: all-atom structure validation for macromolecular crystallography. *Acta Crystallogr. D Biol. Crystallogr.* **66**, 12-21
19. The PyMOL molecular graphics system, version 1.3, Schrödinger, LLC., http://www.pymol.org
20. Pettersen, E. F., Goddard, T. D., Huang, C. C., Couch, G. S., Greenblatt, D. M., Meng, E. C., and Ferrin, T. E. (2004) UCSF Chimera - A visualization system for exploratory research and analysis. *J. Comput. Chem.* **25**, 1605-1612

CHAPTER 3. CHARACTERIZATION AND COMPARISON OF ACETOLACTATE SYNTHASE AND ACETOHYDROXYACID SYNTHASE FROM *KLEBSIELLA PNEUMONIAE*

3.1 Introduction

In 1955, Strassman *et al*. (1) published the first evidence showing that acetolactate is a direct precursor to the amino acid valine, and that it is derived solely from two molecules of pyruvate (Figure 1.13 A) in *E. coli*. Subsequently, it was shown that, in *Aerobacter aerogenes*, two distinct enzymes were able to form acetolactate (2). Both enzymes were found to only be active in the presence of a divalent cation and thiamin diphosphate (ThDP); yet, they exhibited different pH optima and inhibition patterns. The two enzymes responsible for this were termed the pH 6.0 acetolactate-forming enzyme and the pH 8.0 acetolactate-forming enzyme. Shortly after, it was then shown that the pH 8.0 enzyme from *E. coli* was also able to form acetohydroxybutyrate (Figure 1.13 B), a compound that had earlier been identified as an important precursor to isoleucine (3), from one molecule of pyruvate and one molecule of α-ketobutyrate (4). Finally, it was shown that the pH 8.0 enzyme has an absolute requirement for FAD in addition to ThDP (5). A couple of years later, the pH 6.0 enzyme from *A. aerogenes* was isolated in crystalline form by Störmer, who then characterized the enzyme (6). Interestingly, it showed no dependence on FAD, and with a catalytic rate of ~500 s^{-1}, it was found to be much faster than the pH 8.0 enzyme (7,8). In fact, the pH 6.0 enzyme remains the fastest thiamin diphosphate-dependent enzyme known (9).

For quite some time both enzymes were referred to as acetolactate synthases, despite the fact that they have been shown to have distinct properties. This terminology proved to be quite confusing and a new naming convention was proposed in which the pH 6.0 enzyme should be called acetolactate synthase (ALS), while the pH 8.0 enzyme should be called acetohydroxyacid synthase (AHAS) (10).

Since the identification of AHAS as the enzyme responsible for synthesizing the acetolactate and acetohydroxybutyrate necessary for branched chain amino acid (BCAA) biosynthesis (1,3,4,11), orthologs of the enzyme have been studied from bacteria, fungi, and plants (10). Conversely, ALS enzymes have only been identified in bacteria, and the ALSs from *A. aerogenes* (6-8), *Bacillus subtilis* (12,13), *Serratia marcescens* (14), *Enterobacter cloacae* (15), and *Klebsiella pneumoniae* (9,16) have been studied to varying degrees.

3.1.1 General differences between AHASs and ALSs

AHASs and ALSs show even more differences than simply optimal pH, catalytic rate, and dependence on FAD. First, the genes encoding for the enzymes are found on different operons. AHASs are generally found on the *ilv* operon, while ALSs are found the *bud* operon. The *ilv* operon contains the genes involved with BCAA production while the *bud* operon contains genes for the production of 2,3-butanediol. Indeed, AHASs and ALSs have been shown to be essential for the production of BCAAs and 2,3-butanediol, respectively (12,14,15,17-19).

Second, AHASs generally contain two subunits, a catalytic and regulatory subunit, and form dimers in solution (20). Conversely, ALSs do not rely on a regulatory subunit, and form tetramers in solution (6,12,14,15).

The presence of a regulatory subunit in AHAS is of particular interest because it has been implicated as the target for feedback inhibition by valine, a common feature among AHAS enzymes. Concomitantly, the lack of a regulatory subunit has been used to explain why some ALSs are generally resistant to such inhibition (10). However, this explanation seems insufficient after the discovery of the valine sensitive ALSs from *S. marcescens* and *E. cloacae* which do not rely on any known regulatory subunits (14,15). The source of valine sensitivity in these ALS enzymes has largely not been studied, and as such, is currently not well known.

3.1.2 Substrate specificity in ALS and AHAS enzymes

As acetolactate and acetohydroxybutyrate are chemically very similar, they are difficult to differentiate spectroscopically. As a consequence, the preference for pyruvate or α-ketobutyrate as an acceptor substrate in the AHASs was not known for quite some time. Additionally, whether ALSs were able to form any significant amount of acetohydroxybutyrate was also unclear. This was due primarily to the lack of specific detection methods for the two products.

Formation of acetolactate and acetohydroxybutyrate is often detected by adaptation of the method developed by Westerfeld (21), which involves monitoring the formation of a colored complex after reaction of acetoin with creatine and naphthol. This was made possible by the discovery (22) that acetolactate and acetohydroxybutyrate undergo non-oxidative decarboxylation to acetoin and 3-hydroxy-2-pentanone, respectively, when heated under acidic conditions (Figure

3.1). As such, the method provided a reliable way to measure total concentrations of acetolactate and acetohydroxybutyrate in solution.

One of the pitfalls of the Westerfeld method is the non-specific nature of the technique, *i.e.* both products produce the same colored complex. However, it was later discovered that 2-aceto-2-hydroxyacids undergo oxidative decarboxylation when heated in the presence of iron salts (23). The oxidative decarboxylation results in the formation of volatile diketones (Figure 3.1), which can then be separated for analysis by gas chromatography (GC). This technique allowed for the simultaneous quantification of both acetolactate and acetohydroxybutyrate (24), and has been recently adapted to allow for detection of a third possible product, propiohydroxybutyrate. Propiohydroxybutyrate is formed by the condensation of two molecules of α-ketobutyrate. The ability of at least one ALS and one AHAS to catalyze the formation of this product is discussed later in this chapter.

Using the GC separation method, it was shown that AHASs generally show a strong preference for α-ketobutyrate over pyruvate as an acceptor substrate (24). That said, at least one enzyme, the AHAS I isozyme from *E. coli*, was shown to have almost no preference between the two acceptor substrates (25). Conversely, when the product distributions of the ALSs from *B. subtilis* and *A. aerogenes* were examined using this method, it was found that both enzymes largely favored the formation of acetolactate over acetohydroxybutyrate, indicating a strong preference for pyruvate as an acceptor substrate (26).

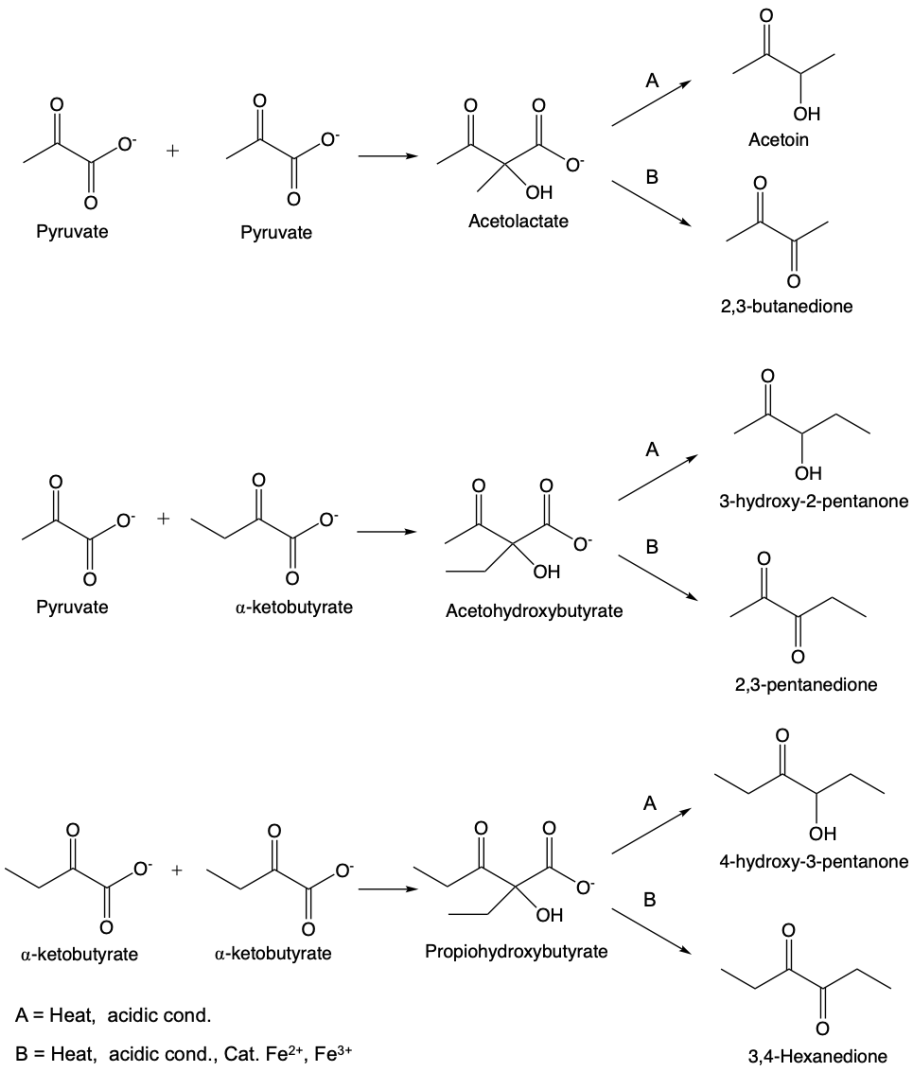

Figure 3.1: Conversion of acetolactate, acetohydroxybutyrate, and propiohydroxybutyrate to A) α-hydroxyketones, and B) diketones.

3.1.3 Stereospecificity of ALS and AHAS enzymes

Although acetolactate and acetohydroxybutyrate are both chiral, the stereochemistry of the products formed by ALS and AHAS was unknown for quite some time. However, in 1979, Sylvester and Stevens (27) showed that synthesis of valine and isoleucine requires the formation of (*S*)-acetolactate and (*S*)-acetohydroxybutyrate, respectively. By extension, this meant that the products formed by AHAS must be in the (*S*)- configuration. The stereospecificity of ALS remained unknown for another two decades until circular dichroism (CD) was used to show the product was also in the (*S*)- configuration (9,28) by comparison with products formed by AHAS.

To date, only crude extracts of an ALS and an AHAS from the same organism have been studied, and then only to determine the ratio of acetohydroxybutyrate and acetolactate formed (29). This chapter describes the kinetic characterization and comparison of the purified ALS and AHAS enzymes from *Klebsiella pneumoniae* (*Kp*ALS and *Kp*AHAS).

3.2 Kinetic analyses on *Kp*ALS and *Kp*AHAS

3.2.1 Expression and purification of *Kp*ALS and *Kp*AHAS

Construction of expression vectors, protein expression, and purification, were performed as described in Chapter 2. Both *Kp*ALS and *Kp*AHAS were expressed as N-terminal 6x Histidine-tagged variants and were purified by nickel affinity chromatography. Purity was determined by SDS-PAGE and protein concentration was determined by the Bradford assay (30). The catalytic (*Ilv*G), and regulatory (*Ilv*M) subunits of *Kp*AHAS were co-expressed and co-purified, and all attempts to express and purify the catalytic subunit alone were unsuccessful. The molecular weight of each enzyme was calculated from their respective amino acid sequences by the ProtParam tool on the ExPASy server (31). The molecular weight of *Kp*ALS was found to be ~62.5 kDa, while the combined molecular weight of both subunits of *Kp*AHAS was found to be ~70.5 kDa.

3.2.2 Kinetic characterization of *Kp*ALS

The kinetic characterization of the ALS from *A. aerogenes* (*Aa*ALS) by Störmer (7) showed that the enzyme was extremely sensitive to the buffer in which it is assayed. This included activation by acetate, and inhibition by phosphate and sulfate. Additionally, the enzyme was shown to exhibit Michaelis-Menten kinetics only in acetate buffer. All other buffers tested showed sigmoidal kinetics, indicating the requirement for substrate activation. A few years later, a similar analysis was performed on the ALS from *B. subtilis* (*Bs*ALS). The kinetics of this enzyme also showed a strong dependence on the buffer used (12). However, there were some interesting differences in the kinetic profiles of *Bs*ALS and *Aa*ALS.

First, Michaelis-Menten kinetics were observed for *Bs*ALS in phosphate, but not acetate. Second, the pH optimum of *Bs*ALS was found to be ~7.0, while it was found to be ~6.0 for *Aa*ALS. Finally, while acetate was found to be the strongest activator of *Aa*ALS, isobutyrate was found to

be the strongest activator of *Bs*ALS. In both cases however, only compounds containing a carboxylate group showed any activating effect.

In the present work, a similar study was proposed, with the steady-state kinetics of *Kp*ALS to be examined in three buffer systems: acetate, MES, and phosphate, all at pH 6.0 (Figure 3.2). Initially, kinetics were monitored using the colorimetric method (21). Later a CD method was employed, and the methods were compared.

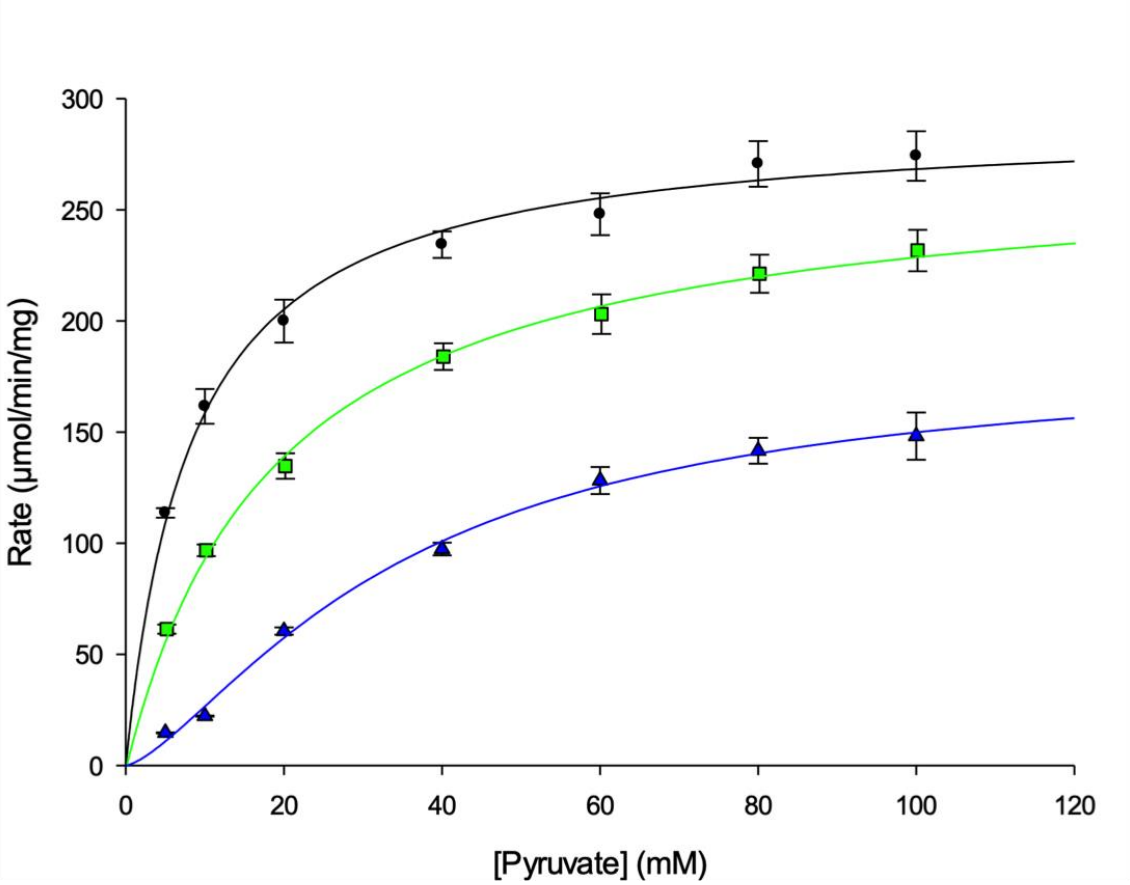

Figure 3.2: Plots of steady-state kinetic data for *Kp*ALS catalyzed formation of (*S*)-acetolactate in acetate (black), MES (green), and phosphate (blue) buffers at pH 6.0.

Table 3.1: Michaelis-Menten parameters for *Kp*ALS in 50 mM of each acetate, MES, and potassium phosphate buffers at 30 °C.

	k_{cat} (s^{-1})	K_m (mM)	k_{cat}/K_m ($mM^{-1}s^{-1}$)
Acetate	310 ± 20	8 ± 1	39
MES	290 ± 30	19 ± 1	15
Phosphate	230 ± 20	37 ± 8	6

The steady-state kinetic parameters (Table 3.1) for *Kp*ALS were found to be different in each buffer, and, in addition, the kinetics changed from Michaelis-Menten in acetate and MES to sigmoidal in phosphate (Figure 3.2). The lowest K_m and highest k_{cat} values were observed in acetate buffer, while the highest K_m value, or more correctly, S_{05} value, and lowest k_{cat} value were observed in phosphate buffer. The buffers appear to affect K_m values more than k_{cat} values. In MES and acetate the k_{cat} values were similar, but a ~2-fold increase in K_m was observed going from 8 mM in acetate to 19 mM in MES. While there was only a ~25% reduction in k_{cat}, a ~4-5-fold increase was observed between the K_m determined in acetate and the S_{05} value measured in phosphate buffer.

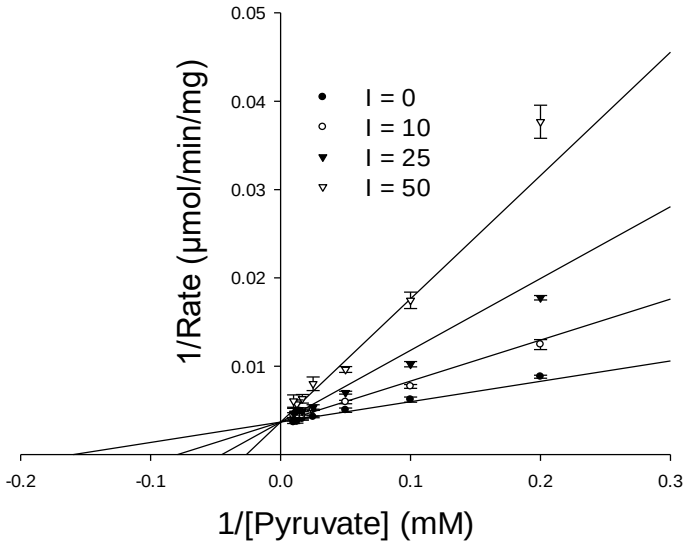

Figure 3.3: Lineweaver-Burk plot showing competitive inhibition of *Kp*ALS by up to 50 mM phosphate at pH 6.0 when assayed in 50 mM acetate buffer at pH 6.0

The change in kinetics prompted an investigation into potential inhibition by phosphate. As with *Aa*ALS, phosphate was shown to act as a competitive inhibitor of*Kp*ALS (Figure 3.3).

Inhibition was observed in both acetate and MES buffers but there was a 4-fold difference in K_i values. Phosphate inhibition was stronger in acetate, with a K_i value of 10 mM, compared to that in MES where K_i was found to be 40 mM.

After examining phosphate inhibition, the possibility of activation by acetate was also examined (Table 3.2), as, similar to *Aa*ALS, the fastest rates and best substrate binding were observed in acetate. Acetate activation was apparent in both MES and phosphate buffers. Just as was observed for phosphate inhibition, the effect was shown to be different in each buffer. However, the activating effects were found to be stronger in MES than in phosphate

Table 3.2: Steady-state parameters obtained in acetate activation experiments in 50 mM MES and phosphate buffers.

	k_{cat} (s^{-1})	K_m (mM)	k_{cat}/K_m ($mM^{-1}s^{-1}$)
MES	290 ± 30	19 ± 1	15
MES + Acetate	280 ± 40	9 ± 0.5	31
Phosphate	230 ± 20	38 ± 8	6
Phosphate + Acetate	200 ± 40	23 ± 7	9

In MES, the addition of 50 mM acetate resulted in kinetic constants matching those found in acetate alone. This indicated that acetate does have some activating effect, at least on substrate binding, and that MES shows no apparent inhibition. As may be expected, Michaelis-Menten kinetics were observed in the presence and absence of acetate.

Some evidence of acetate activation was also apparent in phosphate buffer, though the effect was less in magnitude than observed that in MES. As with activation in MES, acetate activation had no effect on k_{cat}. Additionally, only a small effect on K_m value was observed. Taken together, it is clear that acetate acts as an activator toward *Kp*ALS, and that the activating effect has little to no impact on k_{cat} values, only on K_m values.

3.2.3 Using circular dichroism to detect (*S*)-acetohydroxyacids

It has been shown that it is possible to monitor the formation of (*S*)-acetohydroxyacids directly by CD (28). The CD assay has multiple benefits over to the colorimetric method: i) it is a direct and continuous assay allowing for more precise rate measurement, ii) the assay is much

simpler in that only four components are required: substrate, buffer, enzyme, and water, and iii) the assay procedure is much faster as no quenching and derivatization reaction is required.

Kinetic assays using this technique were performed as described in Chapter 2. Again, the assays were performed in acetate and phosphate buffers (Table 3.3) for comparison with data generated by the colorimetric method (21). While the values for k_{cat} and K_m obtained in the methods are not identical, it was found that they are within reasonable limits. In both methods, Michaelis-Menten kinetics were observed in acetate, while sigmoidal kinetics were observed in phosphate.

Table 3.3: Steady-state parameters for *Kp*ALS using CD and colorimetric methods

	k_{cat} (s^{-1})	K_m (mM)	k_{cat}/K_m ($mM^{-1}s^{-1}$)
Acetate	310 ± 20	8 ± 1	39
Acetate (CD)	430 ± 20	12 ± 2	36
Phosphate	230 ± 20	38 ± 8	6
Phosphate (CD)	190 ± 10	46 ± 2	4

3.2.4 Kinetic characterization of *Kp*AHAS

In a similar study to that performed on *Kp*ALS, kinetic characterization of *Kp*AHAS was carried out in two buffer systems: phosphate and HEPES at pH 8.0. Only minor variations in k_{cat} and K_m were observed between the assays with no evidence of sigmoidal kinetics observed in either buffer (Table 3.4). The effects of added acetate were also tested in phosphate buffer. Addition of acetate was shown to have minimal effect as the calculated values for k_{cat} and K_m remained effectively unchanged compared to the values obtained in phosphate alone (Table 3.4).

Table 3.4: Steady-state parameters for *Kp*AHAS in phosphate and HEPES buffers.

	k_{cat} (s^{-1})	K_m (mM)	k_{cat}/K_m ($mM^{-1}s^{-1}$)
Phosphate	7.5 ± 0.4	3.8 ± 0.4	2
Phosphate + Acetate	3.5 ± 0.2	5.1 ± 1.0	0.7
HEPES	4.5 ± 0.1	3.9 ± 0.4	1

3.2.5 Comparison of the kinetic parameters of *Kp*ALS and *Kp*AHAS

*Kp*AHAS was found to be a much slower enzyme, with a k_{cat} value almost 60-fold lower than that measured for *Kp*ALS. On the other hand, the K_m value for pyruvate in *Kp*AHAS was also lower, with K_m values, on average, at least 2-3-fold lower than those obtained for *Kp*ALS. For a direct comparison, both enzymes were assayed in MOPS at pH 7.0 with the addition of 50 mM acetate. The addition of acetate was required for ALS activity under these conditions. As with assays performed in phosphate at pH 8.0 in the presence of acetate, *Kp*AHAS showed only a 2-fold decrease in k_{cat} value with no observed effect on K_m.

Interestingly, under these conditions *Kp*ALS and *Kp*AHAS were shown to have similar values for K_m. The K_m value of *Kp*ALS for pyruvate was found to the the lowest measured in all conditions at ~6 mM, which is similar to the ~4 mM value obtained for *Kp*AHAS. However, despite the similarity in K_m values, the values for k_{cat} remained significantly different. Notwithstanding *Kp*ALS showing an almost 4-fold decrease in k_{cat} in MOPS, that value was still ~40-fold higher than the value obtained for *Kp*AHAS (Table 3.5).

Table 3.5: Steady-state parameters for *Kp*ALS and *Kp*AHAS in MOPS buffer at pH 7.0.

	k_{cat} (s^{-1})	K_m (mM)	k_{cat}/K_m ($mM^{-1} \bullet s^{-1}$)
*Kp*ALS	120 ± 5	6 ± 1	20
*Kp*AHAS	3.3 ± 0.2	4.0 ± 0.8	0.8

3.2.6 Inhibition by β-fluoropyruvate

β-fluoropyruvate (β-FP), a pyruvate analogue, has been shown to be an inhibitor of pyruvate-utilizing ThDP-dependent enzymes (32,33). Typically, it blocks the active site by acting as a slow alternative substrate where it is converted to acetate following the loss of a fluoride ion. The mechanism of inhibition is discussed in detail in Chapter 4.

Initial-rate data were fit to the equations for competitive, uncompetitive, noncompetitive, and mixed inhibition using the enzyme kinetics package in Sigmaplot 12 (Systat Software). For *Kp*ALS, the pattern of inhibition was found to be mixed with K_i and K_i' values of 40 and 92 μM, respectively. A similar, but not identical, pattern of inhibition was observed for *Kp*AHAS

(Figure 3.4). On balance, the inhibition of *Kp*AHAS by β-fluoropyruvate was deemed to be noncompetitive with a K_i of 100 μM. However, the errors involved in the calculation were such that mixed inhibition was not out of the question.

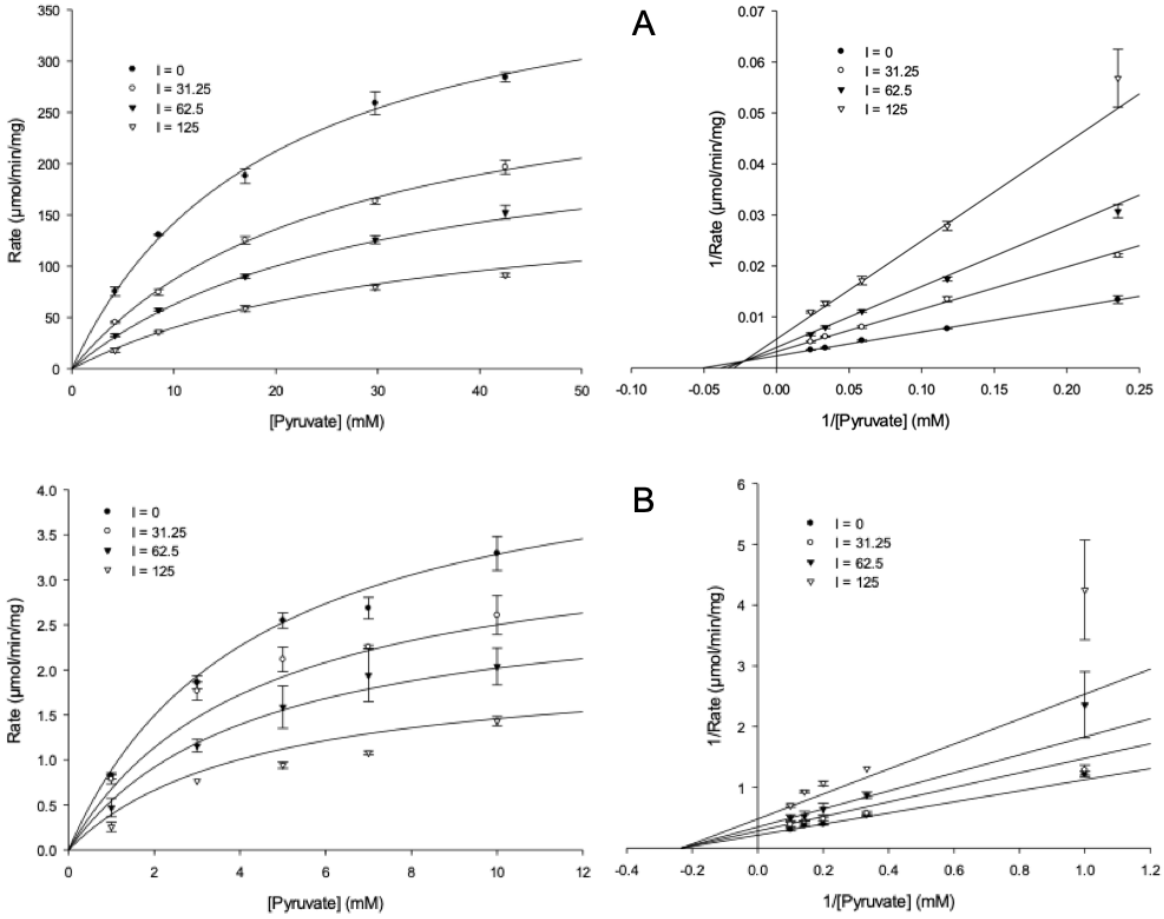

Figure 3. 4: Michaelis-Menten and Lineweaver-Burk plots of A) *Kp*ALS and B) *Kp*AHAS inhibition by micromolar concentrations of β-fluoropyruvate

The patterns of inhibition observed for these enzymes were not unexpected as they can use two identical substrates, of which β-fluoropyruvate is an analogue. The mixed inhibition observed for *Kp*ALS indicates that the inhibitor binds to both the unreacted enzyme, mimicking the donor substrate, and to the E-S complex, mimicking the acceptor substrate. However, the effect appears to be slightly stronger toward the unreacted enzyme than to the E-S complex, potentially indicating that the inhibitor competes more strongly with the donor substrate than the acceptor. The noncompetitive inhibition observed for *Kp*AHAS indicates that the inhibitor binds to both sites

equally, *i.e*., it competes equally with both the donor and acceptor substrates. Interestingly, for both enzymes, the K_i for β-fluoropyruvate was found to be at least an order of magnitude lower than the K_m values calculated for pyruvate.

3.2.7 Use of α-ketobutyrate as an alternative substrate in *Kp*ALS and *Kp*AHAS

One possible product of ALS and AHAS enzymes that is rarely considered is the condensation of two molecules of α-ketobutyrate (αKB) to form propiohydroxybutyrate (Figure 3.1). The lack of interest in this activity is likely due to the fact that it appears propiohydroxybutyrate has no known biological significance. Regardless, the ability of both enzymes to catalyze this reaction was investigated.

For *Kp*ALS, very little ability to form propiohydroxybutyrate was observed. In fact, evidence for formation of a chiral product was only observed after the reaction was allowed to proceed for 16 hours, and even then only a small amount was formed (Figure 3.5, A). This represented less than 10% of the signal observed when the enzyme forms (*S*)-acetolactate from the same concentration (25 mM) of pyruvate (Figure 3.5, B).

Conversely, *Kp*AHAS was shown to readily form this product with a k_{cat} value of 2.4 ± 0.1 s^{-1} and K_m value of 14 ± 1 mM. This represents only a 10-fold decrease in catalytic efficiency for the formation of propiohydroxybutyrate compared to that for acetolactate formation. Given this, it would appear that *Kp*AHAS is able to use the larger substrate not only as an acceptor, but also as a donor.

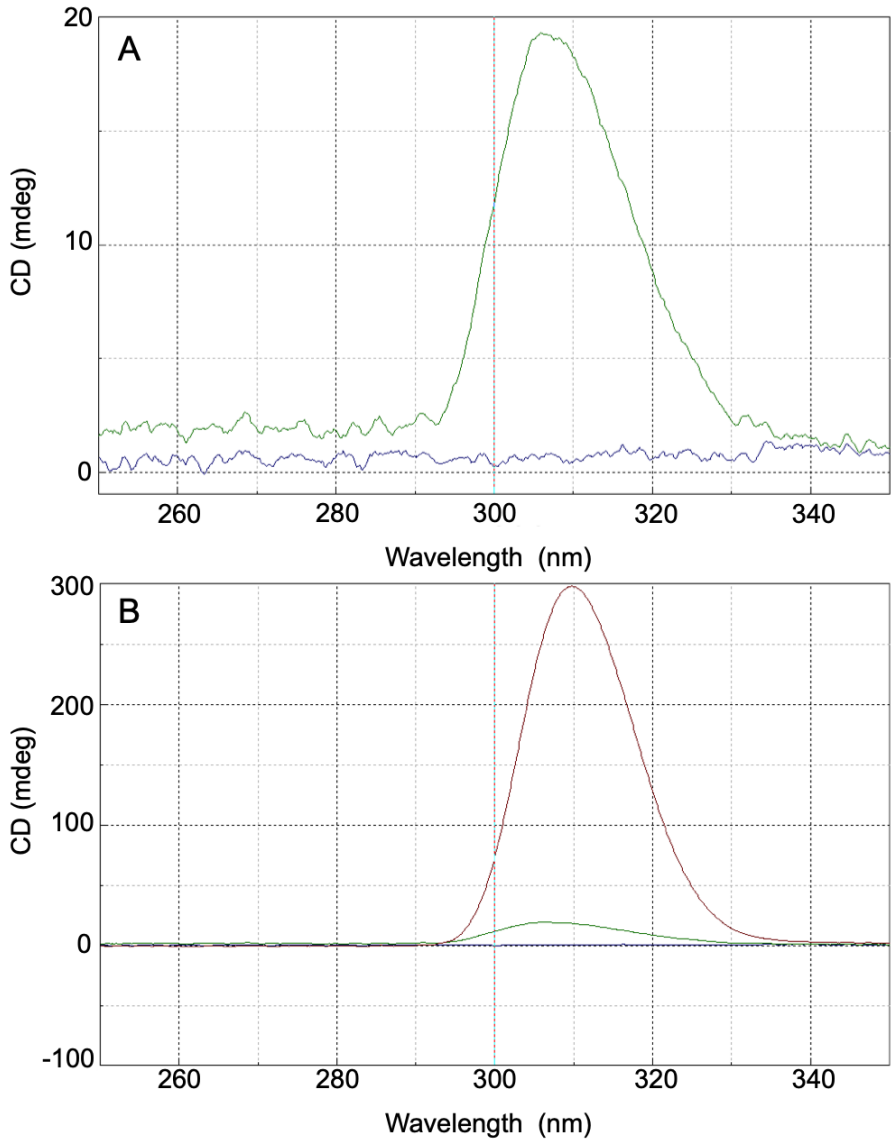

Figure 3.5: CD scan overlays of A) *Kp*ALS reacted with 25 mM α-ketobutyrate after 5 minutes (blue) and 16 hours (green), and B) overlay of A with CD scan of reaction of *Kp*ALS with 25 mM pyruvate after 5 minutes (red).

Figure 3.5 shows that *Kp*ALS is not able to form a chiral product from two molecules of α-ketobutyrate in any significant amount, even after long incubation periods. However, this does not rule out the possibility that the enzyme can form acetohydroxybutyrate, simply that it cannot form significant amounts of propiohydroxybutyrate.

To gain insight on the lack of carboligation activity, experiments were performed to determine if *Kp*ALS could decarboxylate α-ketobutyrate. In this scenario, the reaction would see the conversion of αKB to propionaldehyde. If decarboxylation is observed, it would confirm that

the substrate can bind in the active site as a donor substrate positioned for attack by ThDP. This was certainly not an unreasonable experiment, particularly as *Bs*ALS was shown to be a fairly effective decarboxylase of α-ketoisovalerate, a similar substrate (13). Using the coupled decarboxylase assay (section 2.4.3), no evidence was observed for decarboxylation of α-ketobutyrate. Unfortunately, these results are not conclusive as similar results were obtained when the same experiment was performed to test for *Kp*ALS-catalyzed decarboxylation of pyruvate, a compound known to bind as a donor substrate.

3.3 Product distribution analysis of *Kp*ALS and *Kp*AHAS

3.3.1 Establishment of method for simultaneous product analysis

To determine whether *Kp*ALS and *Kp*AHAS prefer to form acetolactate or acetohydroxybutyrate, the products must be analyzed simultaneously. To do this, a modified form of the gas chromatography based method reported by Gollop *et al.* (24) was designed and implemented. The procedure for this analysis, described in detail in Chapter 2, was carried out in four basic steps:

1) Enzymatic reactions were performed in the presence of both pyruvate and α-ketobutyrate under steady-state conditions.
2) The acetohydroxyacid products were then heated in the presence of catalytic amounts of iron (II) sulfate and iron (III) chloride to form diketones in an oxidative decarboxylation reaction.
3) The volatile diketones were then extracted from the aqueous reaction mixture and captured in methanol using an air distillation apparatus (Figure 3.6).
4) The methanol solution containing the diketone analytes was then injected into a GC-MS equipped with a VF-23 column for separation and analysis.

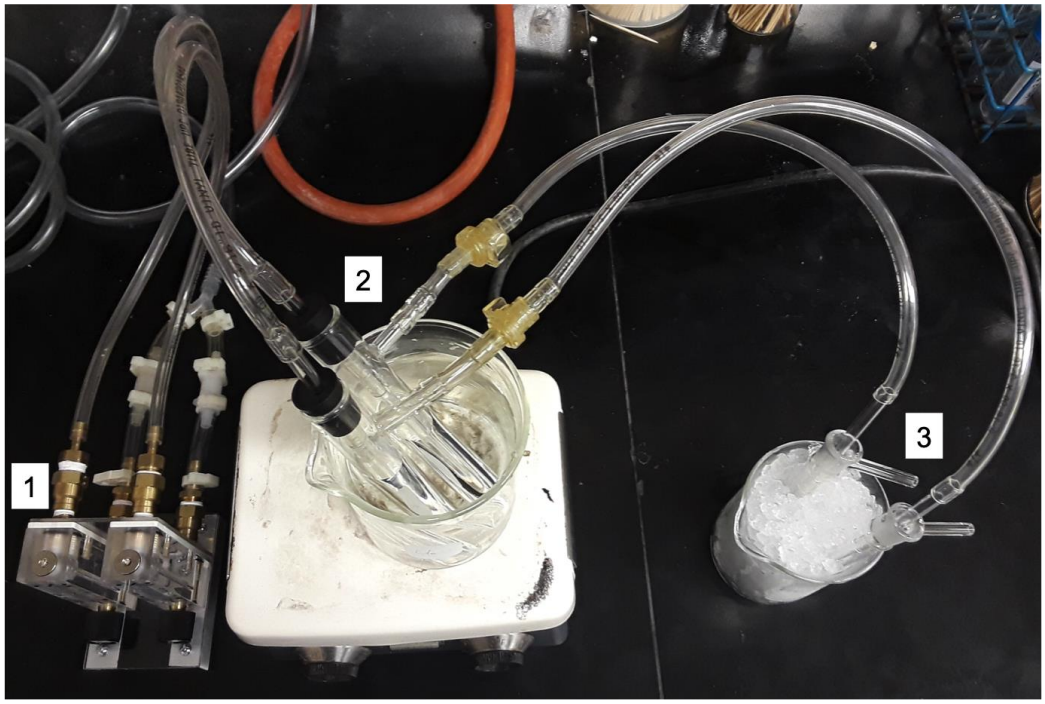

Figure 3.6: Air distillation apparatus. Metered air (~100 mL/min) from the flow valves [1] is passed through the aqueous sample in the large side-arm test tubes [2] held at 60 °C. The air, now containing the volatile diketones, then continues to the collection tubes [3] containing ice-cold methanol.

The first step in establishing the method was to optimize the separation of the diketones by GC. A standard solution was prepared containing 2,3-butanedione, 2,3-pentanedione, 3,4-hexanedione, and acetoin in methanol. 3,4-Hexanedione was added to the standards as it is the diketone product following oxidative decarboxylation of propiohydroxybutyrate (Figure 3.1), and also to ensure it was resolved from the other compounds so any formation would not interfere with peak identification and integration. Finally, acetoin was included as an internal standard.

Using this standard solution, injection volume, split ratio, and column oven temperatures were optimized to provide excellent separation in a short time frame. Mass spectrometric detection was used to identify and quantify compounds as they were eluted. Overall, an efficient separation was achieved with a total run time of 5.4 minutes. Retention times for 2,3-butanedione, 2,3-pentanedione, 3,4-hexanedione, and acetoin were found to be 2.7 minutes, 3.4 minutes, 4.0 minutes, and 4.8 minutes, respectively (Figure 3.7).

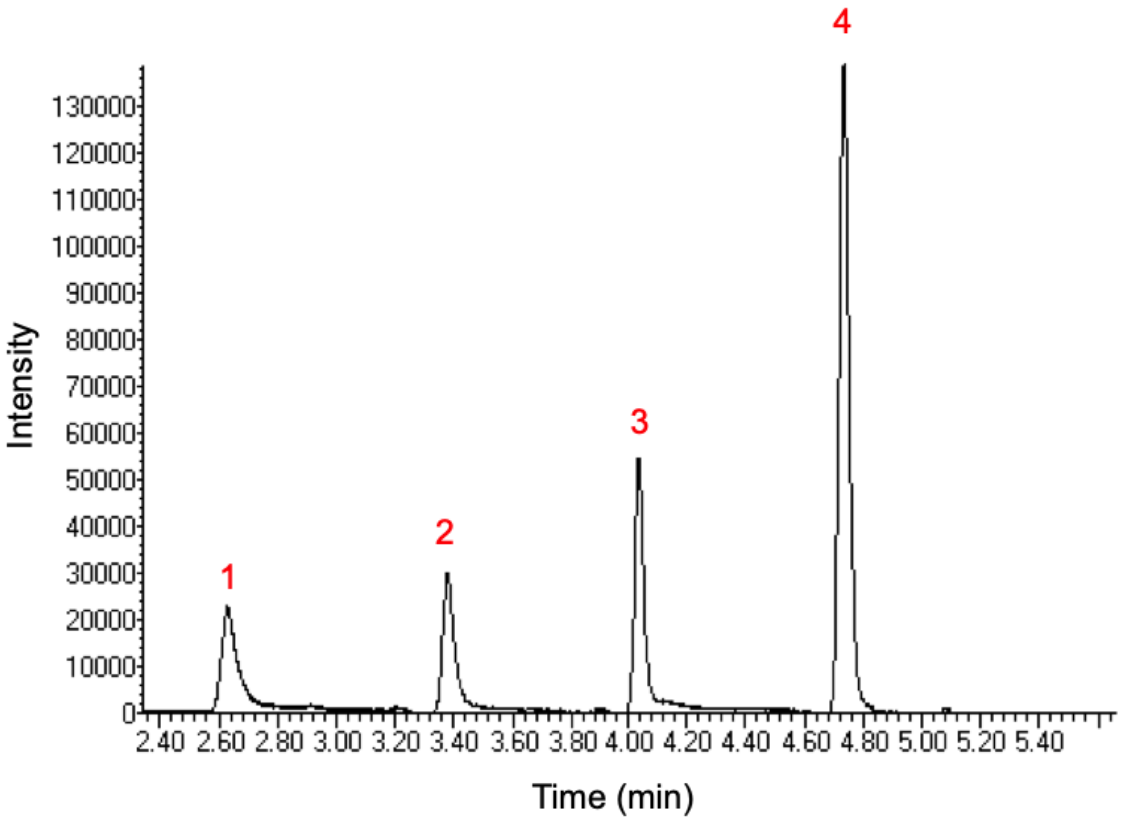

Figure 3.7: Chromatogram of GC separation. Elution order: 1) 2,3-butanedione, 2) 2,3-pentanedione, 3) 3,4-hexanedione, and 4) acetoin.

Following optimization of the procedure, standards were prepared to contain 250 µM, 500 µM, 750 µM, and 1000 µM of each 2,3-butanedione and 2,3-pentanedione in methanol. Acetoin was also added to each standard to a final concentration of 1000 µM. The standards were analyzed, and the resulting peaks were integrated. Normalized peak areas were used to create calibration curves for the diketone analytes (Figure 3.8).

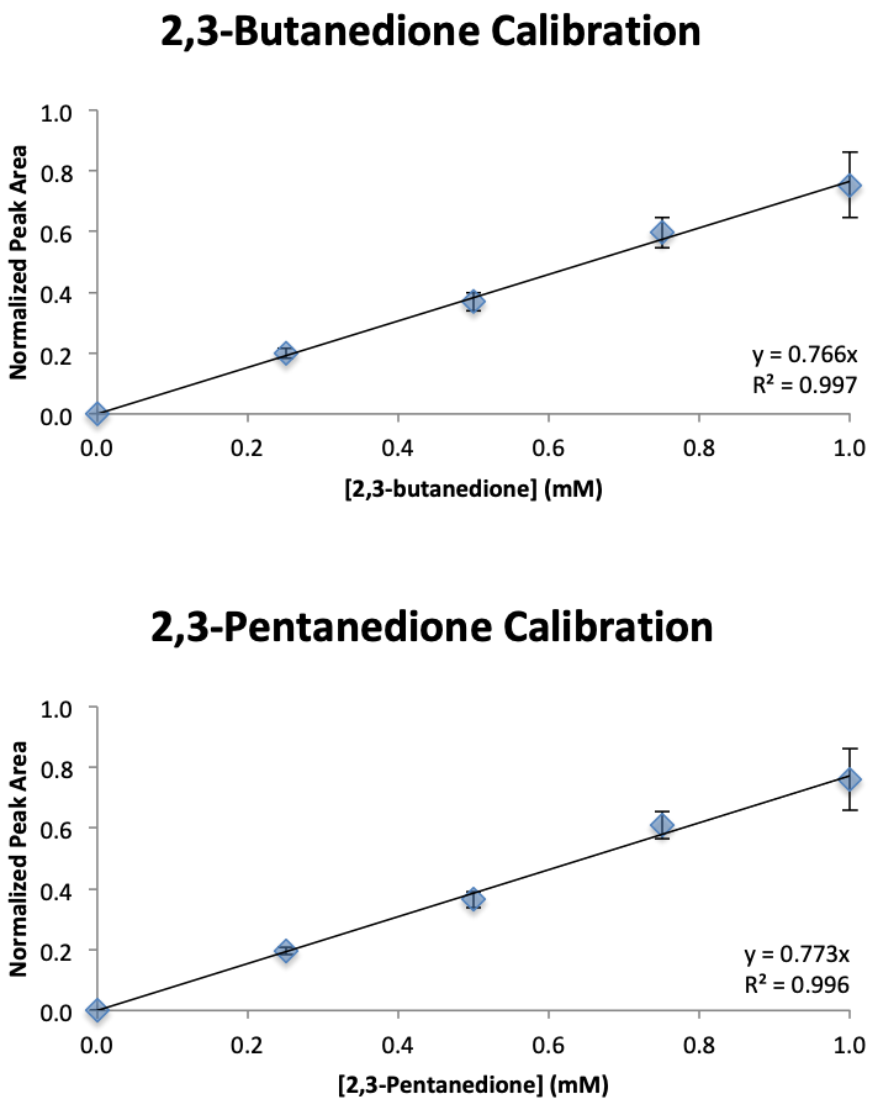

Figure 3.8: Calibration curves for 2,3-butanedione and 2,3-pentanedione.

Normalization was achieved by division of integrated peak areas corresponding to butanedione and pentanedione by the peak area of acetoin. This served to correct for errors in injection volume as well as for errors in methanol capture volume introduced by pipetting errors or evaporation during the extraction step. Signal response was found to be linear over the range tested, and the sensitivity for both butanedione and pentanedione was found to be effectively identical.

Following construction of the calibration curves, the efficiency of the air exchange step was determined. This was achieved by performing the air distillation step on aqueous diketone

standards and then analyzing the extracted samples. Extraction of diketone analytes was found to be fairly linear over the range tested (Figure 3.9), and the extraction efficiency was found to be the almost identical for both 2,3-butanedione and 2,3-pentanedione at ~80 ± 5%.

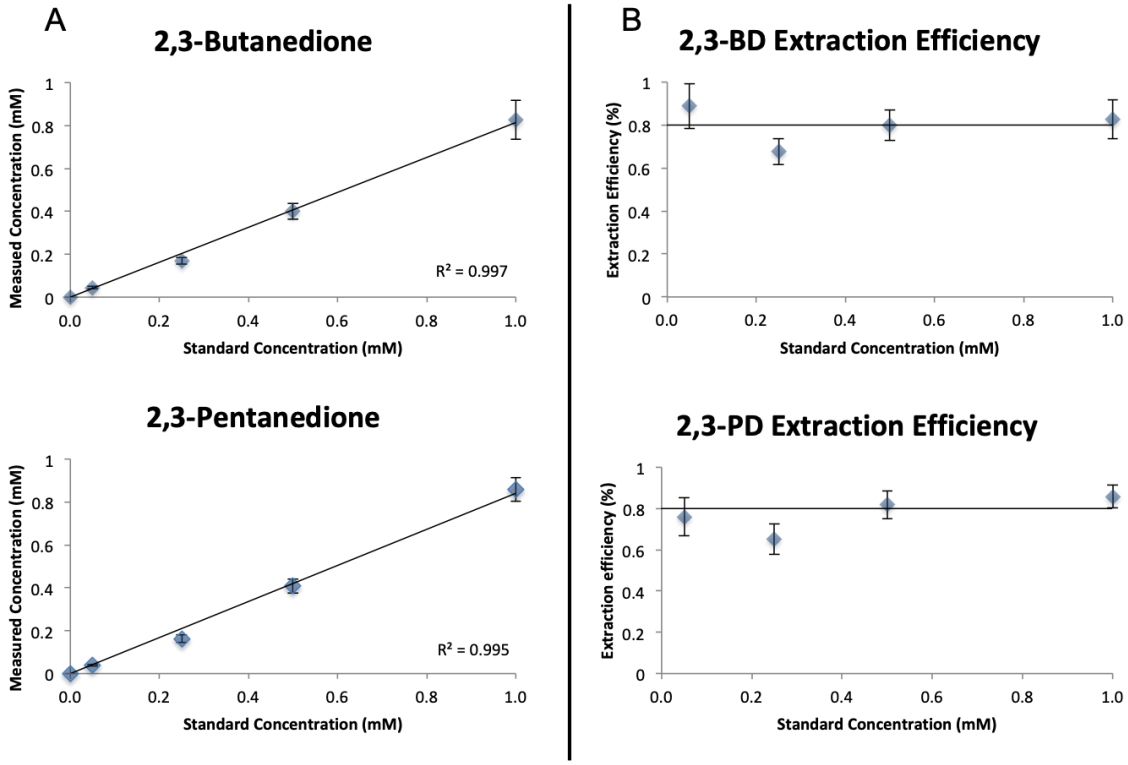

Figure 3.9: Fit of extraction normalized peak areas following extraction. A) shows the concentration calculated after each extraction plotted against the concentration of the standards before extraction. B) shows the extraction efficiency of each standard. Lines are drawn at a constant extraction efficiency of 80%.

3.3.2 Specificity ratio of *Kp*AHAS

The specificity ratio of ALS and AHAS enzymes is a measure of the preference for using either pyruvate or α-ketobutyrate as the acceptor substrate. As defined, a value greater than 1 represents a preference for α-ketobutyrate, while a value less than 1 represents a preference for pyruvate. The ratio (R, Equation 3.1) was defined by Gollop *et al.* (25) as the ratio of the rates formation of acetohydroxybutyrate (AHB) to acetolactate (AL) divided by the ratio of the initial concentrations of α-ketobutyrate (αKB) to pyruvate (Pyr).

Equation 3.1: $$R = \frac{V_{AHB}/V_{AL}}{[\alpha KB]/[Pyr]}$$

To examine the acceptor preference in *Kp*AHAS, reactions were performed under initial rate conditions in 100 mM phosphate buffer at pH 8.0 in the presence of both pyruvate and α-ketobutyrate. Pyruvate concentration was held constant at 10 mM while the concentration of α-ketobutyrate was varied from 100 μM to 1000 μM. Each reaction was run for 5 minutes before quenching with phosphoric acid.

Following extraction, GC-MS chromatograms were obtained for each sample. Each chromatogram contained three peaks. By comparison of the retention times with the standards and inspection of the fragmentation data from the mass spectrometer, the peaks were identified as 2,3-butanedione, 2,3-pentanedione, and acetoin, as expected (Figure 3.10). It was immediately noticeable that the peak corresponding to 2,3-pentanedione was much larger than that for 2,3-butanedione. This indicated that *Kp*AHAS formed much more acetohydroxybutyrate than acetolactate. Interestingly, no evidence of 3,4-hexanedione was obtained in any of the reactions, regardless of the concentration of α-ketobutyrate.

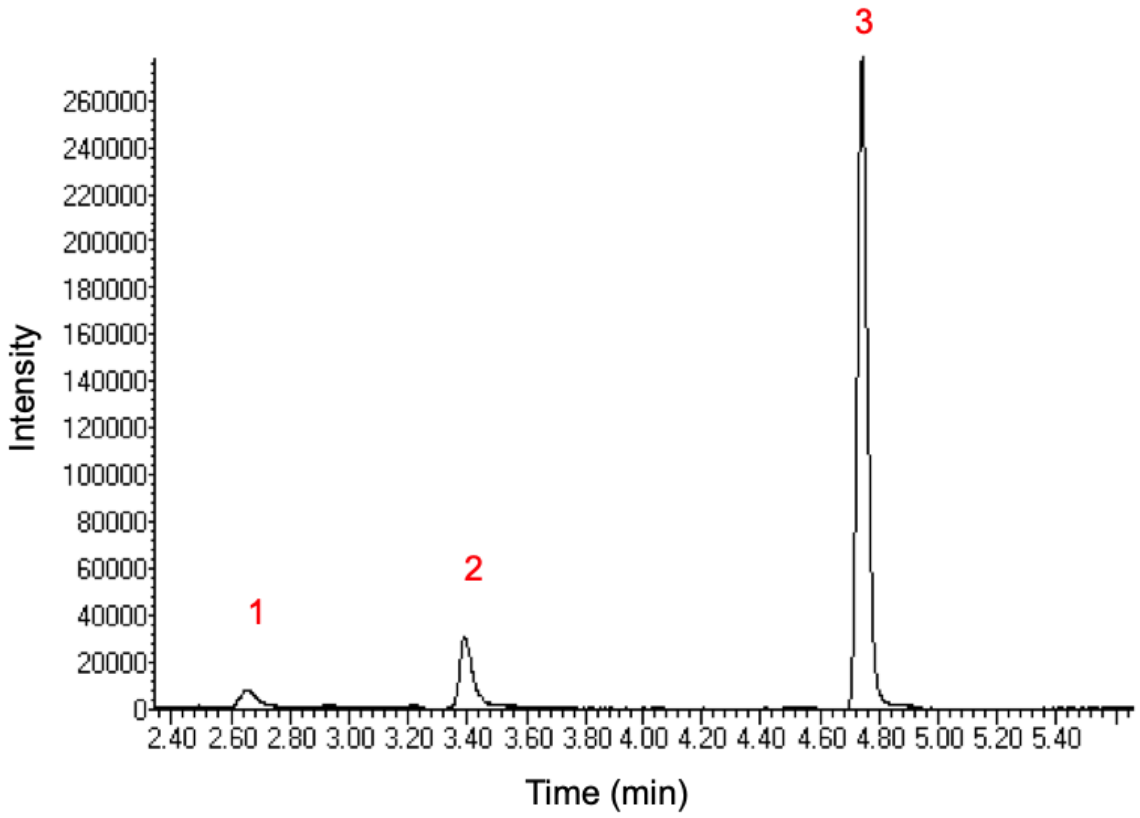

Figure 3.10: Typical chromatogram obtained following diketone extraction from reactions catalyzed by *Kp*AHAS. Labeled peaks: 1) 2,3-butanedione, 2) 2,3-pentanedione, and 3) acetoin.

When the ratios of the rates of product formation are plotted against the ratio of the initial substrate concentrations, the slope of the linear fit is the specificity ratio (Figure 3.11). The specificity ratio was found to be close to 70, indicating that *Kp*AHAS, as with most AHASs studied to date (26), shows a strong preference for α-ketobutyrate as the acceptor substrate.

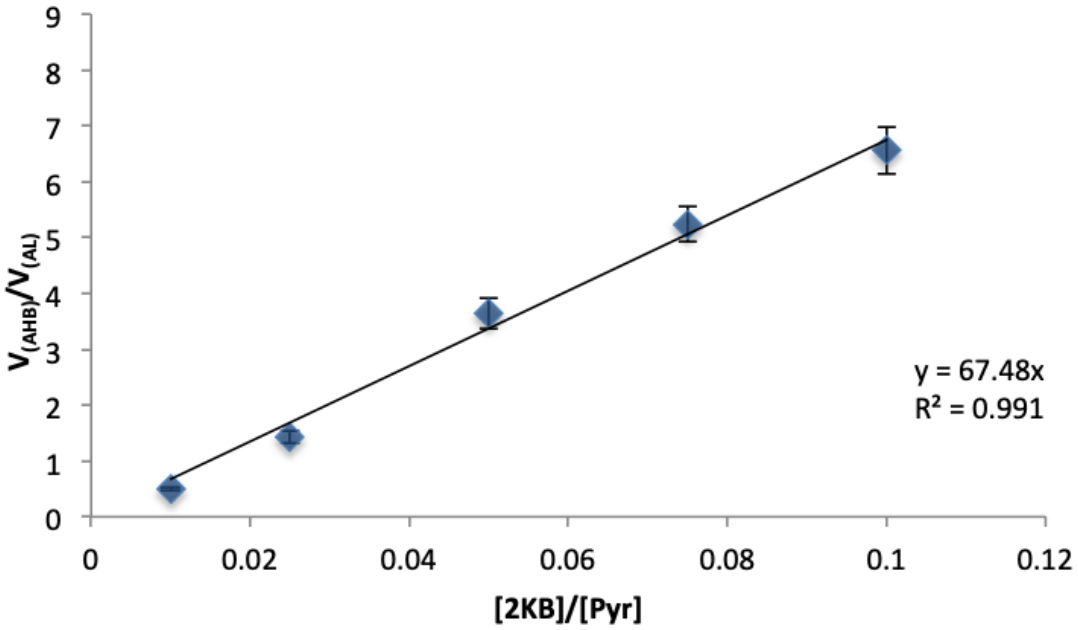

Figure 3.11: Fit of product ratios to determine the specificity ratio for *Kp*AHAS.

The ability to separate the formation of acetohydroxybutyrate and acetolactate makes it possible to calculate the steady-state parameters for the formation of acetohydroxybutyrate. Fitting of the initial rate data showed that formation of acetohydroxybutyrate followed Michaelis-Menten kinetics (Figure 3.12).

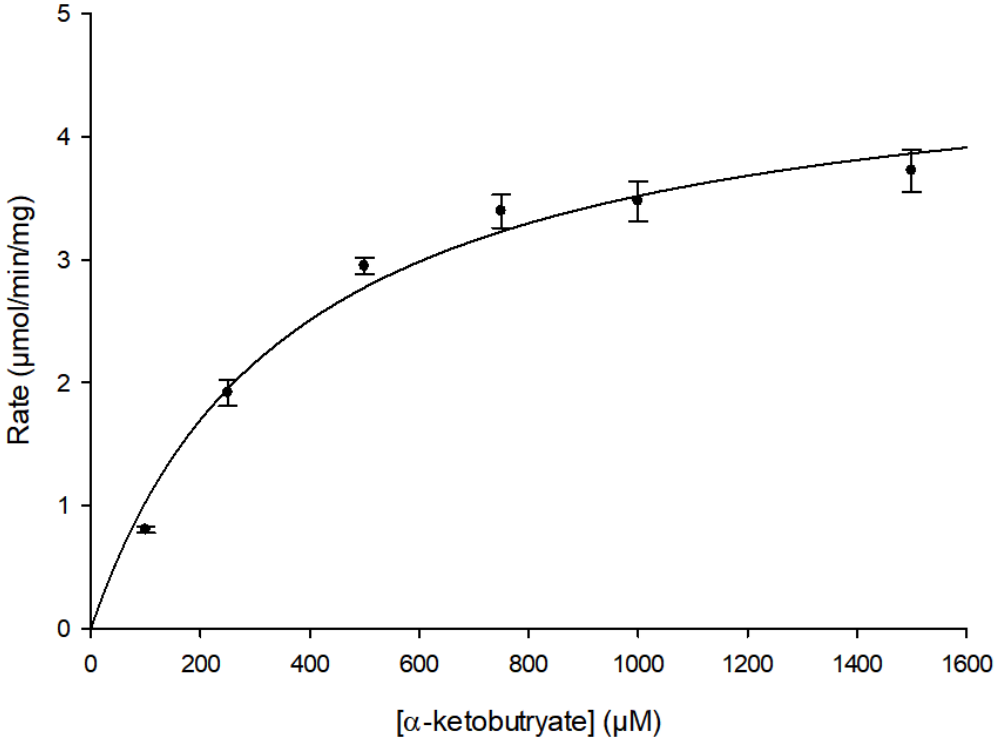

Figure 3.12: Michaelis-Menten plot for formation of acetohydroxybutyrate by *Kp*AHAS.

Table 3.6: Kinetic parameters for formation of varied products in *Kp*AHAS in phosphate buffer at pH 8.0. The assay method is in parenthesis.

Product	k_{cat} (s^{-1})	K_m (mM)	k_{cat}/K_m ($mM^{-1} \bullet s^{-1}$)
Acetolactate (CD)	7.5 ± 0.4	3.8 ± 0.4	2
Acetohydroxybutyrate (GC-MS)	5.8 ± 0.3	0.37 ± 0.05	16
Propiohydroxybutyrate (CD)	2.4 ± 0.1	14 ± 1	0.2

The value obtained for k_{cat} was found to be similar, though slightly lower than, the k_{cat} obtained from monitoring acetolactate formation via CD (Table 3.6). The slightly lower value of k_{cat} is not unexpected as the higher k_{cat} obtained for acetolactate formation was obtained with only pyruvate present in the reaction mixture. The slow formation of acetolactate likely contributes, at least in part, to the slightly reduced k_{cat} value. Even at semi-saturating conditions of α-ketobutyrate, there was still some measurable formation of acetolactate.

As both AHAS and ALS are able to condense two identical molecules to form product, it is difficult to decipher whether the K_m value calculated when monitoring acetolactate or propiohydroxybutyrate is for that of the donor or acceptor site. However, K_m values for α-ketobutyrate as both a donor and acceptor can be estimated by comparison with the data obtained from GC-MS analysis.

The K_m value for α-ketobutyrate obtained by monitoring acetohydroxybutyrate formation was determined to be 0.37 mM. This is at least 10-fold lower than that calculated by following either acetolactate or propiohydroxybutyrate formation. As acetohydroxybutyrate is formed when the enzyme uses pyruvate as the donor and α-ketobutyrate as the acceptor, the K_m value obtained for α-ketobutyrate must be for it acting as an acceptor.

Given that the K_m value obtained from monitoring formation of propiohydroxybutyrate by CD in is ~40-fold higher than that for acetohydroxybutyrate formation, the K_m value for formation of propiohydroxybutyrate must be for α-ketobutyrate acting as the donor substrate.

While this analysis is quite reasonable, there is one caveat that must be considered: the assumption that the binding of the donor substrate, whether it is pyruvate or α-ketobutyrate, does not significantly impact the ability of either substrate to act as an acceptor. If it were to be shown that binding of one substrate over another as a donor influenced binding of the acceptor, then the analysis would need to be revisited. However, inspection of the active site in a *Kp*AHAS homology model shows that it is possible for α-ketobutyrate to bind without any major arrangement of active site architecture (Figure 3.13).

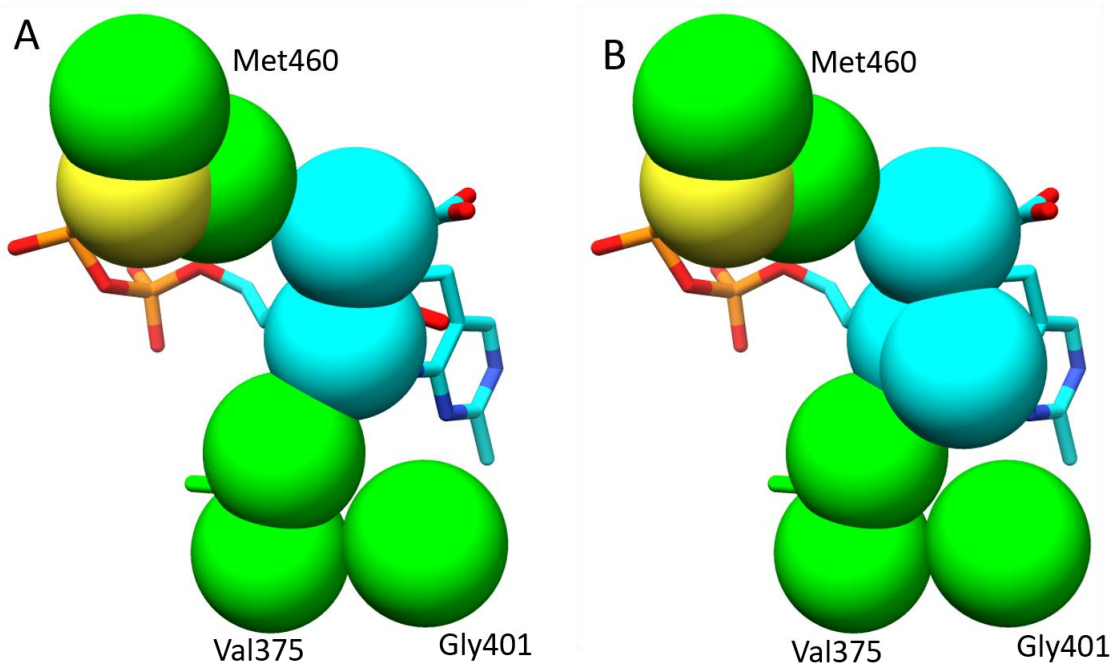

Figure 3.13: Active site of *Kp*AHAS with A) pyruvate as a donor substrate, and B) α-ketobutyrate as a donor substrate. Van der Waals radii for the spheres were calculated using standard options in UCSF Chimera based on radii reported by Tsai *et al.* (34).

A model of *Kp*AHAS was generated using the Phyre2 web portal (35) with AHAS from yeast (PDB ID: 1T9B) as a template. This model was then aligned with a crystal structure of *Kp*ALS that contained a trapped ALThDP intermediate. Using the model building tool it was possible to add an extra methyl group to mimic the space required for binding of α-ketobutyrate as a donor substrate. All structure alignments, manipulations, and visualizations were performed using UCSF Chimera (36). Some slight clashing is observed with Val375, though it is independent of whether the donor is pyruvate or α-ketobutyrate. Likely this is due to the model being generated in the absence of the ALThDP intermediate.

3.3.3 Specificity ratio of *Kp*ALS

The specificity ratio of *Kp*ALS was also investigated. Reactions were carried out under initial rate conditions using a mixture of 10 mM pyruvate in the presence of 10, 15, 20, and 25 mM α-ketobutyrate. After 5 minutes, the reactions were quenched, products were converted into diketones, and the diketones were extracted to methanol before injection into the GC-MS.

The resulting chromatograms (Figure 3.14) showed that the specificity of *Kp*ALS was the opposite of that observed for *Kp*AHAS in that *Kp*ALS formed more acetolactate than acetohydroxybutyrate. Reaction rates were calculated from the normalized peak areas and the data were fit to equation 3.1 to determine the specificity ratio (Figure 3.15). The ratio was found to be 0.08 indicating that *Kp*ALS shows a ~10-fold preference for pyruvate as an acceptor substrate.

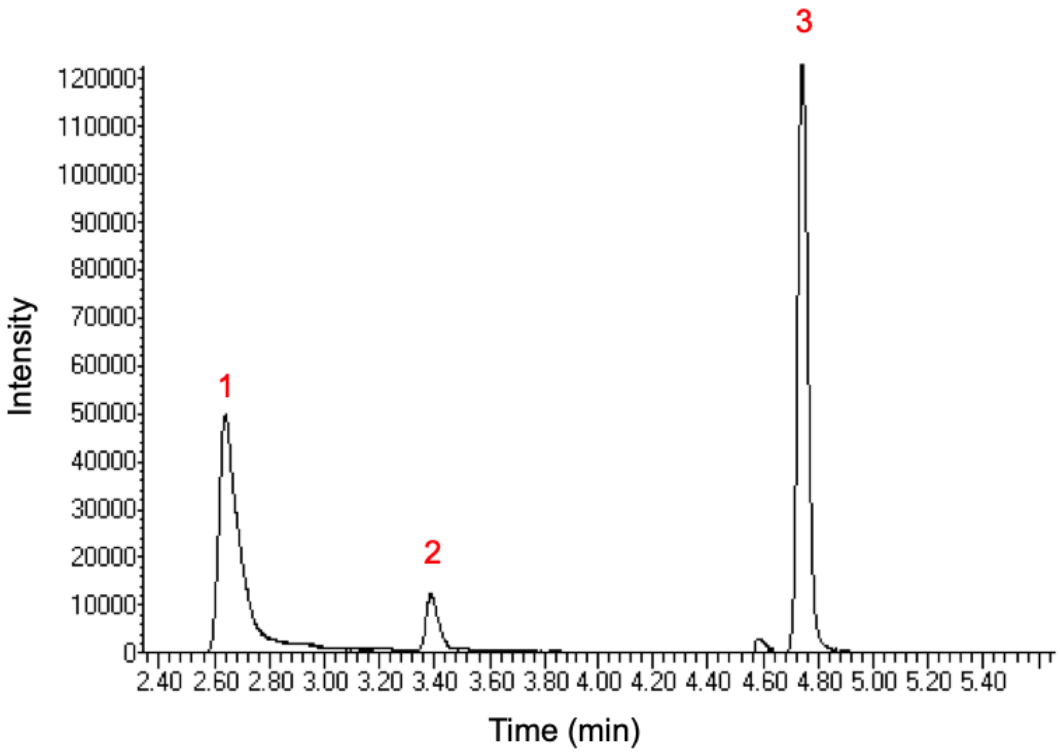

Figure 3.14: Typical chromatogram obtained following diketone extraction from reactions catalyzed by *Kp*ALS. Labeled peaks: 1) 2,3-butanedione, 2) 2,3-pentanedione, and 3) acetoin.

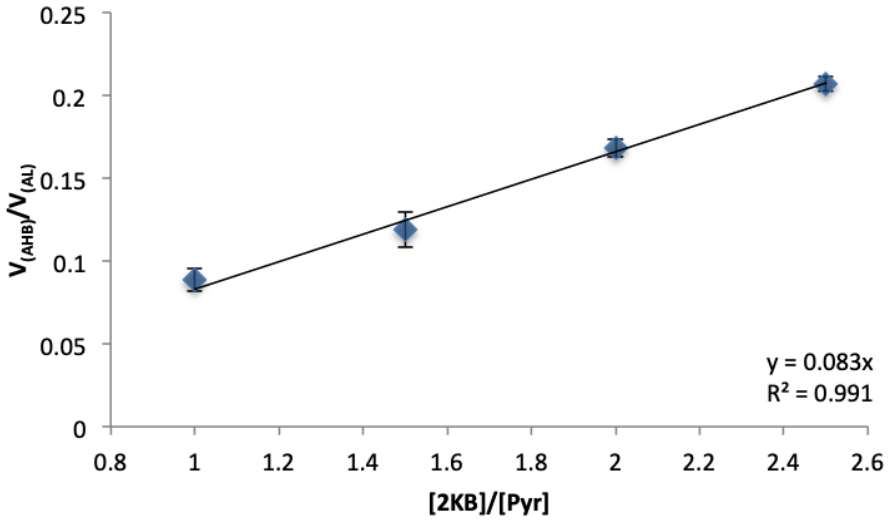

Figure 3.15: Fit of product ratios to determine the specificity ratio for *Kp*ALS.

That being said, while the specificity ratio calculated for *Kp*ALS shows a 10-fold preference for pyruvate as an acceptor, the amount of acetohydroxybutyrate formed in the reactions was not insignificant. This is particularly significant as more acetohydroxybutyrate was formed in the five-minute reactions than propiohydroxybutyrate when α-ketobutyrate was used as a sole substrate over 16 hours. Overall, this indicates that *Kp*ALS is more specific for pyruvate as a donor than it is for pyruvate as an acceptor.

A possible explanation for the lack of propiohydroxybutyrate formation is found by comparing the active site of *Kp*ALS with that of the *Kp*AHAS homology model. In the former, Gln420 occupies the position of Gly401 in the AHAS model. When α-ketobutyrate rather than pyruvate is used as the donor, Gln420 shows strong steric clashes with the extra methyl group. This provides a plausible rationale as to why *Kp*ALS is not able to form any significant amount of propiohydroxybutyrate, *i.e.*, α-ketobutyrate simply cannot fit in the donor site without significant rearrangement of the active site residues (Figure 3.16).

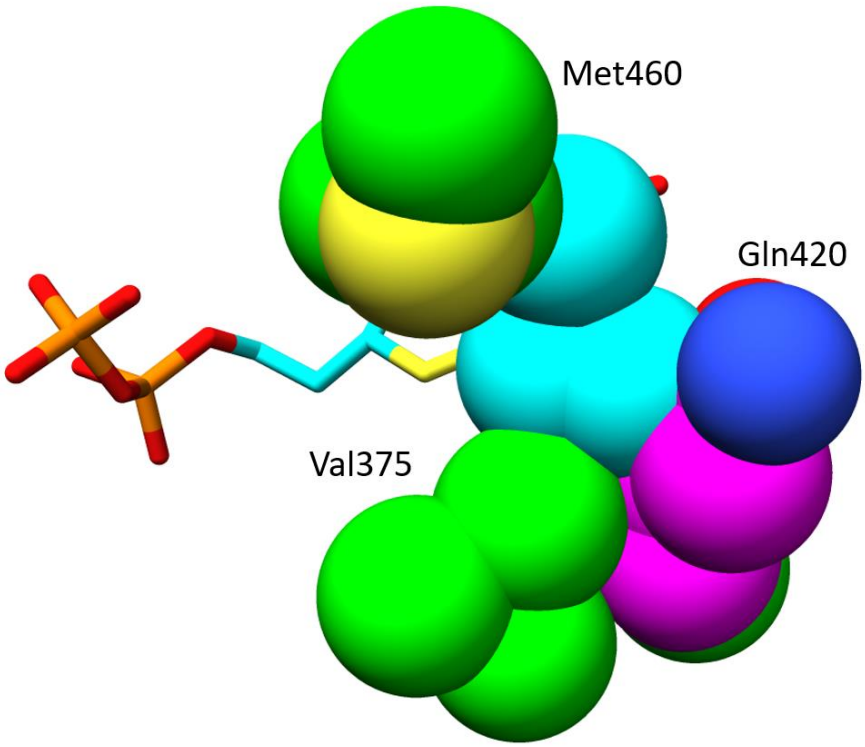

Figure 3.16: Depiction of clash of Gln420 (pink) with α-ketobutyrate (blue) as a donor substrate.

3.4 Summary and conclusions

The work presented in this chapter describes the comparison of the properties of two enzymes, ALS and AHAS, from the same organism that catalyze the same carboligation reaction. The products of that reaction, (*S*)-acetolactate and (*S*)-acetohydroxybutyrate are formed by the condensation of two molecules of pyruvate, or one molecule of pyruvate and one molecule of α-ketobutyrate, respectively. The steady-state kinetics of the two enzymes were studied using three different methods: i) the Westerfeld method (21), ii) the CD method (28), and iii) product conversion to diketones and separation by GC-MS (24). The first two methods were non-specific for acetolactate and acetohydroxybutyrate, while the third method allowed for separation and analysis when the two products are formed simultaneously.

Steady-state analysis monitoring the formation of acetolactate showed that the kinetic parameters of *Kp*ALS were buffer dependent with activation by acetate and inhibition by phosphate being observed. Additionally, the enzyme showed Michaelis-Menten kinetics in acetate

and MES buffers while sigmoidal kinetics were observed in phosphate. This buffer dependence was not observed for *Kp*AHAS.

Both enzymes were shown to be susceptible to inhibition by β-fluoropyruvate, a pyruvate analogue, and the mode of inhibition was found to be similar for both enzymes. β-fluoropyruvate showed a mixed type inhibition for *Kp*ALS, and the K_i values obtained indicated that the inhibitor binds more tightly in the donor site than the acceptor site. Noncompetitive inhibition was observed for *Kp*AHAS with a K_i value slightly higher than that for inhibition of *Kp*ALS. The noncompetitive nature of the inhibition indicates that the compound binds equally to both the donor and acceptor sites.

Finally, the substrate specificities of *Kp*ALS and *Kp*AHAS were investigated. Initially, the enzymes were tested for their ability to condense two molecules of α-ketobutyrate to form propiohydroxybutyrate. *Kp*AHAS was shown to be able to form significant amounts of propiohydroxybutyrate, although the efficiency of this conversion was lower than that for acetolactate formation. Conversely, *Kp*ALS was only able to form miniscule amounts of this product, even after incubation for 16 hours.

*Kp*AHAS was found to form more acetohydroxybutyrate than acetolactate in a given reaction even when the pyruvate concentration was almost 100-fold higher than the α-ketobutyrate concentration. An explanation for this observation came when it was determined that *Kp*AHAS has a ~70-fold preference for α-ketobutyrate as the acceptor substrate.

Highlighting the difference between the enzymes, *Kp*ALS showed the opposite pattern with a ~10-fold preference for pyruvate as the acceptor substrate. On the surface this may not seem to be a particularly strong preference until it is realized that the cellular concentration of pyruvate is ~100-fold higher than that of α-ketobutyrate (25,37,38). Given those levels, it is apparent that *Kp*ALS is not likely to catalyze the formation of any significant amount of acetohydroxybutyrate *in vivo*.

References

1. Strassman, M., Thomas, A. J., and Weinhouse, S. (1955) The biosynthesis of valine. *J. Am. Chem. Soc.* **77**, 1261-1265
2. Halpern, Y. S., and Umbarger, H. E. (1959) Evidence for two distinct enzyme systems forming acetolactate in *Aerobacter aerogenes*. *J. Biol. Chem.* **234**, 3067-3071
3. Umbarger, H. E., and Brown, B. (1958) Isoleucine and valine metabolism in *Escherichia coli* : VIII. The formation of acetolactate. *J. Biol. Chem.* **233**, 1156-1160
4. Leavitt, R. I., and Umbarger, H. E. (1961) Isoleucine and valine metabolism in *Escherichia coli*. X. The enzymatic formation of acetohydroxybutyrate. *J. Biol. Chem.* **236**, 2486-2491
5. Størmer, F. C., and Umbarger, H. E. (1964) The requirement for flavine adenine dinucleotide in the formation of acetolactate by *Salmonella typhimurium* extracts. *Biochem. Biophys. Res. Commun.* **17**, 587-592
6. Störmer, F. C. (1967) Isolation of crystalline pH 6 acetolactate-forming enzyme from *Aerobacter aerogenes*. *J. Biol. Chem.* **242**, 1756-1759
7. Störmer, F. C. (1968) The pH 6 acetolactate-forming enzyme from *Aerobacter aerogenes*. I. Kinetic studies. *J. Biol. Chem.* **243**, 3735-3739
8. Störmer, F. C. (1968) The pH 6 acetolactate-forming enzyme from *Aerobacter aerogenes*. II. Evidence that it is not a flavoprotein. *J. Biol. Chem.* **243**, 3740-3741
9. Pang, S. S., Duggleby, R. G., Schowen, R. L., and Guddat, L. W. (2004) The crystal structures of *Klebsiella pneumoniae* acetolactate synthase with enzyme-bound cofactor and with an unusual intermediate. *J. Biol. Chem.* **279**, 2242-2253
10. Duggleby, R. G., and Pang, S. S. (2000) Acetohydroxyacid Synthase. *J. Biochem. Mol. Biol.* **33**, 1-36
11. Umbarger, H. E. (1978) Amino acid biosynthesis and its regulation. *Annu. Rev. Biochem.* **47**, 533-606
12. Holtzclaw, W. D., and Chapman, L. F. (1975) Degradative acetolactate synthase of *Bacillus subtilis*: purification and properties. *J. Bacteriol.* **121**, 917-922
13. Sommer, B., von Moeller, H., Haack, M., Qoura, F., Langner, C., Bourenkov, G., Garbe, D., Loll, B., and Bruck, T. (2015) Detailed structure-function correlations of *Bacillus subtilis* acetolactate synthase. *ChemBioChem* **16**, 110-118

14. Yang, J. H., and Kim, S. S. (1993) Purification and characterization of the valine sensitive acetolactate synthase from *Serratia marcescens* ATCC 25419. *Biochem. Biophys. Acta* **1157**, 178-184

15. Kaushal, A., Pabbi, S., and Sharma, P. (2003) Characterization of 2,3-butanediol-forming and valine-sensitive α-acetolactate synthase of *Enterobacter cloacae*. *World J. Microb. Biot.* **19**, 487-493

16. Pang, S. S., Guddat, L. W., and Duggleby, R. G. (2002) Crystallization of the FAD-independent acetolactate synthase of *Klebsiella pneumoniae*. *Acta Crystallogr. D Biol. Crystallogr.* **58**, 1237-1239

17. De Felice, M., Guardiola, J., Malorni, M. C., Klopotowski, T., and Iaccarino, M. (1974) Regulation of the pool size of valine in *Escherichia coli* K-12. *J. Bacteriol.* **120**, 1058-1067

18. Guardiola, J., De Felice, M., and Iaccarino, M. (1974) Mutant of *Escherichia coli* K-12 missing acetolactate synthase activity. *J. Bacteriol.* **120**, 536-538

19. Lawther, R. P., Calhoun, D. H., Gray, J., Adams, C. W., Hauser, C. A., and Hatfield, G. W. (1982) DNA sequence fine-structure analysis of *ilv*G (*Ilv*G+) mutations of *Escherichia coli* K-12. *J. Bacteriol.* **149**, 294-298

20. Chang, A. K., and Duggleby, R. G. (1997) Expression, purification and characterization of Arabidopsis thaliana acetohydroxyacid synthase. *Biochem. J.* **327 (Pt 1)**, 161-169

21. Westerfeld, W. W. (1945) A colorimetric determination of blood acetoin. *J. Biol. Chem.* **161**, 495-502

22. Juni, E. (1952) Mechanisms of formation of acetoin by bacteria. *J. Biol. Chem.* **195**, 715-726

23. Postel, W., and Meier, B. (1981) Gaschromatographische Bestimmung von 2-Acetolactat, 2-Acetohydroxybutyrat, Diacetyl, 2,3-Pentandion und Acetoin in Traubenmost und Wein. *Zeitschrift für Lebensmittel-Untersuchung und Forschung* **173**, 85-89

24. Gollop, N., Barak, Z. e., and Chipman, D. M. (1987) A method for simultaneous determination of the two possible products of acetohydroxy acid synthase. *Anal. Biochem.* **160**, 323-331

25. Barak, Z., Chipman, D. M., and Gollop, N. (1987) Physiological implications of the specificity of acetohydroxy acid synthase isozymes of enteric bacteria. *J. Bacteriol.* **169**, 3750-3756

26. Gollop, N., Damri, B., Chipman, D. M., and Barak, Z. (1990) Physiological implications of the substrate specificities of acetohydroxy acid synthases from varied organisms. *J. Bacteriol.* **172**, 3444-3449

27. Sylvester, S. R., and Stevens, C. M. (1979) Stereospecificity of the reductoisomerase-catalyzed step in the pathway of biosynthesis of valine and leucine. *Biochemistry* **18**, 4529-4531

28. Vinogradov, M., Kaplun, A., Vyazmensky, M., Engel, S., Golbik, R., Tittmann, K., Uhlemann, K., Meshalkina, L., Barak, Z. e., Hübner, G., and Chipman, D. M. (2005) Monitoring the acetohydroxy acid synthase reaction and related carboligations by circular dichroism spectroscopy. *Anal. Biochem.* **342**, 126-133

29. Gollop, N., Damri, B., Barak, Z., and Chipman, D. M. (1989) Kinetics and mechanism of acetohydroxy acid synthase isozyme III from *Escherichia coli*. *Biochemistry* **28**, 6310-6317

30. Bradford, M. M. (1976) A rapid and sensitive method for the quantitation of microgram quantities of protein utilizing the principle of protein-dye binding. *Anal. Biochem.* **72**, 248-254

31. Gasteiger, E., Hoogland, C., Gattiker, A., Duvaud, S. e., Wilkins, M., Appel, R., and Bairoch, A. (2005) Protein identification and analysis tools on the ExPASy server. in *The Proteomic Protocols Handbook* (Walker, J. M. ed.), Humana Press. pp 571-607

32. Leung, L. S., and Frey, P. A. (1978) Fluoropyruvate: an unusal substrate for *Escherichia coli* pyruvate dehydrogenase. *Biochem. Biophys. Res. Commun.* **81**, 274-279

33. Flournoy, D. S., and Frey, P. A. (1989) Inactivation of the pyruvate dehydrogenase complex of *Escherichia coli* by fluoropyruvate. *Biochemistry* **28**, 9594-9602

34. Tsai, J., Taylor, R., Chothia, C., and Gerstein, M. (1999) The packing density in proteins: standard radii and volumes. *J. Mol. Biol.* **290**, 253-266

35. Kelley, L. A., Mezulis, S., Yates, C. M., Wass, M. N., and Sternberg, M. J. E. (2015) The Phyre2 web portal for protein modeling, prediction and analysis. *Nat. Protoc.* **10**, 845

36. Pettersen, E. F., Goddard, T. D., Huang, C. C., Couch, G. S., Greenblatt, D. M., Meng, E. C., and Ferrin, T. E. (2004) UCSF Chimera - A visualization system for exploratory research and analysis. *J. Comput. Chem.* **25**, 1605-1612

37. Lowry, O. H., Carter, J., Ward, J. B., and Glaser, L. (1971) The Effect of Carbon and Nitrogen Sources on the Level of Metabolic Intermediates in *Escherichia coli*. *J. Biol. Chem.* **246**, 6511-6521

38. Daniel, J., Dondon, L., and Danchin, A. (1983) 2-ketobutyrate: A putative alarmone of *Escherichia coli*. *Mol. Gen. Genet.* **190**, 452-458

CHAPTER 4. STRUCTURAL STUDIES ON ACETOLACTATE SYNTHASE FROM *KLEBSIELLA PNEUMONIAE*

4.1 Introduction

The biosynthesis of 2,3-butanediol from pyruvate in facultative anaerobes is carried out by a cascade of enzymes including acetolactate synthase, acetolactate dehydrogenase, and butanediol dehydrogenase (1). This pathway is of great interest for commercial synthesis projects as 2,3-butanediol is used as a building block in the synthesis of antifreeze agents, extractants, solvents, and biofuels (2). The first enzyme in this pathway, acetolactate synthase (ALS), is of particular interest as acetolactate is readily decarboxylated into either 2,3-butanedione or acetoin, both of which are important aroma compounds in products such as butter and buttermilk (3). Surprisingly, few acetolactate synthase enzymes have been studied throughout the years. The few that have include those from *Aerobacter aerogenes* (4-6), *Enterobacter cloacae* (7), *Bacillus subtilis* (2,8), and *Klebsiella pneumoniae* (9). Only two of these enzymes, those from *B. subtilis* and *K. pneumoniae*, have been studied using X-ray crystallography. Despite their similarity in function, the two enzymes were shown to cluster in different phylogenetic groups (8), and the structural studies showed many distinctions between them. Given these differences it appears that there is still much to learn about the correlation between structure and function of the ALS family of enzymes.

4.1.1 Structural studies on ALS enzymes

It is notable that the protein data bank contains many structures of acetohydroxyacid synthase (AHAS). These arise from a diverse set of organisms including plants (*Arabidopsis thaliana* (10-13)), fungi (*Saccharomyces cerevisiae* (12-16) and *Candida albicans* (17)), and bacteria (*E. coli* (18,19)). By contrast, ALS is quite rare in plants and fungi, so it is not surprising that the structures that have been solved are those of bacterial enzymes.

In spite of the paucity of structures, several of those that are available are of ALS in complex with trapped reaction intermediates. In the *B. subtilis* (*Bs*ALS) structure, a trapped lactylThDP (LThDP) intermediate was observed, while a hydroxyethylThDP (HEThDP) intermediate was observed in the *K. pneumoniae* (*Kp*ALS) structures (8,9).

When considering the accepted reaction mechanism of ALS, discussed in Chapter 1 (Figure 1.14), the observation of LThDP in *Bs*ALS is not unexpected as it is the intermediate formed following attack by the ThDP ylid on the first (donor) pyruvate substrate. Further, accumulation of enough of this intermediate to be observed in a X-ray structure indicates that the rate-limiting step in the reaction may be decarboxylation. That said, while this may be true in the crystal, this doesn't necessarily indicate that it is the rate-limiting step for *Bs*ALS in solution.

The HEThDP intermediate observed in *Kp*ALS is particularly interesting. This intermediate was somewhat unexpected, as it would more likely to be observed in a simple decarboxylation reaction since its observation requires the carbanion/enamine intermediate to be protonated instead of attacking a second (acceptor) substrate (Figure 4.1). This protonation is more akin to the reaction catalyzed by pyruvate decarboxylase, which yields acetaldehyde (20), than the carboligation reaction catalyzed by ALS, which yields acetolactate.

In order to observe these intermediates, crystals of the *Bs*ALS and *Kp*ALS were soaked with pyruvate. The unexpected observation of an apparent off-pathway HEThDP intermediate in *Kp*ALS, rather than the on-pathway LThDP intermediate in *Bs*ALS, is likely explained by design of the soaking experiments. *Kp*ALS crystals were soaked in pyruvate for a week, whereas the *Bs*ALS crystals were soaked for only 3 seconds before being flash frozen. Given these experimental differences, the observation of different intermediates seems quite reasonable. Presumably, the substrate concentration remained high in the *Bs*ALS crystals due to the short soaking period, while the long soaking period for *Kp*ALS allowed for significant depletion of pyruvate from the soaking solution.

As the decarboxylation step is irreversible, it is likely that any equilibrium established between pyruvate and acetolactate would lie heavily toward the formation of acetolactate. However, this does not preclude the possibility of back reaction of acetolactate to any of the post-decarboxylation steps. Such reaction could see the breakdown of acetolactate to one molecule of pyruvate concomitantly with the formation the carbanion/enamine intermediate. Of course most of this will be immediately converted back into acetolactate but, if even a small amount of pyruvate escaped the active site, the reactive carbanion/enamine could be protonated, potentially leading to the formation and release of acetaldehyde. While experiments described in section 3.2.7 indicate that decarboxylation is not observed on the time scale of a routine assay, over the period of a week, the "occasional" decarboxylation reaction could be repeated many times. Ultimately, pyruvate

would be depleted from the soaking solution and an equilibrium would be established between acetolactate and acetaldehyde. At this point, the equilibrium binding of acetaldehyde to the ThDP cofactor is now much more feasible and the observation of the HEThDP intermediate is not so unlikely.

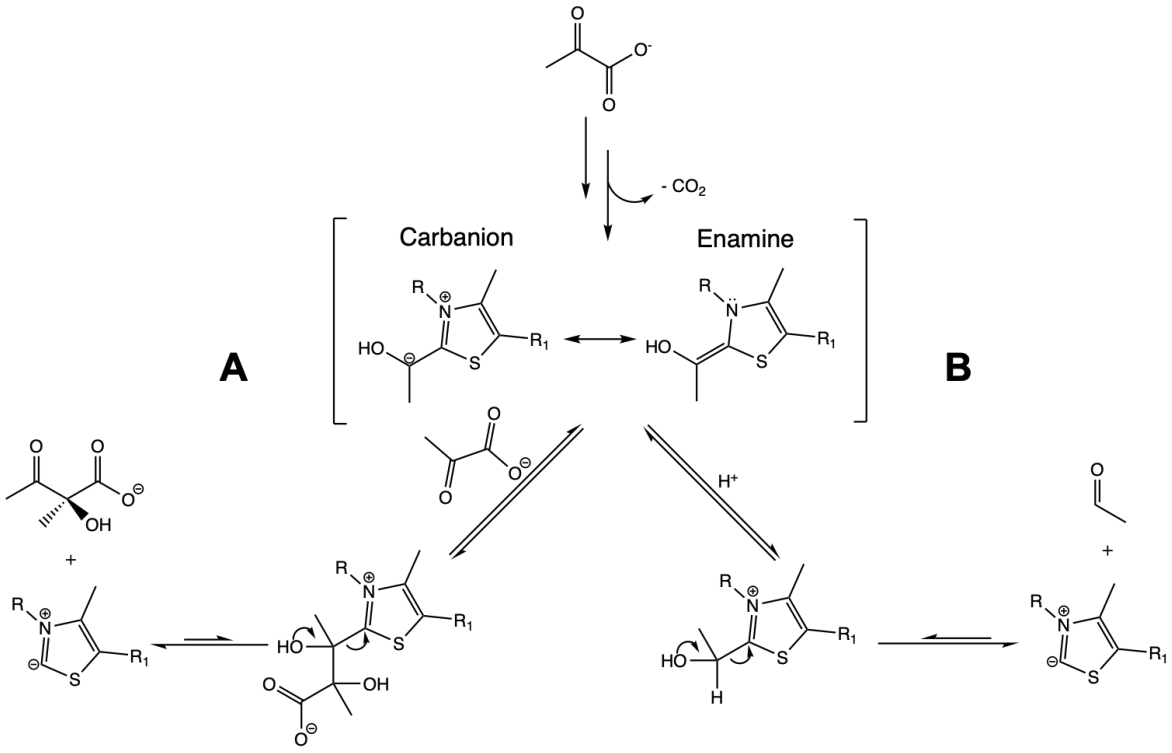

Figure 4.1: Reaction mechanisms of A) acetolactate and B) acetaldehyde formation by ThDP-dependent enzymes.

Another key difference was observed between the trapped intermediates in *Bs*ALS and *Kp*ALS. The trapped intermediate found in *Kp*ALS was found to adopt an unusual tricyclic dihydrothiachrome diphosphate form of ThDP (Figure 4.2). At the time this form of ThDP had never before even been crystallized in solution, much less bound to an enzyme (9). Conversely, no evidence for this form of ThDP was observed in *Bs*ALS. In fact, the tricyclic form of ThDP has only been seen in one other enzyme to date, a phosphoketolase variant from *Bifidobacterium breve* (21).

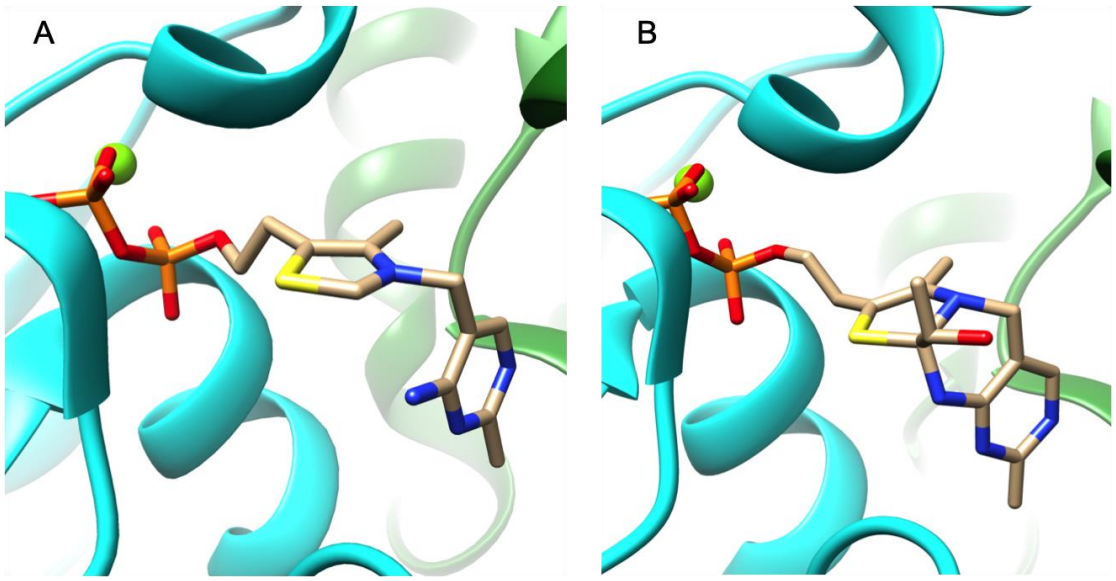

Figure 4.2: Forms of ThDP found in X-ray structures of *Kp*ALS. A) Thiazolium form (PDB ID: 5DX6), and B) dihydrothiachrome form with trapped HEThDP intermediate (PDB ID: 1OZH).

Observation of the dihydrothiachrome form of ThDP immediately led to speculation on its importance in the reaction mechanism of *Kp*ALS. Pang *et al.* (9) proposed a mechanism in which the tricyclic form is formed and broken throughout the catalytic cycle. The mechanism involved the initial formation of a less stable resonance form of ThDP in which a charge migration occurs from the nitrogen atom (N^+ form) to the sulfur atom (S^+ form) in the thiazolium ring (9).

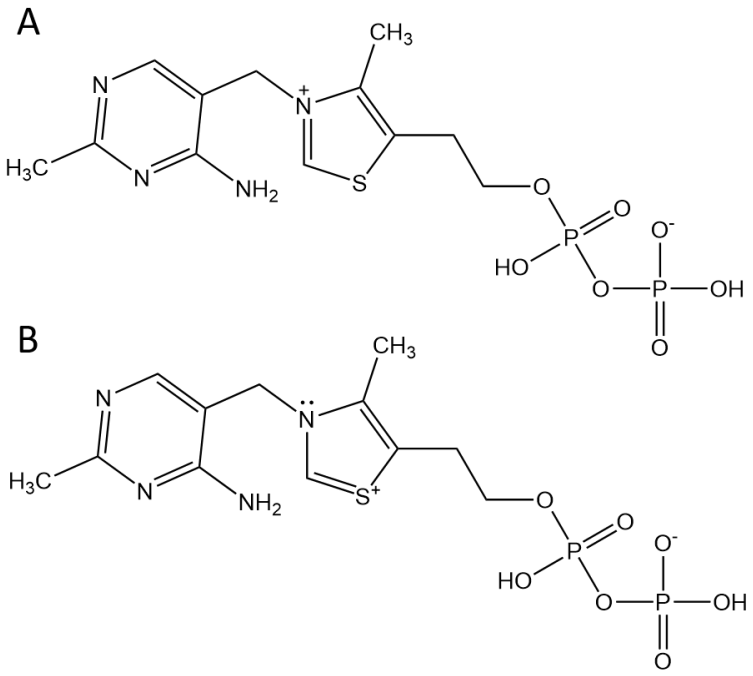

Figure 4.3: A) N^+ and B) S^+ forms of ThDP.

While the S^+ form initially seems like an unlikely resonance form to exist in significant amounts, it has been proposed before in studies of the ThDP cofactor itself. In fact, calculations performed on the crystal structure of ThDP indicated that the N^+ form was only favored over the S^+ form by a factor of ~2:1 (22,23). This would suggest that the latter form exists in significant amounts, at least in crystalline ThDP, providing some support for the proposed mechanism.

A recent computational study looking at the reaction mechanism of benzoylformate decarboxylase (BFDC), suggested that *Kp*ALS is not unique in the formation of the tricyclic form of ThDP (24). The authors postulated that the tricyclic intermediates act as kinetic traps. Although they were found to be more stable than their equivalent thiazolium-type intermediate they have no path to move forward in the reaction cycle, indicating that they are unproductive off-pathway intermediates (24).

In an attempt to (i) determine the importance of soak time on the observation of ALS intermediates and (ii) obtain additional information about the tricyclic intermediates of ThDP, a series of soaking experiments was carried out.

4.2 X-ray Crystallography of *Kp*ALS

*Kp*ALS was crystallized using crystallization conditions described in section 2.7.1, and crystals appeared in drops within 5-7 days at 4 °C (Figure 4.4).

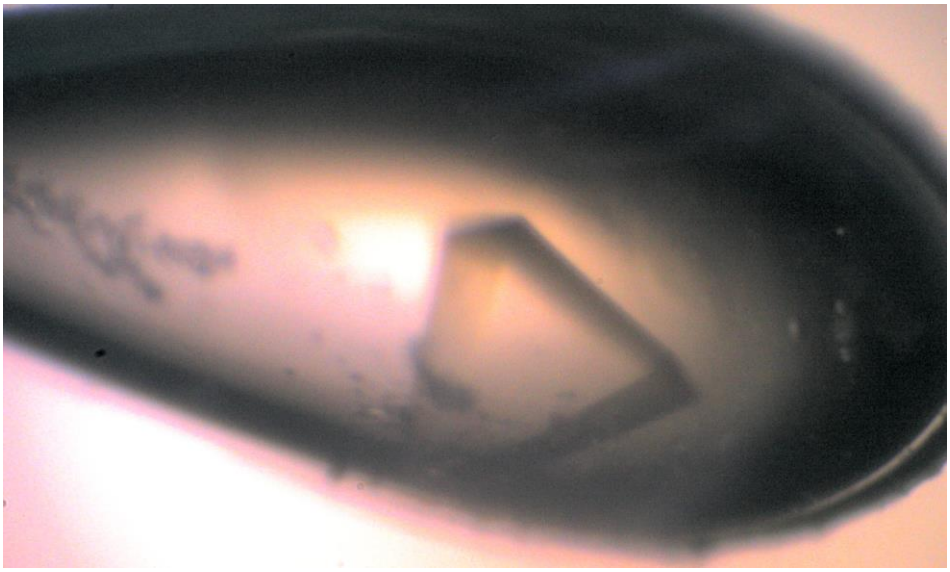

Figure 4.4: Typical *Kp*ALS crystal used for soaking experiments.

In total, these crystals were soaked separately with three compounds (Figure 4.5), pyruvate, phosphonodifluoropyruvate, and β-fluoropyruvate, before diffraction data was collected. These compounds were chosen as it was thought that each might highlight different properties of the enzyme. The first compound, pyruvate, was chosen in hopes that a reaction intermediate could be trapped following a quick soaking experiment. The second compound, phosphonodifluoropyruvate (PnDFP), was chosen in an attempt to provide structural evidence for its proposed mechanism of inhibition of phosphonopyruvate decarboxylase, another ThDP-dependent enzyme (25). Finally, the third compound, β-fluoropyruvate, is a known inhibitor of other pyruvate-utilizing enzymes such as the E1 subunit of the pyruvate dehydrogenase complex (26), and was chosen in an attempt to observe an enzyme-inhibitor complex. Ultimately, these soaking experiments resulted in observation of many unique features of the enzyme that are discussed in this chapter.

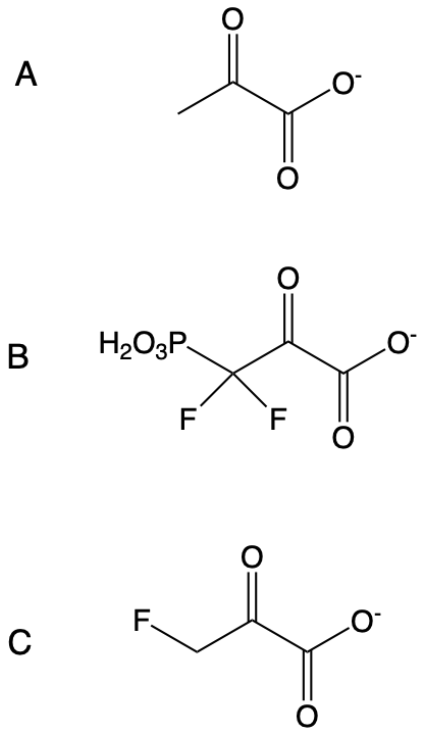

Figure 4.5: Chemical structures of compounds used for ligand soaking experiments. A) Pyruvate, B) PnDFP, and C) β-fluoropyruvate.

4.2.1 General structural features

In all cases, crystals of *Kp*ALS were found to belong to monoclinic spacegroup I121 with unit cell dimensions a = 85, b = 134, and c = 111 Å. The structures were solved by molecular replacement using a search model consisting of a single monomer from a previously published structure of *Kp*ALS (PDB ID: 1OZF) with water molecules and ligands removed. The asymmetric unit was found to consist of two monomers of *Kp*ALS in a non-biologically active dimer. In agreement with previously published structures, analysis by PISA (27) showed that, like many other members of the ThDP-dependent decarboxylase family, including benzoylformate decarboxylase from *Pseudomonas putida* (28), and pyruvate decarboxylase from *Zymomonas mobilis* (29), the biological assembly of *Kp*ALS is a tetramer. Often the tetrameric assembly formed by enzymes in this family is better described as a "dimer of dimers" (Figure 4.6). Additionally, with the exceptions discussed below, each monomer was found to contain at least 1 magnesium ion, 1 molecule of ThDP (or a trapped ThDP complex), and 1 phosphate ion in addition to the protein chain. A summary of crystallographic data, model, and refinement statistics for all data sets is presented in Table 4.1.

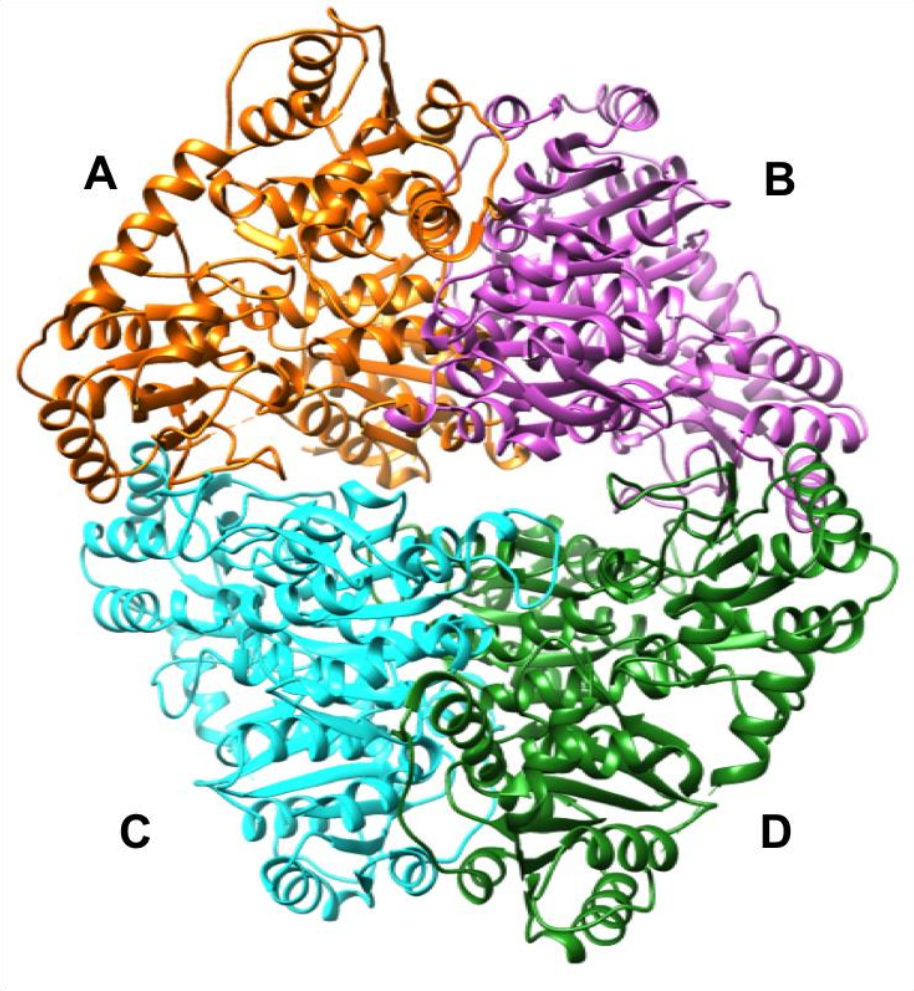

Figure 4.6: Tetrameric structure of *Kp*ALS. The asymmetric unit is represented by monomers A and D, while the functional dimers are represented by monomers A and B and monomers C and D.

Table 4.1: Data, model, and refinement statistics for *Kp*ALS X-ray crystal structures

Data Set	Pyruvate	β-fluoropyruvate	PnDFP
PDB ID	5WDG	5DX6	5D6R
Space group	I121	I121	I121
Unit cell Dimensions			
a, b, c (Å)	85.47, 134.41, 110.75	84.8, 134.01, 110.77	85.12, 133.35, 110.62
α, β, γ (°)	90.0, 95.5, 90.0	90.0, 95.5, 90.0	90.0, 95.4, 90.0
Resolution range (Å)[a]	55.12–2.12 (2.19–2.12)	42.57–1.75 (1.81–1.75)	46.28–2.28 (2.36–2.28)
No. reflections	238251	440033	196557
No. unique reflections	70787	124191	56232
Completeness (%)[a]	99.9 (99.7)	99.9 (99.5)	100.0 (99.8)
Multiplicity[a]	3.4 (3.3)	3.5 (3.4)	3.5 (3.4)
Linear R_{merge}, (%)[b]	10.8 (94.2)	6.6 (82.5)	9.1 (78.2)
Mean I/σ (I)[a]	6.58 (1.75)	9.29 (1.50)	8.57 (1.44)
Refinement statistics			
[c]R_{work}	0.203	0.151	0.208
[d]R_{free}	0.246	0.189	0.237
No. of atoms	8653	9100	8538
Protein	8059	8248	8188
Ligands	98	72	83
Water	496	780	267
B-factors (Å^2)			
Average B-factor	46.27	35.33	54.01
Protein	46.38	34.81	54.33
Ligands	54.44	34.83	55.31
RMSD[e] (bonds, Å)	0.002	0.008	0.003
RMSD[e] (angles, °)	0.49	0.81	0.74
Clashscore	5.91	3.57	1.41

[a]Values in parentheses refer to statistics in the highest-resolution shell.
[b]Linear $R_{merge} = \Sigma|I_{obs} - I_{avg}|/\Sigma I_{avg}$
[c]$R_{work} = \Sigma|F_{obs} - F_{calc}|/\Sigma F_{obs}$
[d]R_{free} was calculated as R_{work} where ~3.5–5% of the reflection data was selected at random as a test set and excluded from refinement.
[e]RMSD – root mean square deviation.

4.2.2 Crystals soaked with pyruvate

The initial experiment was performed by soaking crystals in 100 mM pyruvate for 5 seconds as described in Chapter 2. Theses crystals diffracted to a resolution of 2.1 Å and the structure was refined to a final R_{work}/R_{free} of 0.203/0.246 using the approach outlined in section 2.7.4. Upon molecular replacement and subsequent placing of the ThDP cofactor, extra electron density was observed stemming from C2 on the ThDP cofactor, suggestive of a potential reaction intermediate. Originally, it was thought that this density could correspond to an intermediate similar to that observed in *Bs*ALS, *i.e*. the LThDP intermediate (8). However, all refinement with LThDP resulted in significant extra positive difference density near the carboxylate group. This led to the idea that the trapped intermediate may be of the last step of the reaction immediately before product release, the acetolactylThDP (ALThDP) intermediate, as the bulkier intermediate could potentially fit the extra density. Concomitantly, there appeared extra positive difference density between C2 and the 4′ amino group on the pyrimidine ring suggesting that the cofactor may be in the tricyclic form previously observed in *Kp*ALS. Indeed, upon refinement with the tricyclic ALThDP intermediate, the resulting electron density was observed to fit this intermediate quite well (Figure 4.7).

Observation of this tricyclic intermediate supports the conclusions of the computational study on BFDC (24). The tricyclic forms proposed for BFDC correspond to two intermediates in the mechanism of ALS: i) unreacted ThDP, and ii) the ALThDP intermediate. Given that tricyclic HEThDP had already been seen in *Kp*ALS, the observation of tricyclic ALThDP is not entirely surprising. In fact, it is likely that the stability the tricyclic form is a key factor that allowed for sufficient accumulation of the intermediate to be observed in an X-ray crystal structure.

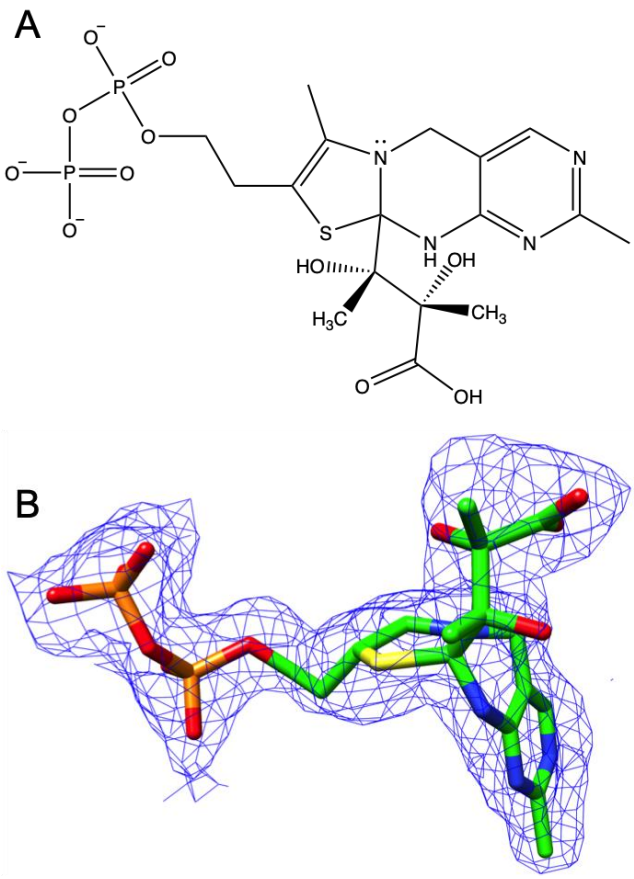

Figure 4.7: A) Chemical structure and B) electron density fit (1 σ) of the tricyclic ALThDP reaction intermediate.

Given the observation of the tricyclic ALThDP species in the crystal structure, and how well it correlates with evidence provided by the computational studies on BFDC, the proposed mechanism of acetolactate formation should be updated to include the tricyclic intermediate. As such, an updated mechanism can be seen in Figure 4.8.

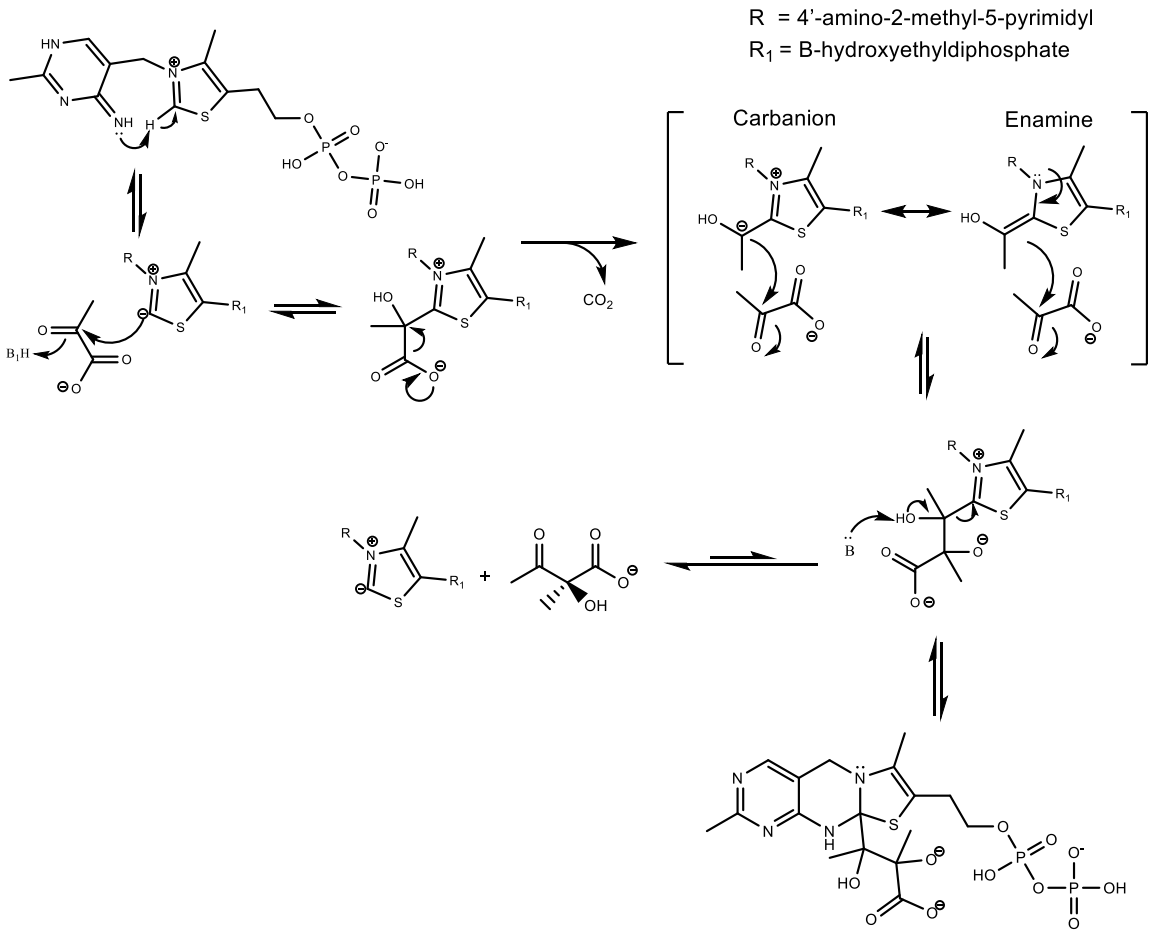

Figure 4.8: Updated mechanism for the formation of (*S*)-acetolactate by *Kp*ALS.

The acetolactyl moiety in ALThDP was observed to be held in place by hydrogen bond interactions with several water molecules held in place by side chain and backbone interactions with Ala35, Lys6, Thr80, Ser81, Gln120, and Gln420 (Figure 4.9).

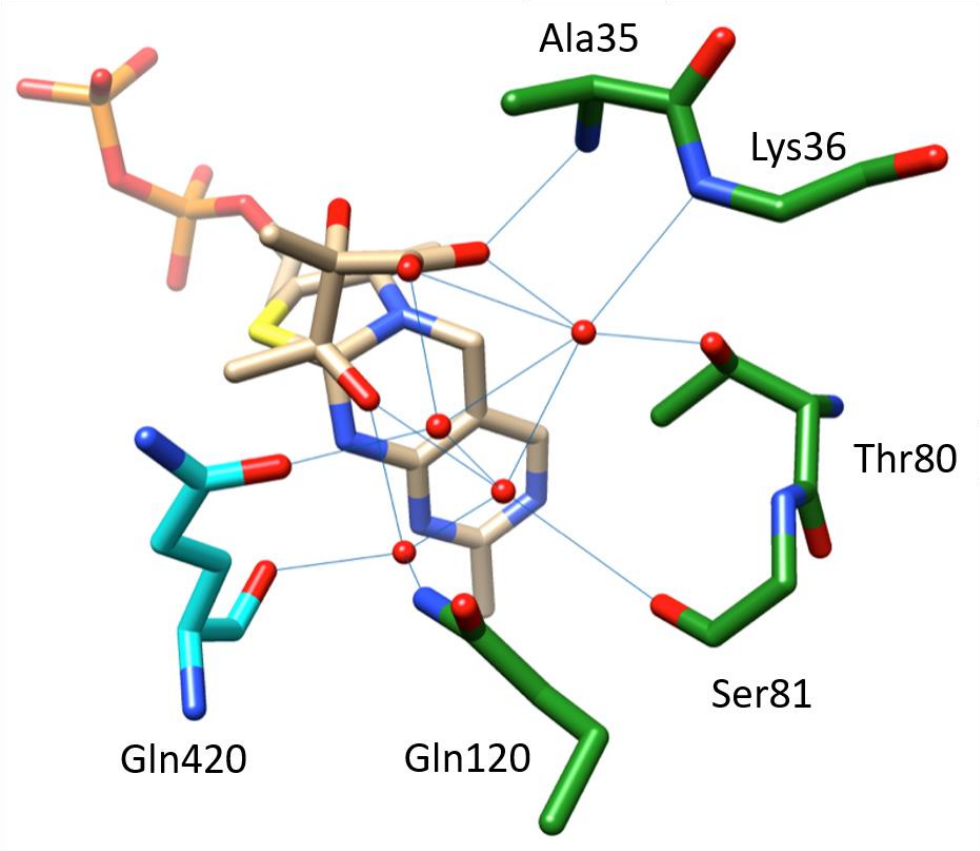

Figure 4.9: Hydrogen bonding interactions (≤ 3.2 Å) of acetolactyl moiety of ALThDP with protein chain and water molecules in the active site.

The acceptor pyruvate is found in a similar position to that suggested by Pang *et al*. in which the acceptor pyruvate molecule approaches the enamine/carbanion intermediate from above and is clearly in position to form (*S*)-acetolactate (Figure 4.10). The model agrees with the observed ALThDP quite well including the prediction of hydrogen bond interactions with Ala35, Lys36, and Gln420 (9).

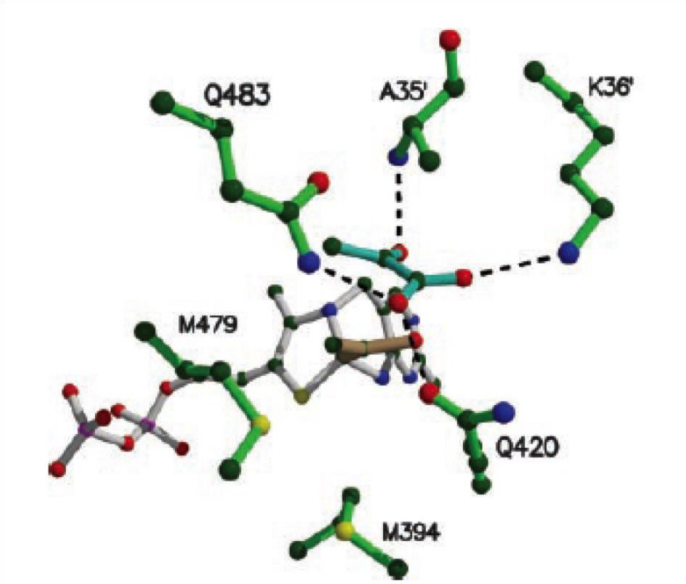

Figure 4.10: Predicted model of second substrate binding in the active site of *Kp*ALS. Reproduced from Pang *et al.* (9).

That said, the proposed model differs from the observed intermediate in a few ways. First, and not unreasonably, the model did not consider water molecules in the active site. Clearly, they are a key feature in the stabilization of the carboxylate group in ALThDP observed here. Second, while the location of the acceptor pyruvate is similar, its orientation differs between the predicted model and the observed intermediate. In the latter, the carboxylate group of the acceptor points toward the backbone nitrogen atoms of Ala35 and Lys36, while it was predicted to point toward Gln420 in the model. In fact, the model predicted an interaction between the backbone nitrogen of Ala35 and the carbonyl oxygen of pyruvate. This interaction was proposed to be one of the interactions explaining the formation of solely (*S*)- rather than (*R*)-acetolactate. In ALThDP however, no such interaction is observed, and the oxygen atom was found to be involved in very few, if any, interactions with active site residues.

Finally, Gln483 was proposed to be involved with coordination of the carboxylate group. This residue is found on a loop folded over the top of the active site. This residue has since been observed to take on multiple conformations depending on presence of reaction intermediates in the active site. In the presence of ALThDP Gln483 was observed to be folded away from the active site, likely to prevent steric clash with the acceptor substrate. However, as seen in Figure 4.9, it reaches down into the active site when either no, or smaller, reaction intermediates are in the site.

Looking at the binding mode and conformation of ALThDP, the positioning of the acceptor in the active site appears to be controlled by hydrophobic interactions as much as by hydrogen bonding. The methyl groups found in the acetolactyl moiety are in close proximity with residues Met394 and Met479 (Figure 4.11). Due to the proximity of these residues to the acetolactyl moiety, they likely contribute to substrate orientation in the active site, and, by extension, the stereospecificty of the enzyme.

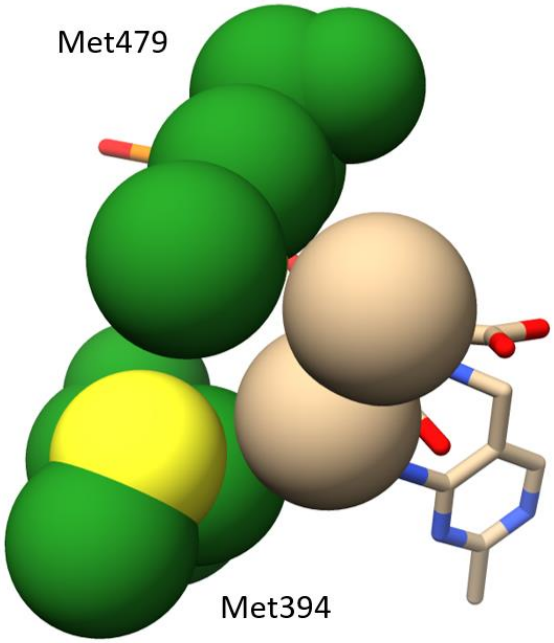

Figure 4.11: Interaction of the methyl groups of ALThDP (tan) and side-chains of Met394 and Met479 (green) shown as spheres.

4.2.3 Crystals soaked with phosphonodifluoropyruvate (PnDFP)

In a second experiment, crystals of *Kp*ALS were soaked in PnDFP for two weeks before being flash frozen in liquid nitrogen. These crystals diffracted to 2.28 Å, and the model was refined to a final R_{work}/R_{free} of 0.208/0.237 using the approach outlined in section 2.7.4. As with the crystals soaked with pyruvate, upon molecular replacement and subsequent placing of the ThDP cofactor, extra electron density was observed stemming from C2 of the ThDP cofactor.

PnDFP was originally synthesized (25) as a mechanism-based inhibitor of phosphonopyruvate decarboxylase (PnPyrDC). However, as PnPyrDC is refractory to crystallization, no structural evidence of the inhibitor complex has previously been obtained.

*Kp*ALS is more easily crystallized, acts on a similar substrate, and has a relatively large binding pocket. Consequently, it was thought that ALS could act as a surrogate for PnPyrDC to gain structural insight about the mechanism of inactivation by PnDFP.

As shown in Figure 4.12, inactivation of PnPyrDC by PnDFP was postulated to occur through irreversible modification of the ThDP cofactor at C2 (25). In effect, it acts as a mechanism-based inhibitor in which the initial steps of the inactivation reaction follow the proposed mechanism of catalysis with standard 2-ketoacid substrates. First the ThDP ylid performs a nucleophilic attack on the carbonyl of PnDFP to form a tetrahedral intermediate which then undergoes decarboxylation. If pyruvate was used, this would result in the formation of the carbanion/enamine intermediate which would then become protonated. However, with PnDFP, decarboxylation is proposed to be concerted with the loss of a fluoride ion. Finally, this results in the formation of an "enolThDP" intermediate, which can tautomerize to form phosphonofluoracetylThDP (Figure 4.12 A).

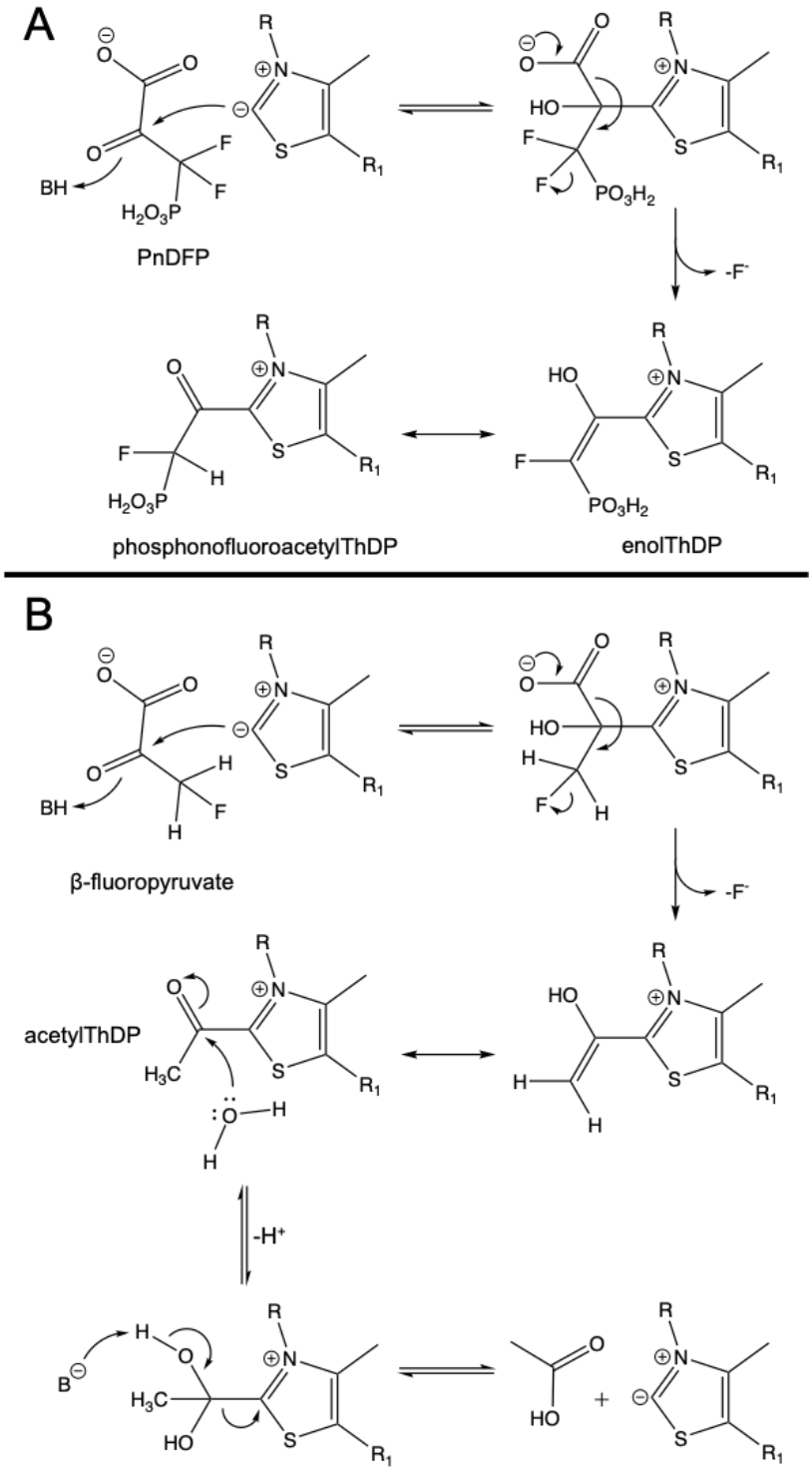

Figure 4.12: Proposed mechanisms of A) inactivation of PnPyrDC by PnDFP, and B) formation of acetate from β-fluoropyruvate by the E1 component of PDH.

The loss of the fluoride ion and subsequent formation of the enolThDP complex is similar to the proposed mechanism of acetate formation (Figure 4.12 B) by the E1 component of PDH when incubated with β-fluoropyruvate (26,30). β-fluoropyruvate appears to inhibit the E1 component of PDH by acting as a slow alternate substrate ultimately resulting in the formation of acetate through addition of a water molecule following loss of the fluoride ion. Conversely, reaction of PnPyrDC with PnDFP was shown to cause irreversible inactivation of PnPyrDC making it a true inhibitor instead of an alternate substrate. The irreversible nature of the inhibition indicates that the phosphonofluoroacetylThDP complex is not likely to break down to form phosphonofluoroacetate the same way that acetylThDP breaks down to form acetate in the E1 component of PDH.

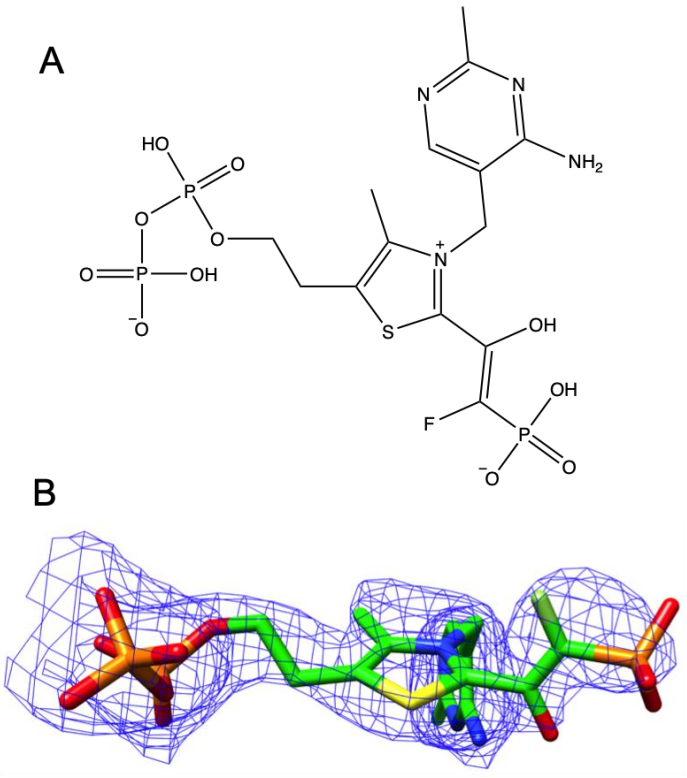

Figure 4.13: Electron density fit (1 σ) of the enolThDP complex.

As seen in Figure 4.13, the electron density stemming from C2 was determined to be from the enol/keto tautomers of phosphonofluoroacetylThDP. The moderate resolution of the structure makes determination of whether the complex exists primarily in the enol or keto form difficult. It is likely that both tautomers exist in significant amounts and the electron density represents an

average between them. Given that the geometry of the carbon bound to the fluorine and phosphate moieties will be different, a higher resolution structure may provide more insight into the distribution of keto and enol tautomers. In the enol form, the form modeled in Figure 4.13, this carbon is sp^2 hybridized and the fluorine, phosphate, and alcohol groups lie on the same plane. In the keto form, however, this carbon will be sp^3 hybridized and the geometry would be tetrahedral. It should also be noted that, without appropriate resolution, it is difficult to speculate on the stereochemistry of the keto tautomer, *i.e.*, would it be in the (*R*)-, or (*S*)- configuration.

4.2.4 Crystals soaked with β-fluoropyruvate

In a final experiment, crystals of *Kp*ALS were soaked in β-fluoropyruvate for 5 minutes before being flash frozen in liquid nitrogen as described in Chapter 2. These crystals diffracted to 1.75 Å, and the model was refined to a final R_{work}/R_{free} of 0.151/0.189 using the approach outlined in section 2.7.4. As with the crystals soaked with pyruvate and PnDFP, upon molecular replacement and subsequent placing of the ThDP cofactor, extra electron density was observed stemming from C2 of the ThDP cofactor. However, in contrast to the crystals soaked with pyruvate, this extra density was only observed in one of the two monomers in the asymmetric unit. The second monomer was found to contain unmodified ThDP. The extra density was determined to belong to a fluorohydroxyethylThDP (FHEThDP) complex (Figure 4.14). Finally, no evidence of the tricyclic form of ThDP was observed.

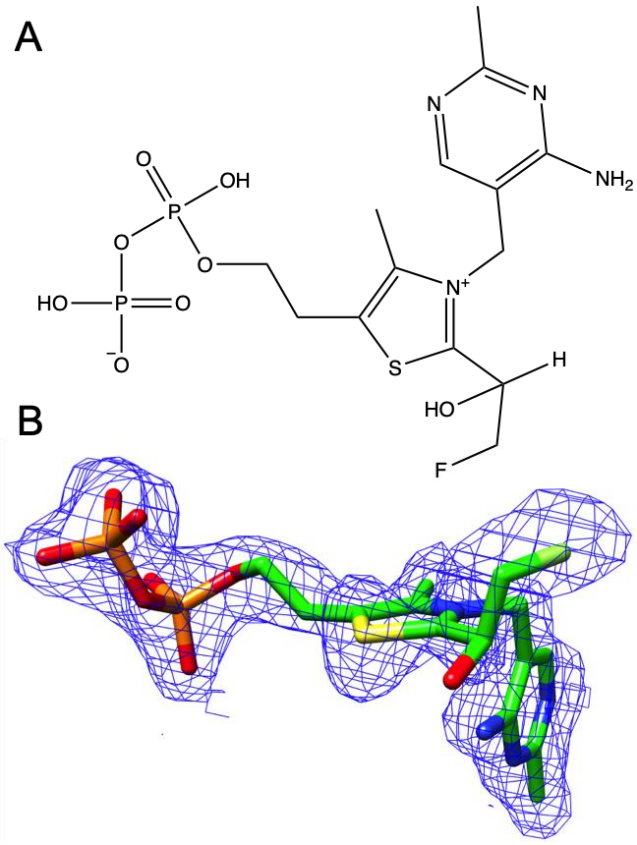

Figure 4.14: A) Chemical representation and B) Electron density fit (1 σ) of the FHEThDP complex.

Observation of the FHEThDP complex was somewhat unexpected as previous studies using β-fluoropyruvate showed the loss of the fluoride group following decarboxylation in the E1 component of the pyruvate dehydrogenase complex from *E. coli* (26,30). The loss of the fluoride ion was shown to result in formation of acetylThDP and the eventual release of acetate (Figure 4.12). The intermediate observed here would be expected if the final product were to be fluoroacetaldehyde in a reaction directly analogous to that catalyzed by pyruvate decarboxylase. While β-fluoropyruvate does act as an inhibitor of *Kp*ALS (see Chapter 3), the mechanism of inhibition is currently not known. Additionally, it has not been established whether incubation with β-fluoropyruvate results in either the loss of a fluoride ion, or the formation of acetate. However, the inhibition was found to be reversible by dilution assay indicating that β-fluoropyruvate, unlike PnDFP is unlikely to be a mechanism-based inhibitor.

Surprisingly, and unlike the crystals soaked with pyruvate in which ALThDP is found in all active sites, FHEThDP is only observed in one of the two monomers in the asymmetric unit

and thus only two of the four monomers in the tetramer. At first glance, this provides evidence that ThDP-dependent enzymes do not use all active sites simultaneously. It has been reported the decarboxylase family of ThDP-dependent enzymes show alternating-site reactivity, with negative cooperativity between the sites (31,32). Consequently, if true, in a tetramer such as *Kp*ALS, only 2 of the 4 active sites would be occupied at any given time during a catalytic cycle. More specifically, only one site in each functional dimer would be occupied, *i.e.*, one of the two sites in pairs A-B and C-D (Figure 4.6). However, this is not the pattern that is observed in this instance. Here, the occupied sites are found in the A-B dimer, while the C-D dimer contains unreacted ThDP. This immediately suggests two possibilities. First, alternating-sites reactivity does not express itself in *Kp*ALS in the same fashion as the other enzymes for which alternating-site activity was observed. Second, some other factor led to the observation of only one dimer containing a reaction complex. Close inspection of the structure indicates that the latter explanation is the more likely.

An intriguing observation is that the C-terminal residues 555-559, normally a disordered region, form an alpha helix in the monomers containing unmodified ThDP. As shown in Figure 4.15 the helix that appears to close over the active site and completely block substrate access to the site. From this point, the monomers containing the closed active site will be referred to as the "closed" structure, while monomers without the ordered C-terminal helix will be referred to as the "open" structure.

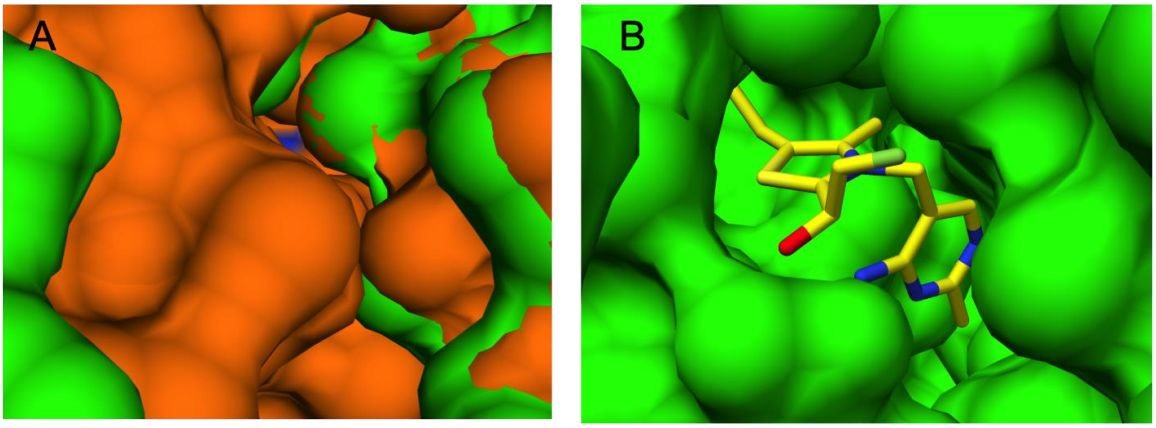

Figure 4.15: Space filling model showing the closure of the active site by residues the C-terminus. Dimers containing FHEThDP (green) and unmodified ThDP (orange) were aligned in UCSF Chimera (33). A) Shows the closed structure of the active site, and B) Shows the open structure of the active site.

When aligned, the dimers appear reasonably similar with an RMSD of only 0.703 Å over all residues. Interestingly, the C-terminus is not the only region that shows deviation when the sets of dimers are aligned. While the interior loops, particularly those surrounding the active site, align with almost no deviation, many solvent accessible loops show positional changes ranging from 2.5 Å to over 8 Å. Two of the loops showing these movements also show varying degrees of disorder. For example, in the open structure residues 116-122 form a disordered loop that cannot be modeled. In the closed structure however, the residues form an ordered α-helix (Figure 4.16 A) that sits directly across the substrate channel from the C-terminal residues.

Differences also arise with residues 354-366. In the open structure these residues form the end of an ordered α-helix, while in the closed structure all α-helical character is lost In fact, residues 358-366 in the closed structure show too little electron density to be modeled (Figure 4.16 B).

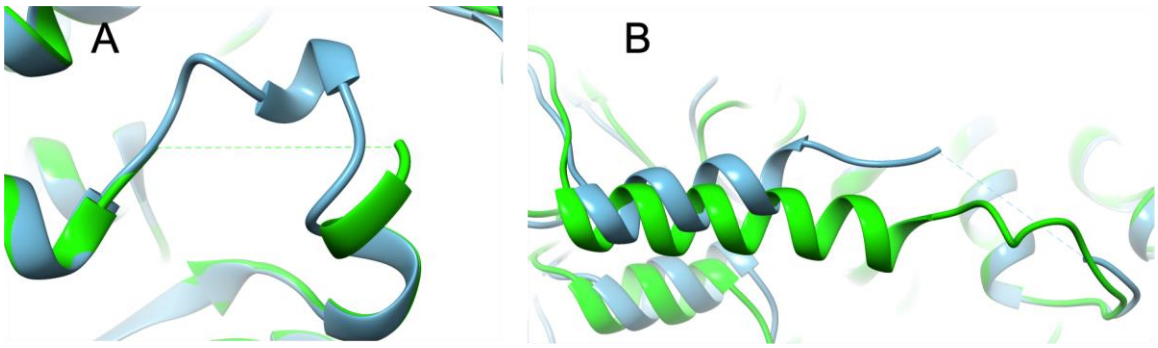

Figure 4.16: Movement of loops A) 116-122, and B) 354-366. Residues from closed structure are shown in blue. Residues from open structure are shown in green.

Closure of the active site does not necessarily explain the movement of these loops. More likely, movement of the loops potentially explains the closure of the active site. This leads to the question of what forces are inducing the loop movements. Indeed some of the same mobility of the surface loops is observed when dimer components of the structure from crystals soaked with pyruvate are aligned, indicating that the loop movements and the closure of the active site may be unrelated. However, the movements in crystals soaked with pyruvate appear smaller in magnitude than those observed in the crystals soaked with β-fluoropyruvate.

One simple explanation for these observations is that crystal-packing forces cause the closure of the active site. This seems unlikely as no other structures of *Kp*ALS show this closed

C-terminal conformation. However, this possibility cannot be eliminated as the increased resolution and moderately lower B-factors from these crystals indicate a higher degree of order, and thus potential observation of regions in which previous models showed little or no electron density.

An alternative, and more intriguing, explanation for the loop movement could lie in the possibility of regulatory phosphate-binding site. In all structures of *Kp*ALS, except from crystals soaked with β-fluoropyruvate, a phosphate molecule is observed bound to each monomer of the enzyme. Initially, the site was not considered significant and the bound phosphate was potentially only present because the enzyme was stored in phosphate buffer. In crystals soaked with β-fluoropyruvate however, two of the four phosphate-binding sites are occupied by a molecule of β-fluoropyruvate, while the other two remain occupied by phosphate. Intriguingly, the sites occupied by β-fluoropyruvate belong to the same monomers containing the closed active site. Only the monomers containing phosphate in the site showed the open conformation of the active site. Additionally, many of the solvent accessible mobile loops surround the phosphate binding site (Figure 4.17).

Currently, this evidence suggests that it is possible that displacement of the phosphate molecule in the active site may be inducing changes in residues surrounding the active site. These observations, in concert with the buffer-dependent change of kinetic profile of *Kp*ALS, as discussed in Chapter 3, suggest that this site may be important for regulation of the enzyme.

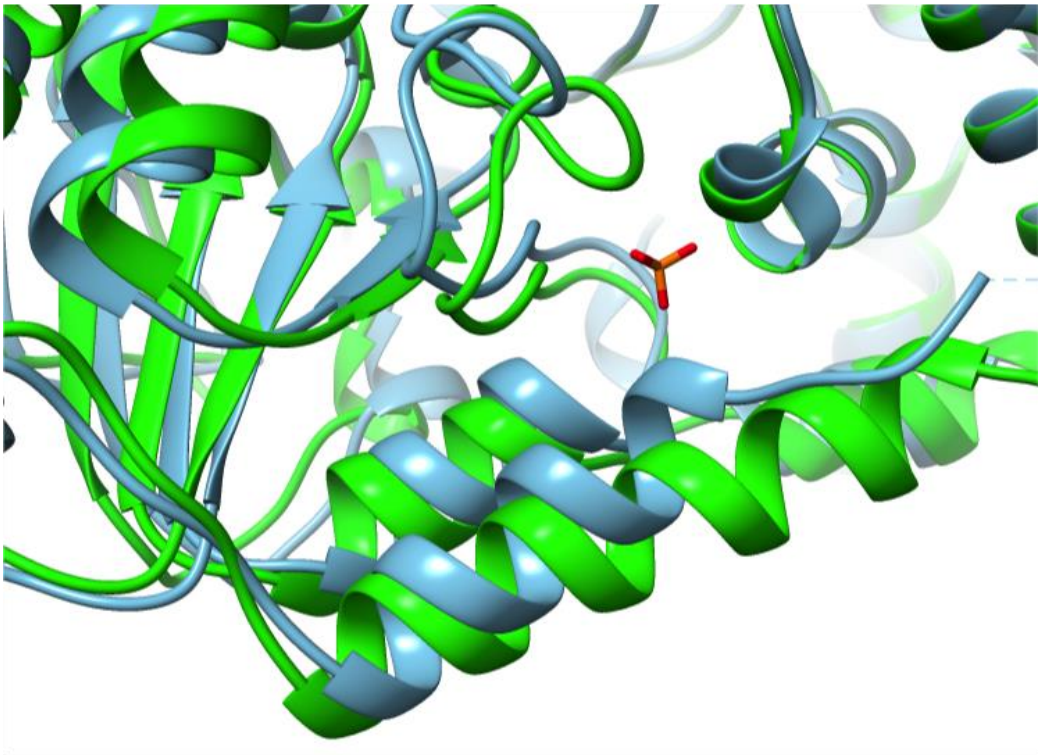

Figure 4.17: Movement of loops surrounding the phosphate binding site. Residues in green are from dimer bound with phosphate (orange). Residues in blue are from dimer bound to β-fluoropyruvate. For clarity, β-fluoropyruvate is not shown.

4.3 Investigation into the phosphate binding site as the site of allosteric activation

The observation of sigmoidal kinetics only in phosphate buffer (see Chapter 3) as well as the displacement of the bound phosphate molecule in the crystal soaked with β-fluoropyruvate led to a mutagenesis study to probe the possibility of the phosphate binding site as the source of the buffer dependence of the kinetic profile.

Potentially-important residues were identified by comparing the binding mode of phosphate to that of β-fluoropyruvate (Figure 4.18). Residues Arg259, Gln266, Arg352, and Tyr406 were found to have hydrogen bond interactions with the bound phosphate. Of these, only Arg259 and Arg352 showed direct interactions with β-fluoropyruvate. However, binding of β-fluoropyruvate is additionally accompanied by significant movement of the side chain of Gln266. Tyr406 showed little movement upon displacement of phosphate, and appears to have no interaction with β-fluoropyruvate.

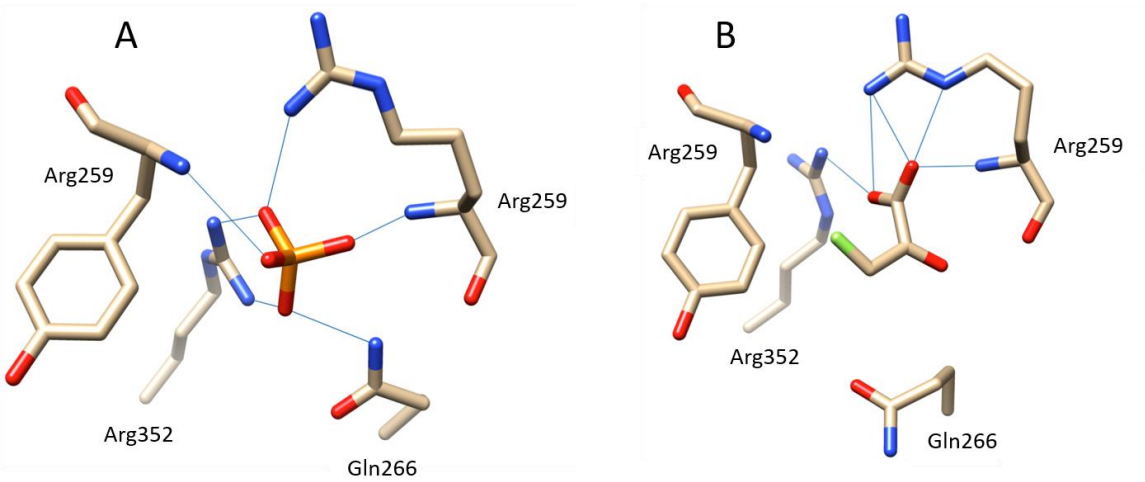

Figure 4.18: Hydrogen bond interactions of A) phosphate, and B) β-fluoropyruvate in the phosphate binding site.

While hydrogen bond interactions are observed with each of the oxygen atoms in the phosphate molecule, such interactions are only observed with the carboxylate group in β-fluoropyruvate. This is particularly interesting when considering that the carboxylate group in acetate could potentially allow the compound to bind in a similar manner, possibly leading to the acetate activation discussed in Chapter 3. Additionally, the β-fluoropyruvate binding mode suggests that this site could also be the origin of the substrate activation required when the kinetics of *Kp*ALS are measured in phosphate buffer. Given that pyruvate and β-fluoropyruvate differ only by the presence of the fluorine atom, it is likely that pyruvate binds and displaces phosphate in an almost identical way.

To investigate this, site-directed mutagenesis was performed on Arg259, Gln266, and Arg352 to determine the contribution of each residue to the buffer dependence on kinetic profile. Using the primer sequences listed in Table 4.2, theses residues were mutated to alanine in an attempt to eliminate any contribution to potential binding of phosphate, pyruvate, or acetate in the site. Mutagenesis was performed as described in Chapter 2.

Table 4.2: Sequences of primers used for mutagenesis of phosphate binding site residues.*

Primer Name	Sequence
R259A Forward	5'-TCTCGCTTCGCCGGCgccGTTGGGCTGTTTAAC-3'
R259A Reverse	5'-GTTAAACAGCCCAACggcGCCGGCGAAGCGAGA-3'
R352A Forward	5'-GAGATCCTCCGCGACgctCAGCACCAGCGCGAG-3'
R352A Reverse	5'-CTCGCGCTGGTGCTGagcGTCGCGGAGGATCTC-3'
Q266A Forward	5'-GTTTAACAACgcGGCCGGGGACCGTCTGCTaCAGCTCGCCGACC-3'
Q266A Reverse	5'-GGTCGGCGAGCTGtAGCAGACGGTCCCCGGCCgcGTTGTTAAAC-3'

*Lowercase bases indicate a mismatch with the template DNA.

In total, five *Kp*ALS variants were constructed: R259A, R352A, Q266A, R259A/R352A, and R259A/R352A/Q266A. Each of the variants was expressed and purified in the same manner as the wild type enzyme. Once purified, the variants were assayed in the same three buffer systems as the wild type enzyme: acetate, MES and phosphate at pH 6.0 using the CD method following the formation of (*S*)-acetolactate. The plots, and the steady-state kinetic parameters derived from them, are presented in Figure 4.19 and Table 4.3, respectively.

In acetate buffer, only variants containing the R259A mutation showed any significant change in K_m value. R259A showed a four-fold increase in K_m, while R352A showed a K_m relatively close to that obtained for the wild-type enzyme. In phosphate, the R259A mutation resulted in Michaelis-Menten kinetics, *i.e*., sigmoidal kinetics were not observed for this variant. The kinetics in MES were more difficult to evaluate as the near linear plots indicated that the K_m value is well in excess of 120 mM. Higher pyruvate concentrations were tested, however using over 150 mM resulted poor data quality due to its absorbance at 310 nm.

The R352A variant was found to be largely similar to wild-type *Kp*ALS in both acetate and phosphate buffers. However, in MES, the k_{cat} and K_m values both showed increases. Most importantly, as was observed for the wild-type enzyme, R352A showed Michaelis-Menten kinetics in acetate and MES, and sigmoidal kinetics in phosphate buffer.

Perhaps the most interesting feature of the single variants was the appearance of sigmoidal kinetics for Q266A in all three buffers. The S_{05} and k_{cat} values in MES and phosphate were similar, while a lower S_{05} value and higher k_{cat} value were found in acetate. It is notable that the Hill coefficients for reaction in acetate and MES buffers were lower than that observed in phosphate buffer, although the meaning of that observation is still unclear.

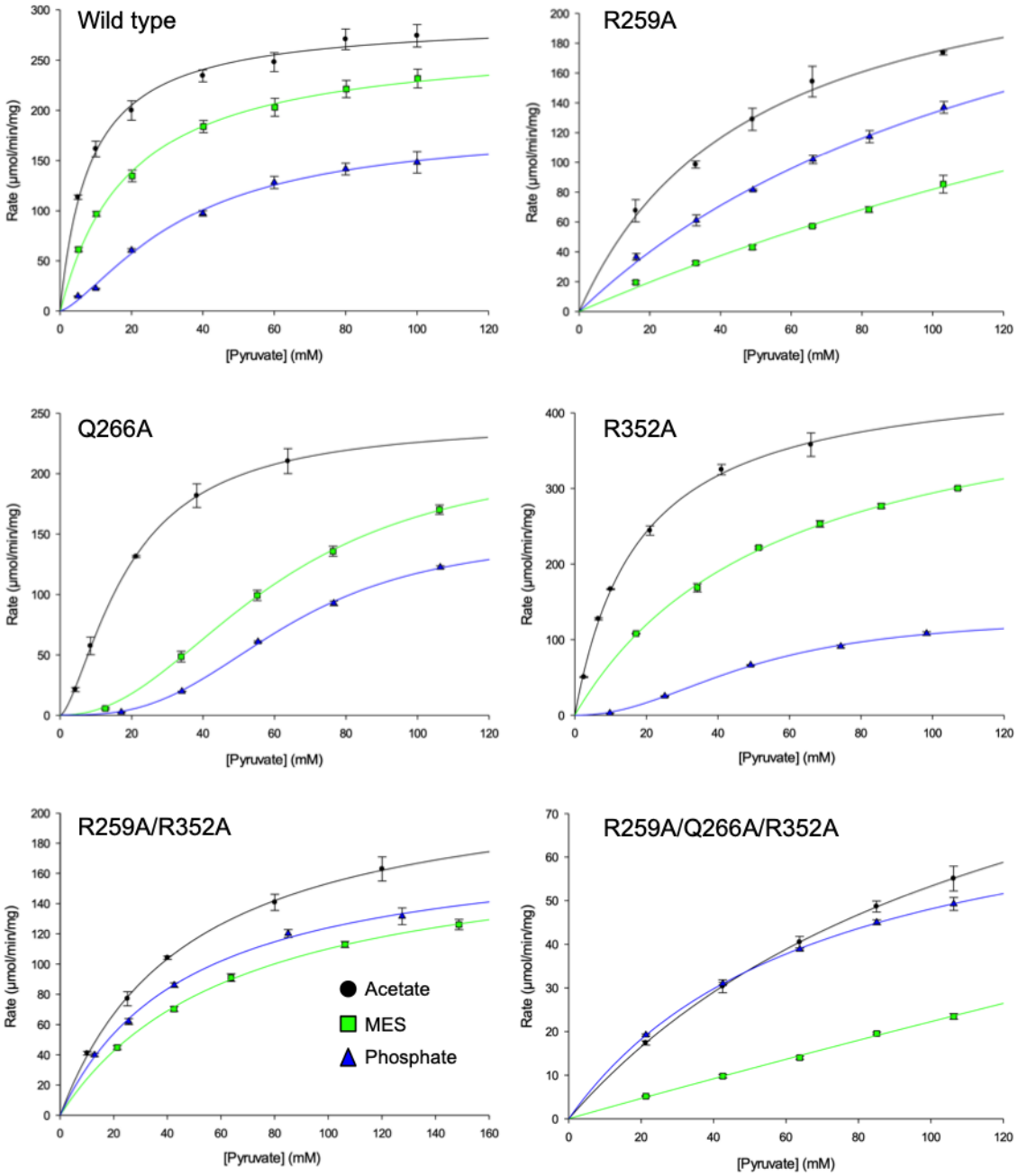

Figure 4.19: Plots of steady-state kinetic data for each allosteric site variant in acetate (black), MES (green), and phosphate (blue).

Table 4.3: Steady-state kinetic parameters of allosteric site variants.

Acetate				
Variant	K_m or S_{05} (mM)	k_{cat} (s^{-1})	k_{cat}/K_m	n
Wild Type	8 ± 2	310 ± 20	39	-
R259A	49 ± 9	270 ± 20	6	-
Q266A	19 ± 3	250 ± 20	13	1.5
R352A	18 ± 1	480 ± 10	27	-
R259A/R352A	40 ± 5	240 ± 10	6	-
R259A/R352A/Q266A	130 ± 30	130 ± 20	1	-
MES				
Variant	K_m or S_{05} (mM)	k_{cat} (s^{-1})	k_{cat}/K_m	n
Wild Type	19 ± 1	290 ± 30	15	-
R259A*	-	-	0.9	-
Q266A	61 ± 6	230 ± 20	4	2.2
R352A	67 ± 4	480 ± 10	7	-
R259A/R352A	66 ± 5	190 ± 7	3	-
R259A/R352A/Q266A*	-	-	0.2	-
Phosphate				
Variant	K_m or S_{05} (mM)	k_{cat} (s^{-1})	k_{cat}/K_m	n
Wild Type	37 ± 8	230 ± 20	6	2.2
R259A	141 ± 23	330 ± 40	2	-
Q266A	64 ± 2	155 ± 5	2	2.9
R352A	41 ± 2	138 ± 7	3	2.1
R259A/R352A	48 ± 5	191 ± 8	4	-
R259A/R352A/Q266A	69 ± 5	85 ± 3	1	-

n – Hill coefficient

* k_{cat}/ K_m was calculated as the slope of the linear kinetic plots (i.e., V/K conditions).

Neither the double (R259A/R352A) nor the triple (R259A/Q266A/R352A) variant showed any evidence of sigmoidal kinetics. The double variant was interesting in that the K_m values in MES and phosphate buffers were significantly lower than that of the R259A variant suggesting that the increased sensitivity to MES buffer observed in the R259A variant was lost after introduction of the R352A mutation. In acetate, the triple variant showed a ~10-fold increase in K_m value when compared to the wild type enzyme. This was the largest increase in any of the variants in this buffer. In fact, this is the only variant tested that shows a K_m value lower in phosphate than in acetate. Finally, the triple variant showed the lowest k_{cat} values of all variants.

Taken together, these results indicate that the phosphate binding site is likely to be the site of allosteric activation in *Kp*ALS. Mutation of Gln266 to alanine results in sigmoidal kinetics in all conditions tested, while mutation of Arg259 to alanine results in Michaelis-Menten kinetics in all conditions. In fact, all variants carrying the R259A mutation showed Michaelis-Menten kinetics in all conditions, even when the Q266A mutation was also present. Clearly, Gln266 and Arg259 are important for allosteric regulation of the enzyme. Conversely, the R352A single variant showed no effect on the kinetic profile, and only a minimal effect on K_m values.

It is interesting that while the R259A single variant showed no evidence of sigmoidal kinetics, it showed one of the largest buffer effects on K_m values ranging from ~50 mM (acetate) to an estimated 400 mM (MES). Conversely the R259A/R352A double variant showed the smallest range of K_m values. This indicates that, while Arg259 has a profound effect on the requirement for allosteric activation in phosphate, and influences buffer effects overall, it is not the only residue responsible for these effects. It required a combination two mutations, R259A and R352A, to see the sigmoidal kinetics and buffer effects on kinetic parameters effectively eliminated. However, addition of a third mutation, Q266A, led to some odd effects. For example, the pyruvate K_m value for reaction in MES buffer increased greatly, returning that observed for the R259A variant, while the k_{cat} values were at least a 2-3-fold lower than those observed for any other variants.

4.4 Summary and Conclusions

This chapter discusses three X-ray structures of *Kp*ALS solved following the soaking of ALS crystals with three compounds: pyruvate, phosphonodifluoropyruvate, and β-fluoropyruvate.

All three structures showed the presence of covalent reaction intermediate complexes of ThDP in the active site.

Crystals soaked with pyruvate resulted in the observation of a tricyclic form of ALThDP. This was the second time the tricyclic dihydrothiachrome form of ThDP had been observed in *Kp*ALS, and only the third time for ThDP-dependent enzymes in general. Overall, the observation of this intermediate is important as it provides insight into the binding mode of pyruvate as the acceptor substrate in the formation of (*S*)-acetolactate. Unexpectedly, it was discovered that, in addition to hydrogen bonding, hydrophobic interactions appear to play a significant role in positioning of the acceptor to ensure the (*S*)-enantiospecificty of the reaction. Finally, the ALThDP complex permitted the identification of those active site residues likely to be involved in substrate specificity. The analysis and subsequent testing of these observations are discussed in Chapter 5.

Crystals soaked with phosphonodifluoropyruvate showed evidence of a trapped phosphonofluoroacetylThDP intermediate. The intermediate provided evidence in support of the proposed mechanism of inactivation of phosphonopyruvate decarboxylase by PnDFP. Unfortunately, the structure was not of sufficient resolution to determine whether the keto or enol tautomer of the intermediate was the major contributor to its stability although, on balance, the latter was more likely.

In a final soaking experiment, crystals soaked with β-fluoropyruvate exhibited a number of surprising and noteworthy features. These included a FHEThDP intermediate in two of the four active sites in the *Kp*ALS tetramer, β-fluoropyruvate displacing phosphate in two of its four possible binding sites, and a C-terminal helix closing over two of the four active sites. The observation of the FHEThDP intermediate was somewhat surprising as it was expected that the fluorine would be eliminated following decarboxylation as was seen in the E1 component of PDH. Currently, it is unknown whether the retention of the fluorine in *Kp*ALS is due to the enzyme being in crystalline form, or if the enzyme simply catalyzes a different reaction with β-fluoropyruvate.

Observation of β-fluoropyruvate bound in place of phosphate is interesting for two reasons. First, the enzyme displays sigmoidal kinetics when assayed in phosphate buffer, but exhibits Michaelis-Menten kinetics when it is assayed in acetate buffer at the same pH. This suggests that phosphate may be playing some sort of regulatory role. The second relates to the observation that, in monomers where β-fluoropyruvate displaces phosphate, a C-terminal helix closes over the active site. It is currently unclear whether the two events are related. This region is generally

disordered in other published structures of ALS and it is feasible that some other force such as crystal packing may be contributing. That said, the link is striking and, to explore this further, a mutagenesis study on the phosphate binding site was carried out.

Lastly, a mutagenesis study was performed that provided evidence that the phosphate binding site is indeed the site responsible for the requirement of substrate activation in *Kp*ALS. Initially, it was clear that Arg259 and Gln266 are both involved in allosteric regulation by this site. While the R259A variant showed a significantly increased K_m value in MES buffer, it exhibited no evidence of sigmoidal kinetics. Conversely, the Q266A variant required substrate activation in all conditions tested. The R352A variant showed wild-type like kinetic patterns, and showed little effect on K_m and k_{cat} values indicating that Arg352, by itself, has little effect on binding. However, when in concert with the R259A mutation in the R259A/R352A double variant, the sensitivity to MES and phosphate buffers that was observed with the R259A variant was eliminated. Further, introduction of the Q266A mutation to the double variant saw the restoration of sensitivity to MES, along with a 2-3-fold reduction in k_{cat} values in both acetate and phosphate buffers. Taken together, these results indicate that the phosphate binding site is most likely to be responsible for the requirement of substrate activation in *Kp*ALS and that all three residues examined, Arg259, Gln266, and Arg352, are important in the buffer effects exhibited by the enzyme.

References

1. Stormer, F. C. (1975) 2,3-Butanediol biosynthetic system in *Aerobacter aerogenes*. *Methods Enzymol.* **41**, 518-532
2. Atsumi, S., Li, Z., and Liao, J. C. (2009) Acetolactate synthase from *Bacillus subtilis* serves as a 2-ketoisovalerate decarboxylase for isobutanol biosynthesis in *Escherichia coli*. *Appl Environ Microbiol* **75**, 6306-6311
3. Wang, M., Fu, J., Zhang, X. Y., and Chen, T. (2012) Metabolic engineering of *Bacillus subtilis* for enhanced production of acetoin. *Biotechnol. Lett.* **34**, 1877-1885
4. Störmer, F. C. (1967) Isolation of crystalline pH 6 acetolactate-forming enzyme from *Aerobacter aerogenes*. *J. Biol. Chem.* **242**, 1756-1759
5. Störmer, F. C. (1968) The pH 6 acetolactate-forming enzyme from *Aerobacter aerogenes*. I. Kinetic studies. *J. Biol. Chem.* **243**, 3735-3739
6. Störmer, F. C. (1968) The pH 6 acetolactate-forming enzyme from *Aerobacter aerogenes*. II. Evidence that it is not a flavoprotein. *J. Biol. Chem.* **243**, 3740-3741
7. Kaushal, A., Pabbi, S., and Sharma, P. (2003) Characterization of 2,3-butanediol-forming and valine-sensitive α-acetolactate synthase of *Enterobacter cloacae*. *World J. Microb. Biot.* **19**, 487-493
8. Sommer, B., von Moeller, H., Haack, M., Qoura, F., Langner, C., Bourenkov, G., Garbe, D., Loll, B., and Bruck, T. (2015) Detailed structure-function correlations of *Bacillus subtilis* acetolactate synthase. *ChemBioChem* **16**, 110-118
9. Pang, S. S., Duggleby, R. G., Schowen, R. L., and Guddat, L. W. (2004) The crystal structures of *Klebsiella pneumoniae* acetolactate synthase with enzyme-bound cofactor and with an unusual intermediate. *J. Biol. Chem.* **279**, 2242-2253
10. McCourt, J. A., Pang, S. S., King-Scott, J., Guddat, L. W., and Duggleby, R. G. (2006) Herbicide-binding sites revealed in the structure of plant acetohydroxyacid synthase. *Proc. Natl. Acad. Sci. U. S. A.* **103**, 569-573
11. Wang, J.-G., Lee, P. K. M., Dong, Y.-H., Pang, S. S., Duggleby, R. G., Li, Z.-M., and Guddat, L. W. (2009) Crystal structures of two novel sulfonylurea herbicides in complex with Arabidopsis thaliana acetohydroxyacid synthase. *FEBS J.* **276**, 1282-1290

12. Lonhienne, T., Garcia, M. D., Noble, C., Harmer, J., Fraser, J. A., Williams, C. M., and Guddat, L. W. (2017) High resolution crystal structures of the acetohydroxyacid synthase-pyruvate complex provide new insights into its catalytic mechanism. *ChemistrySelect* **2**, 11981-11988
13. Lonhienne, T., Garcia, M. D., Pierens, G., Mobli, M., Nouwens, A., and Guddat, L. W. (2018) Structural insights into the mechanism of inhibition of AHAS by herbicides. *Proc. Natl. Acad. Sci. U. S. A.* **115**, E1945-E1954
14. Pang, S. S., Duggleby, R. G., and Guddat, L. W. (2002) Crystal structure of yeast acetohydroxyacid synthase: a target for herbicidal inhibitors. *J. Mol. Biol.* **317**, 249-262
15. Pang, S. S., Guddat, L. W., and Duggleby, R. G. (2003) Molecular basis of sulfonylurea herbicide inhibition of acetohydroxyacid synthase. *J. Biol. Chem.* **278**, 7639-7644
16. Lonhienne, T., Nouwens, A., Williams, C. M., Fraser, J. A., Lee, Y. T., West, N. P., and Guddat, L. W. (2016) Commercial herbicides can trigger the oxidative inactivation of acetohydroxyacid synthase. *Angew. Chem. Int. Ed.* **55**, 4247-4251
17. Garcia, M. D., Chua, S. M. H., Low, Y. S., Lee, Y. T., Agnew-Francis, K., Wang, J. G., Nouwens, A., Lonhienne, T., Williams, C. M., Fraser, J. A., and Guddat, L. W. (2018) Commercial AHAS-inhibiting herbicides are promising drug leads for the treatment of human fungal pathogenic infections. *Proc. Natl. Acad. Sci. U. S. A.* **115**, E9649-E9658
18. Kaplun, A., Vyazmensky, M., Zherdev, Y., Belenky, I., Slutzker, A., Mendel, S., Barak, Z. e., Chipman, D. M., and Shaanan, B. (2006) Structure of the Regulatory Subunit of Acetohydroxyacid Synthase Isozyme III from Escherichia coli. *J. Mol. Biol.* **357**, 951-963
19. Karanth, N. M., and Sarma, S. P. (2013) The coil-to-helix transition in *Ilv*N regulates the allosteric control of *Escherichia coli* acetohydroxyacid synthase I. *Biochemistry* **52**, 70-83
20. Schellenberger, A. (1967) Structure and mechanism of action of the active center of yeast pyruvate decarboxylase. *Angew. Chem. Int. Ed.* **6**, 1024-1035
21. Suzuki, R., Katayama, T., Kim, B.-J., Wakagi, T., Shoun, H., Ashida, H., Yamamoto, K., and Fushinobu, S. (2010) Crystal structures of phosphoketolase thiamine diphosphate-dependent dehydration mechanism. *J. Biol. Chem.* **285**, 34279-34287
22. Pletcher, J., and Sax, M. (1972) Crystal and molecular structure of thiamine pyrophosphare hydrochloride. *J. Am. Chem. Soc.* **94**, 3998-4005

23. Kluger, R. (1987) Thiamin diphosphate: a mechanistic update on enzymic and nonenzymic catalysis of decarboxylation. *Chem. Rev.* **87**, 863-876

24. Planas, F., Sheng, X., McLeish, M. J., and Himo, F. (2018) A theoretical study of the benzoylformate decarboxylase reaction mechanism. *Front. Chem.* **6**

25. Pallitsch, K., Rogers, M. P., Andrews, F. H., Hammerschmidt, F., and McLeish, M. J. (2017) Phosphonodifluoropyruvate is a mechanism-based inhibitor of phosphonopyruvate decarboxylase from *Bacteroides fragilis*. *Bioorganic Med. Chem.* **25**, 4368-4374

26. Flournoy, D. S., and Frey, P. A. (1989) Inactivation of the pyruvate dehydrogenase complex of *Escherichia coli* by fluoropyruvate. *Biochemistry* **28**, 9594-9602

27. Krissinel, E., and Henrick, K. (2007) Inference of macromolecular assemblies from crystalline state. *J. Mol. Biol*. **372**, 774-797

28. Hasson, M. S., Muscate, A., McLeish, M. J., Polovnikova, L. S., Gerlt, J. A., Kenyon, G. L., Petsko, G. A., and Ringe, D. (1998) The crystal structure of benzoylformate decarboxylase at 1.6 Å resolution: diversity of catalytic residues in thiamin diphosphate-dependent enzymes. *Biochemistry* **37**, 9918-9930

29. Dobritzsch, D., König, S., Schneider, G., and Lu, G. (1998) High resolution crystal structure of pyruvate decarboxylase from *Zymomonas mobilis*. Implications for substrate activation in pyruvate decarboxylases. *J. Biol. Chem.* **273**, 20196-20204

30. Leung, L. S., and Frey, P. A. (1978) Fluoropyruvate: an unusal substrate for *Escherichia coli* pyruvate dehydrogenase. *Biochem. Biophys. Res. Commun.* **81**, 274-279

31. Nemeria, N., Chakraborty, S., Baykal, A., Korotchkina, L. G., Patel, M. S., and Jordan, F. (2007) The 1′,4′-iminopyrimidine tautomer of thiamin diphosphate is poised for catalysis in asymmetric active centers on enzymes. *Proc. Natl. Acad. Sci. U. S. A.* **104**, 78-82

32. Schroder-Tittmann, K., Meyer, D., Arens, J., Wechsler, C., Tietzel, M., Golbik, R., and Tittmann, K. (2013) Alternating sites reactivity is a common feature of thiamin diphosphate-dependent enzymes as evidenced by isothermal titration calorimetry studies of substrate binding. *Biochemistry* **52**, 2505-2507

33. Pettersen, E. F., Goddard, T. D., Huang, C. C., Couch, G. S., Greenblatt, D. M., Meng, E. C., and Ferrin, T. E. (2004) UCSF Chimera - A visualization system for exploratory research and analysis. *J. Comput. Chem.* **25**, 1605-1612

CHAPTER 5. GROWTH COMPLEMENTATION STUDIES ON ACTIVE SITE VARIANTS OF *KLEBSIELLA PNEUMONIAE* ACETOLACTATE SYNTHASE

5.1 Introduction

Acetohydroxyacid synthase (AHAS), a ThDP-dependent enzyme, has long been known as the target of the broadly used imidazolinone and sulfonylurea herbicides (1-7). These classes of herbicides are used worldwide and accounted for approximately $2.3 billion in annual sales in 2014 (8). These compounds are quite potent with application rates of 10-100 g per hectare and show low toxicity toward humans. In fact, some non-herbicidal derivatives of the sulfonylureas are even used in the treatment of diabetes mellitus type 2 (9,10). The relative safety of these compounds makes them attractive for use in fields to control unwanted weed growth. However, many crops of interest are also negatively affected by these compounds, making non-targeted treatment of a whole field difficult. This problem could be mediated if a resistant form of the desired crop were to be engineered. Planting of the engineered crop would then allow for nonspecific application of these herbicides to a whole field without negative effects toward the engineered plant. This chapter describes the initial steps toward achieving such a goal including: i) identification of an enzyme resistant to the herbicidal inhibitors, ii) establishment of a growth complementation assay to probe for AHAS activity in knockout stains of *E. coli,* and iii) preliminary mutagenesis studies on engineering an enzyme capable of fulfilling the biosynthetic role of AHAS while maintaining resistance to the sulfonylurea and imidazolinone herbicides.

5.1.1 Basis for herbicidal activity of AHAS inhibitors

In plants, bacteria and fungi, branched chain amino acids (BCAAs) are synthesized from two compounds, acetolactate and acetohydroxybutyrate (Figure 5.1).

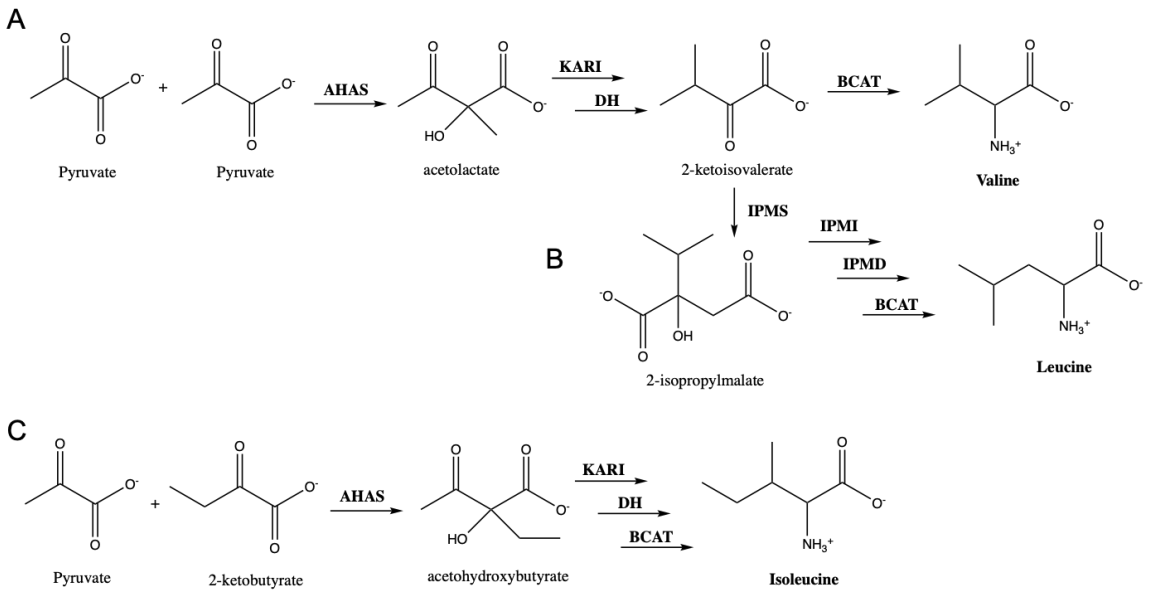

Figure 5.1: Biosynthesis of A) valine, B) leucine, and C) isoleucine starting with pyruvate and α-ketobutyrate. Abbreviations used are: AHAS, acetohydroxyacid synthase; KARI, ketol-acid reductoisomerase; DH, dihydroxyacid dehydratase; BCAT, branched-chain amino acid aminotransferase; IPMS, 2-isopropylmalate synthase; IPMI, isopropylmalate isomerase; IPMD, 3-isopropylmalate dehydrogenase.

Figure 5.1 shows that acetolactate is a precursor to valine and leucine, while acetohydroxybutyrate is a precursor to isoleucine. Acetolactate is formed by the condensation of two molecules of pyruvate, while acetohydroxybutyrate is formed by the condensation of one molecule of pyruvate and one molecule of α-ketobutyrate. The formation of both compounds is catalyzed by AHAS, the first step in the pathway.

One of the interesting and unique features of these pathways is the fact that the same enzyme cascade catalyzes the formation of both valine and isoleucine, as well as many of the precursors to leucine. In order to maintain a consistent level of each amino acid, the pathways are heavily regulated, although the mechanisms of regulation are not completely understood (9). Accordingly, inhibition of the enzymes, AHAS, ketol-acid reductoisomerase (KARI), dihydroxyacid dehydratase (DH), or branched-chain amino acid aminotransferase (BCAT) would likely prevent formation of not one, but all three amino acids. Since these amino acids are essential for growth, inhibition of this pathway would, presumably, lead to death of the target organism.

By contrast, mammals do not possess these biosynthetic pathways; they must acquire these amino acids through dietary means (9). Targeting these pathways and their regulation mechanisms

provides an opportunity for development of herbicidal and antibacterial compounds with low human toxicity. Indeed, at least two enzymes in these pathways, AHAS and KARI, have been targeted in herbicide development (11). Additionally, the enzyme catalyzing the final step in valine and isoleucine biosynthesis, BCAT, has been identified as susceptible to inhibition by PLP inactivators. However, BCAT is a less desirable target as mammals express homologues of this enzyme for amino acid degradation pathways (12), thus increasing the possibility of toxicity towards humans and animals.

The imidazolinone and sulfonylurea herbicides are two classes of AHAS inhibitors that prevent the formation of acetolactate and acetohydroxybutyrate for BCAA production. They have been shown to be potent herbicides with low toxicity toward mammals. Reported LD_{50} values for the sulfonylurea compounds are as high as 6 g/kg of body weight in rats (9), likely this is due to the lack of mammalian homologues of AHAS (13).

Interestingly, although plants and bacteria use the same pathways to synthesize the BCAAs, growth studies on various bacterial strains have shown differential levels of bacterial toxicity when exposed to these herbicides. This indicates some level of specificity toward the plant-derived enzymes, differential levels of cell uptake, or the presence of degradation pathways. As many studies report similar levels of inhibition of purified AHASs from plants and bacteria, degradation pathways and varied levels of cellular uptake are likely explanations for the disparity in toxicity. Regardless, these studies showed that many of the compounds still have significant toxic effects toward many bacteria (14,15).

Off-target toxic effects, *i.e.*, undesired toxicity toward crops such as corn, beans, etc., by these herbicides are reported at concentrations as low as 1/100 of a typical effective dose (16). This makes whole field treatment an unattractive option in most cases, as it would cause a large reduction in total crop yield. Therefore, to allow for broad application to whole fields will necessitate the development of crops resistant to these herbicides.

5.1.2 Design of herbicide resistant crops

Development of herbicide-resistant plants has previously seen wild success. In 1974, glyphosate, or trade name Roundup®, was brought to market by Monsanto. As with the sulfonylurea and imidazolinone herbicides, glyphosate was quickly found to be a “broad spectrum” herbicide effectively killing almost every plant on which it was applied. Unfortunately, glyphosate

is as effective at killing crops as it is at controlling weeds. To remedy this, Monsanto released the first glyphosate resistant "Roundup Ready®" crop in 1996 (17). Since then, the range of Roundup Ready® crops has grown and glyphosate has become the most widely-used herbicide around the world. However, this widespread and consistent use has led to the emergence of more than 30 different species of glyphosate-resistant weeds, necessitating the development of new crop treatment options (18-20).

Glyphosate acts by inhibiting 5-enolpyruvylshikimate-3-phosphate (EPSP) synthase, an enzyme important in biosynthesis of aromatic amino acids and other essential biological compounds (21). It was discovered that while the EPSP synthases from plants are inhibited by glyphosate, not all of the orthologues from bacteria were subject to the same inhibition. Eventually, a resistant enzyme from *Agrobacterium* sp. CP4 was identified and inserted into the plant genome, conferring herbicide resistance to the host plant (22).

It is not unreasonable to speculate that, in a similar manner, insertion of an AHAS enzyme resistant to inhibition by sulfonylurea and imidazolinone herbicides into a plant genome could confer herbicide resistance to that plant. In this chapter, we explore the possibility that acetolactate synthase from *Klebsiella pneumoniae* (*Kp*ALS) might act as such an enzyme.

5.1.3 ALS as a potential replacement for AHAS in herbicide resistant crops

Like AHAS, ALS catalyzes the ThDP-dependent formation of acetolactate from pyruvate. Although they catalyze the same reaction, ALS and AHAS exhibit distinct differences including reaction kinetics, as shown in Chapter 3, cofactor dependence, and substrate profile. While these differences do not necessarily prohibit the use of ALS as a replacement for AHAS, they should be investigated to determine the potential for an ALS, such as *Kp*ALS discussed here, to fulfill the biosynthetic role of AHAS.

With the X-ray structure solution of AHAS from a yeast (*Saccharomyces cerevisiae*) and a plant (*Arabidopsis thaliana*), both in complex with sulfonylurea and imidazolinone herbicides, the binding mode of the compounds can be identified (6,7,23). Interestingly the sulfonylurea herbicides, specifically chlorsulfuron, do not bind in the active site. Instead they bind in the channel leading to the active site, thereby blocking substrate access (6,7,23). Figure 5.2A shows the interactions of chlorsulfuron in the active-sites of the AHAS from *S. cerevisiae* (*Sc*AHAS) and a homology model of AHAS from *K. pneumoniae* (*Kp*AHAS) generated by the PHYRE2 Protein

Fold Recognition Server (24) using the *Sc*AHAS:chlorsulfuron structure (PDB ID:1T9B) as the template. Even a cursory inspection of the chlorsulfuron binding pocket in both *Sc*AHAS and *Kp*AHAS shows that the majority of the enzyme-chlorsulfuron interactions are conserved. Given that *Sc*AHAS is inhibited by chlorsulfuron, *Kp*AHAS would be expected to be similarly inhibited.

The AHAS:chlorsulfuron structures were then aligned with an X-ray structure of *Kp*ALS (PDB ID: 5WDG) in order to compare binding interactions between the yeast and bacterial AHAS, and a bacterial ALS (Figure 5.2B). It was readily apparent that *Kp*ALS had several unfavorable steric interactions with the inhibitor suggesting that chlorsulfuron is unlikely to be an inhibitor of *Kp*ALS.

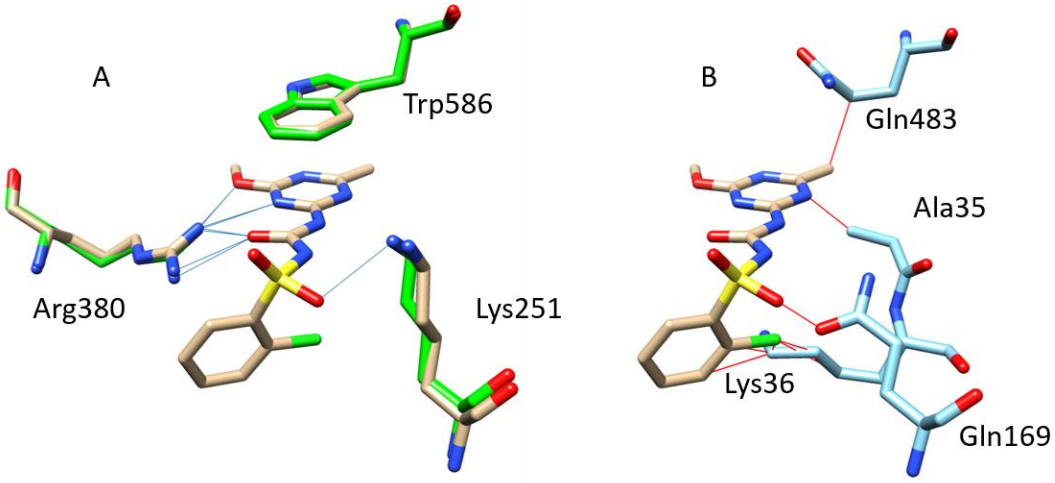

Figure 5.2: A comparison of chlorsulfuron binding sites. A) Overlay of *Sc*AHAS with bound chlorsulfuron (tan) with aligned homology model of *Kp*AHAS (green). Hydrogen bonds are shown as blue lines. B) Model of chlorsulfuron binding in *Kp*ALS (blue). Steric clashes are shown as red lines. Hydrogen bond and steric clash analyses were performed in UCSF Chimera (25).

As seen in Figure 5.2, Arg380 shows strong hydrogen bonding interactions with the carbonyl oxygen, one of the nitrogen atoms in the triazine ring, and with the hydroxyl substituent on the triazine ring in the inhibitor. Additionally, a strong π-stacking interaction is observed between the triazine ring and Trp586. Interestingly, an additional interaction is predicted between one of the sulfone oxygens in chlorsulfuron and Lys251 in the model of *Kp*AHAS. While this residue is conserved in both *Kp*AHAS and *Sc*AHAS, they are present in different rotamers with the residue in *Sc*AHAS pointed away from the herbicide. As such, it is likely that the difference is simply a result of the modeling process.

In contrast to the picture in AHAS, the putative chlorsulfuron binding-site in *Kp*ALS shows no obvious hydrogen bond interactions and the aromatic tryptophan residue (Trp586) has been replaced by a glutamine (Gln483) thereby removing any possibility of π-stacking interactions. Indeed, it appears that almost all of the favorable binding interactions observed in AHAS have been replaced with unfavorable interactions in *Kp*ALS. The hydrogen bond with Lys251 is replaced with a clash with Gln169, and many close contacts are observed between the chlorine of chlorsulfuron and Lys36 of *Kp*ALS. The latter clash is avoided in AHAS as lysine is replaced by an alanine in that position. Given the presence of several strong H-bond and π-stacking interactions, and the lack of any obvious steric clashes, it is not surprising that this class of AHAS inhibitors generally have reported K_i values in the low nM range (9).

Surprisingly, a literature search showed no reports of these compounds being tested for inhibition of ALS. Accordingly, to test the hypothesis that ALS would not be inhibited by compounds of this type, chlorsulfuron was used in a preliminary inhibition study carried out with both *Kp*ALS and *Kp*AHAS (see sections 2.6.1 and 2.6.2 for a detailed description).

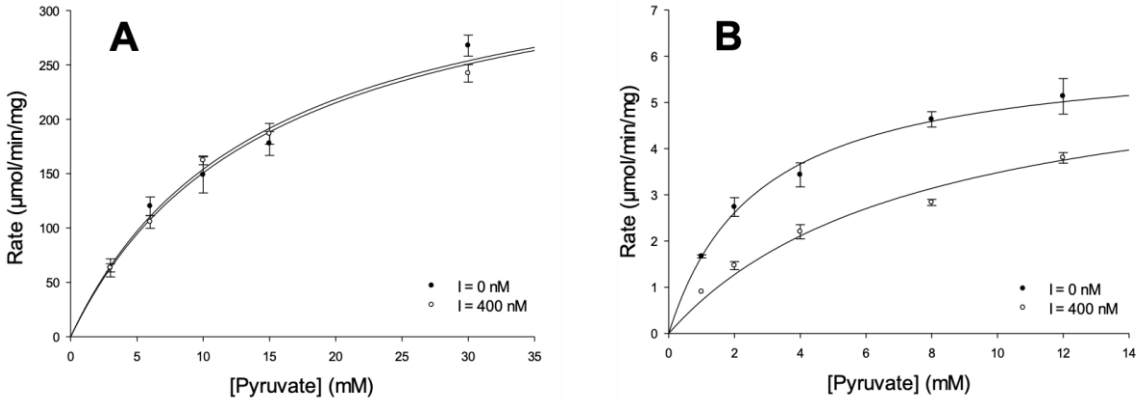

Figure 5.3: Steady-state kinetic plots for A) *Kp*ALS, and B) *Kp*AHAS in the presence (●) and absence (○) of chlorsulfuron (400 nM).

As expected from the structural analysis, *Kp*ALS was essentially unaffected by the presence of 400 nM chlorsulfuron. Conversely, *Kp*AHAS was clearly inhibited at that concentration. The inhibition appeared competitive in nature, and the K_i for chlorsulfuron was determined to be 220 nM. This value is still in the nM range, although it is 10-fold higher than that reported for the plant homologue from *A. thaliana* at 21 nM (26), and ~2-fold higher than that

reported for the yeast enzyme (27). These differences may be ascribed to the fact that *Kp*AHAS is a bacterial enzyme, possibly with some distinctive yet to be characterized properties. Alternatively, they could be due, at least in part, to the fact that these compounds commonly show time-dependent inhibition with full inhibition observed only after long incubation periods (28). As this was a simple screening for *Kp*ALS resistance, no pre-incubation was performed before initial rates were measured.

The role of the FAD cofactor in the AHAS mechanism, is currently the subject of some discussion. Certainly it has been implicated in the time-dependent inactivation (29). As can be seen in the X-ray structures, binding of the sulfonylurea herbicides blocks substrate access to the active site thereby causing the initial inhibition. This is followed by time-dependent oxidation of the FAD cofactor, which is required to be in its reduced form during catalysis (23,29-31). Given that ALS does not generally contain FAD (32) it is unlikely that similar time-dependent inactivation will be seen in *Kp*ALS. The lack of FAD and absence of any rapid-onset inhibition indicates that it is possible that *Kp*ALS will remain active during any *in vivo* treatment with the sulfonylurea herbicides.

While not specifically germane to the subject at hand, it is interesting to report on the current debate about the role of FAD. Why AHAS requires reduced FAD for catalysis is still largely unknown, although it has generally been accepted that the cofactor plays a structural role in the reaction rather than an active redox role (9,33). In the past year or so, a new reaction mechanism has been proposed for *Sc*AHAS, a mechanism that disputes the idea that the role of FAD is purely structural (34). This mechanism suggests that the FAD cofactor and an oxygen molecule bound in the active site participate in two single electron transfers each in the catalytic cycle (Figure 5.4).

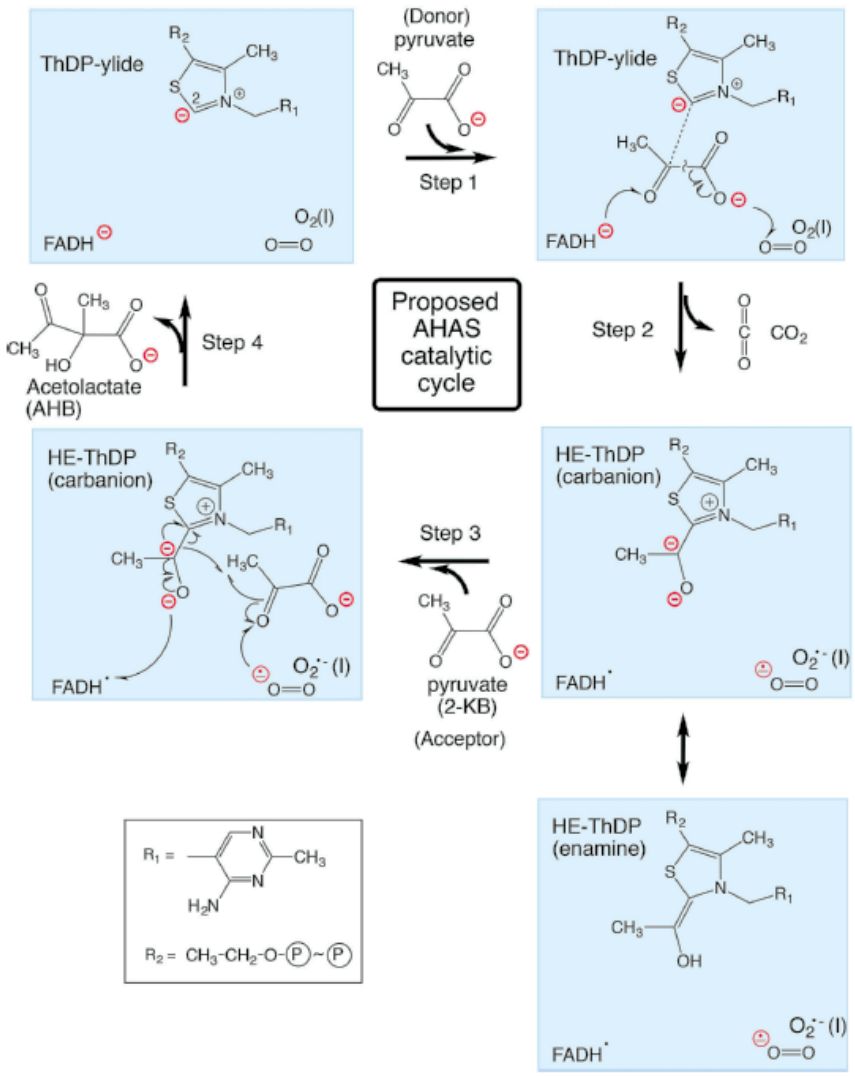

Figure 5.4: Proposed mechanism in *Sc*AHAS involving FAD.
Reproduced from Lonhienne *et al.* (34).

This new mechanism is quite different to the widely accepted mechanism (Figure 1.15) that was discussed in Chapter 1. While it does provide an explanation as to why reduced FAD is required for AHAS activity, previous experiments indicate that it might not be completely correct. NMR studies on AHAS from *E. coli* (*Ec*AHAS) showed clearly the presence of the LThDP intermediate (35,36). However, if the newly proposed mechanism was correct, this observation would be unlikely as attack on the first substrate is proposed to be in concert with decarboxylation (34), meaning that the LThDP intermediate should not be observed.

A similar concerted mechanism is also proposed for attack on the second substrate. In the same way, this would prevent the observation of ALThDP, yet it was also seen in the NMR

experiments (35,36). This indicates either the bacterial *Ec*AHAS and the fungal *Sc*AHAS operate by different mechanisms, or that the concerted steps in the new mechanism cannot be correct. It would be informative to see the NMR experiments carried out on *Sc*AHAS. If LThDP/ALThDP were to be observed in that study it would mitigate strongly against the new mechanism. Certainly, if proved to be correct, this mechanism challenges the long-held belief that ALS and AHAS employ the same reaction mechanism. Put simply, that would be impossible as ALS does not possess, or show a need for, FAD.

5.2 Establishment of a growth complementation assay

After finding that *Kp*ALS appears resistant to inhibition by chlorsulfuron *in vitro*, the next step in testing the viability of using ALS to confer herbicide resistance is to determine whether it is able to act as a functional AHAS *in vivo*. One potential problem may preclude the enzyme being used as a replacement for AHAS is that ALS is known to have a strong preference for pyruvate, not α-ketobutyrate, as the acceptor substrate. This results in acetolactate being the predominant product (37-40), although it is not impossible that some acetohydroxybutyrate can be produced. The origins of this specificity are yet to be established, although there does appear to be some differences in the active sites of AHAS and ALS. Regardless, the ability of ALS to act as a functional AHAS *in vivo* has never before been examined. Testing this would be a major undertaking if one were to insert *Kp*ALS into a plant genome to test viability in plants directly. Fortunately, a simpler system can be used in which formation of acetolactate and acetohydroxybutyrate can be tested using knockout strains of *E. coli* (41).

To take this further, four *E. coli* strains were identified that lack the ability to form isoleucine and valine. The strains are derivatives of *E. coli* K12 and contain one or more mutations of the three *E. coli* AHAS isozymes, thereby rendering them unable to form acetolactate and acetohydroxybutyrate. These strains are designated MI168 (*ilvH612, λ⁻, relA1, thiE1*) (42), MI253 (*thr-10, araC14, ilvI614, ilvH612, λ⁻, relA1, thiE1*) (42), MI262 (*leuB6*(Am), *ilvI614, ilvH612, λ⁻, relA1 spoT1, ilvB619, ilvG605*(Am), *ilvG603*(Act), *thiE1*) (43), and FD1062 (*araC14, ilvI614, ilvH612, λ⁻, glyA18, relA1, spoT1, ilvB619, bglR20, rbs-5: :Tn5, ilvG468*(Act), *thiE1* (44). Sikdar and Kim (41) showed that transformation of a plasmid carrying a functional AHAS gene into each of these strains allows growth on minimal media lacking isoleucine and valine.

5.2.1 Construction of the pBAD*Kp*ALS expression vector

As these knockout strains do not contain the λ(DE3) lysogen, protein expression under control of the T7 promoter cannot be used. To overcome this, the *Kp*ALS gene was cloned into the pBAD/Myc-HisA expression vector, which uses the araBAD promoter. When using this vector, protein expression is induced in the presence of arabinose, and levels of expression can easily be modulated by manipulating the concentration of arabinose in the growth media (45).

Before ligation into the pBAD vector, PCR mutagenesis was used to remove an internal Nco1 restriction site from the *Kp*ALS gene. Mutagenesis primers were designed according to the QuikChange protocol and can be seen in Table 5.1. After removal of the internal Nco1 site, plasmid pBAD*Kp*ALS was constructed as described in section 2.2.2.

Table 5.1: PCR mutagenesis primers for removal of internal Nco1 site in the *Kp*ALS gene. Mismatches with template DNA are shown in lower case.

Primer Name	Sequence
*Kp*ALS* -Nco For	5'-GCGCgATGGCGGTGAAAGTGGATGTTTCTGACC-3'
*Kp*ALS* -Nco Rev	5'-GGTCAGAAACATCCACTTTCACCGCCATcGCGC-3'

5.2.2 Expression testing and strain selection

Following construction of the pBAD*Kp*ALS expression vector, it was transformed into *E. coli* BL21(DE3) to check the ability of the system to express the *Kp*ALS. The resulting colonies were used to inoculate small-scale expression cultures (5 mL) with and without 1% arabinose. Excellent over-expression was observed with no evidence of leaky expression in cultures without arabinose.

To test protein expression in the target system, the pBAD*Kp*ALS plasmid was transformed into each of the four AHAS deficient *E. coli* strains (MI168, MI253, MI262, and FD1062) together with *E. coli* Bl21(DE3) as a positive control. Cells were grown in 5 mL cultures of LB media overnight with and without addition of 1% arabinose. Crude cells extracts were then analyzed by SDS-PAGE to check for protein expression (Figure 5.5).

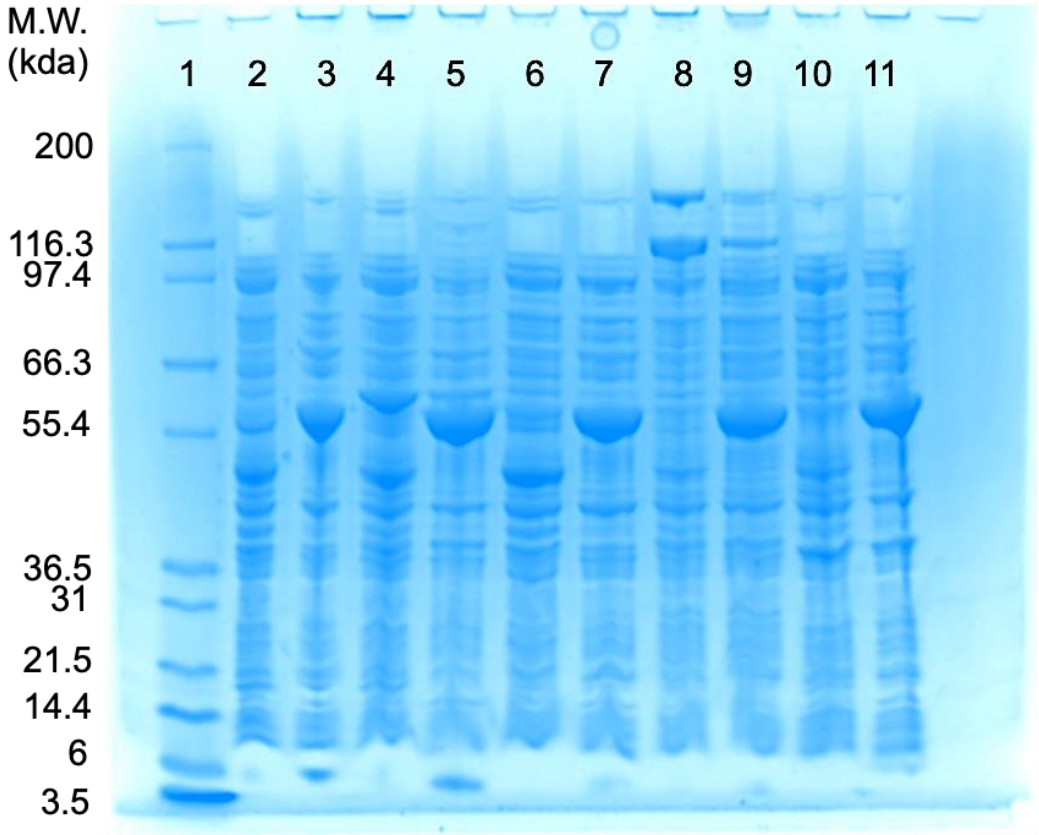

Figure 5.5: SDS-PAGE gel showing crude extracts of cells from expression test. A description of the lane contents can be found in the text. Expression of *Kp*ALS can be seen in lanes 3, 5, 7, 9, and 11.

Lane 1 contains Mark12™ protein standards (Life Technologies). Lane 2 contains a sample of transformed MI168 cells from a culture grown without (-) arabinose while lane 3 contains a sample of the same cells from culture grown with (+) arabinose. This (-)/(+) pattern continues across the gel. Lanes 4 and 5 contain MI253 cells; Lanes 6 and 7, MI262 cells; lanes 8 and 9 contain FD1062 cells; lanes 10 and 11 contain BL21(DE3) cells. The cultures containing 1% arabinose saw a heavy band appear between 55 and 66 kDa. This is consistent with arabinose-mediated expression of *Kp*ALS which has a calculated molecular mass of ~62.5 kDa.

Although the knockout strains all showed good expression of *Kp*ALS (Figure 5.5), MI262 was chosen as the optimal strain with which to carry out growth complementation experiments. This decision was made on two grounds. First, MI262 contains more mutations in the AHAS gene than MI168 and MI253, making it less likely to present false positives through reactivation of the AHAS genes. Second, although strain FD1062 contained the same number of AHAS mutations, it

exhibited a strange phenotype in which colonies were not well defined on the agar plates, making it overall inferior to MI262.

5.2.3 Growth on minimal media

The initial expression test cultures were grown in rich media (LB), *i.e.*, the cells were provided all amino acids required for growth. To test the ability of the expressed *Kp*ALS to act as a functional AHAS, the cells must be grown in media without isoleucine and valine supplements. As such, the expression test cultures were streaked on plates containing M9 minimal media without isoleucine and valine. The plates also contained 1% arabinose to induce protein expression (See section 2.6.4). After 36 hours, the only strain showing growth on these plates was BL21(DE3).

This result was expected if *Kp*ALS is not able to act as a functional AHAS. Presumably, this was due to *Kp*ALS not being able to form enough acetohydroxybutyrate for isoleucine synthesis. However, before this conclusion could be drawn, other factors had to be considered as potential explanations for the lack of cell growth. To understand these required the screening of multiple factors such as, arabinose concentration, supplementation with isoleucine and/or valine, and presence of selection antibiotic. The number of conditions to be tested led to the establishment of a liquid media based analysis employing a 96-well plate reader. The plate reader was set to take optical density measurements at 595 nm every 15 minutes over a 24 hour period. Throughout the growth period the 96-well plates were maintained at 37 °C with shaking between measurements. The readings were then plotted and growth curves were obtained.

To eliminate the possibility of slow or negligible growth being the result of too much selection pressure, the concentration of arabinose and the presence of antibiotic were tested as experimental variables. As the arabinose concentration controls expression levels, it was considered that, when cells were grown in minimal media, a high arabinose concentration could exhaust cellular stocks of amino acids by inducing too much protein expression. Although less likely, the effect of the ampicillin antibiotic was tested also, as the over-expression of β-lactamase could have a similar effect.

To test these possibilities, MI262 cells carrying the pBAD*Kp*ALS plasmid were grown in minimal media while the arabinose concentration was varied from 0.2% to 0.00002% in ten-fold increments, in the presence and absence of ampicillin. The plate layout can be seen in Table 5.2,

and the growth curves can be seen in Figure 5.6. In Table 5.2 each box represents a unique condition tested in triplicate.

The data presented in Figure 5.6 shows that arabinose concentration and presence of ampicillin had little to no effect on growth in minimal media. Most importantly however, the experiment confirmed that *Kp*ALS is not able to complement growth in media lacking both isoleucine and valine, concluding that direct replacement of AHAS by wild type ALS is not a viable option to confer herbicide resistance.

Table 5.2: Plate layout for testing arabinose concentration and presence of ampicillin on MI262 cell growth in minimal media. Each box represents conditions tested in triplicate.

	1	2	3	4	5	6	7	8	9	10	11	12
A	Water Blank			Media -Ilv			Media +Ilv			Media +Ilv +Amp		
B	MI262 -Ilv			MI262 +Ilv			MI262 +*Kp*ALS -Ilv			MI262 +*Kp*ALS +Ilv		
C	*Kp*ALS –Ilv +Amp			*Kp*ALS +Ilv +Amp			-			-		
D	*Kp*ALS -Ilv +Amp +0.00002% Ara			*Kp*ALS +Ilv +Amp +0.00002% Ara			*Kp*ALS -Ilv +0.00002% Ara			*Kp*ALS +Ilv +0.00002% Ara		
E	*Kp*ALS -Ilv +Amp +0.0002% Ara			*Kp*ALS +Ilv +Amp +0.0002% Ara			*Kp*ALS -Ilv +0.0002% Ara			*Kp*ALS +Ilv +0.0002% Ara		
F	*Kp*ALS -Ilv +Amp +0.002% Ara			*Kp*ALS +Ilv +Amp +0.002% Ara			*Kp*ALS -Ilv +0.002% Ara			*Kp*ALS +Ilv +0.002% Ara		
G	*Kp*ALS -Ilv +Amp +0.02% Ara			*Kp*ALS +Ilv +Amp +0.02% Ara			*Kp*ALS -Ilv +0.02% Ara			*Kp*ALS +Ilv +0.02% Ara		
H	*Kp*ALS -Ilv +Amp +0.2% Ara			*Kp*ALS +Ilv +Amp +0.2% Ara			*Kp*ALS -Ilv +0.2% Ara			*Kp*ALS +Ilv +0.2% Ara		

*Kp*ALS – indicates media was inoculated with MI262 cells transformed with pBAD*Kp*ALS
+Ilv – indicates media is supplemented with isoleucine and valine
-Ilv – indicates media without isoleucine and valine
% Ara – indicates final arabinose concentration in weight percent

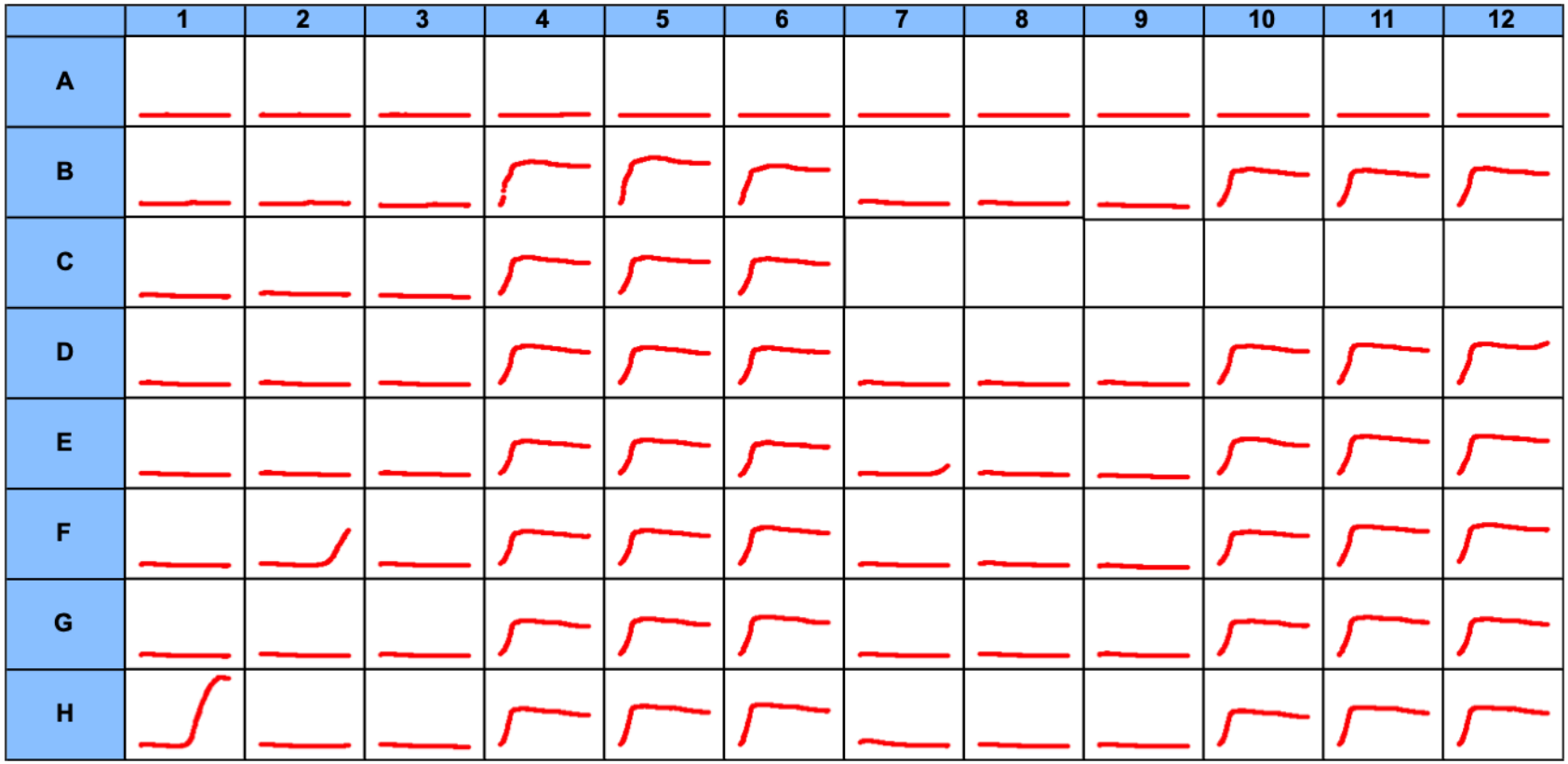

Figure 5.6: Growth curves of MI262 cells in minimal media with and without isoleucine and valine.

5.2.4 Growth complementation in media without valine supplementation

To determine whether *Kp*ALS can complement growth under any conditions, experiments were performed using media that contained only one of the amino acids, either isoleucine or valine.

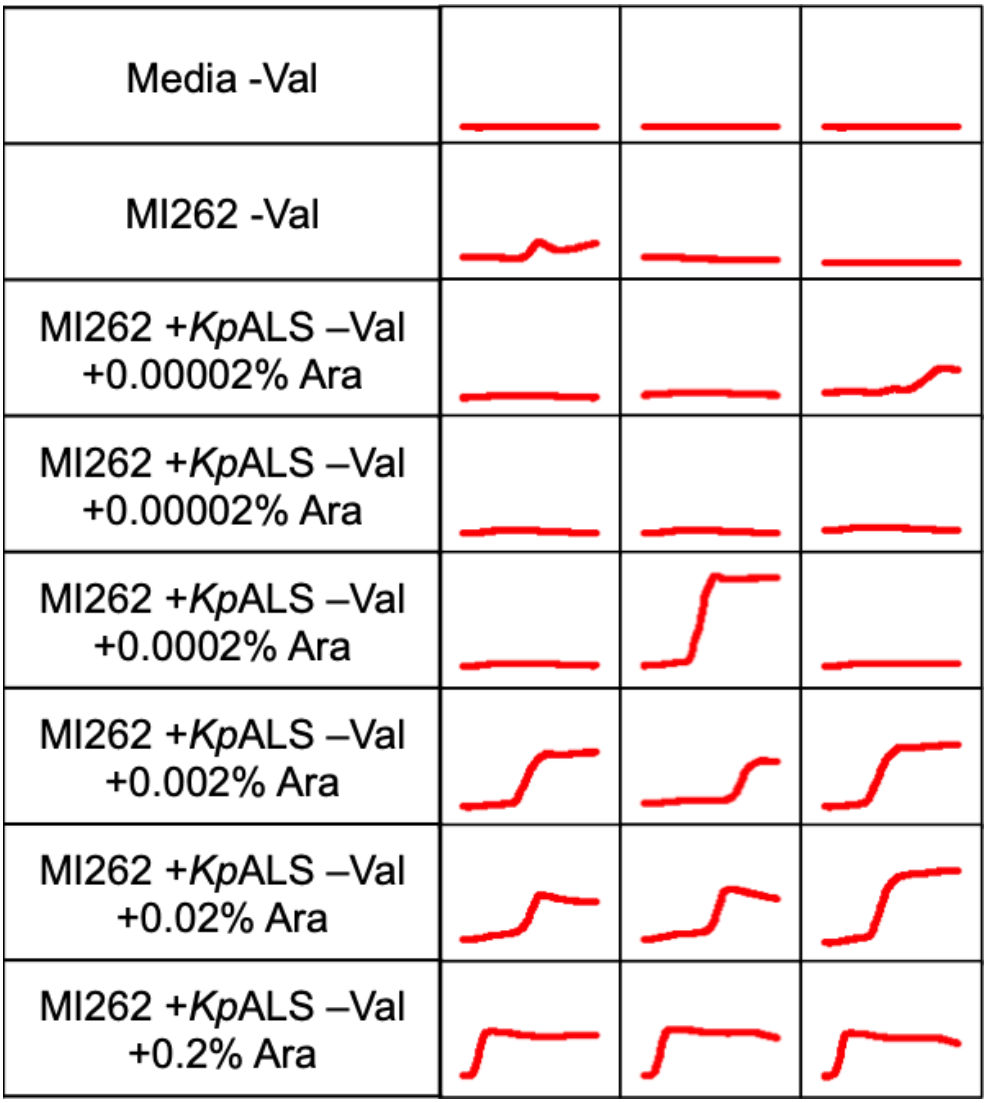

Figure 5.7: Plate setup and results from growth complementation studies in media without valine. Each condition was tested in triplicate.

Figure 5.7 shows clearly that, when sufficient *Kp*ALS is expressed, the enzyme is able to complement growth in media lacking valine. Consistent growth complementation was observed at arabinose concentrations of 0.002% and higher. However, long lag phases were observed at

arabinose concentrations below 0.2%. Unfortunately, no growth was observed in media lacking isoleucine (data not shown).

One problem arising from these experiments was the observation of false positives. A prime example of this is the growth seen in one of the wells containing 0.0002% arabinose (Figure 5.7). This was ruled a false positive as growth was only observed in one out of three replicates. False positives were observed in other experiments so care was taken to verify results.

In a final experiment to determine the viability of the methodology, MI262 cells were transformed with an expression vector containing the gene encoding for *Kp*AHAS. The plasmid, pBAD*Kp*IlvGM, was constructed as described in Section 2.2.3. The transformed MI262 cells were then grown in three minimal media conditions: i) -valine, ii) -isoleucine, and iii) -isoleucine and -valine. As seen in Figure 5.8, excellent growth complementation was observed all media conditions when *Kp*AHAS was expressed in the cells.

In summary, *Kp*ALS was able to promote growth only in media that contained supplemental isoleucine whereas *Kp*AHAS was able to promote growth in media lacking both isoleucine and valine.

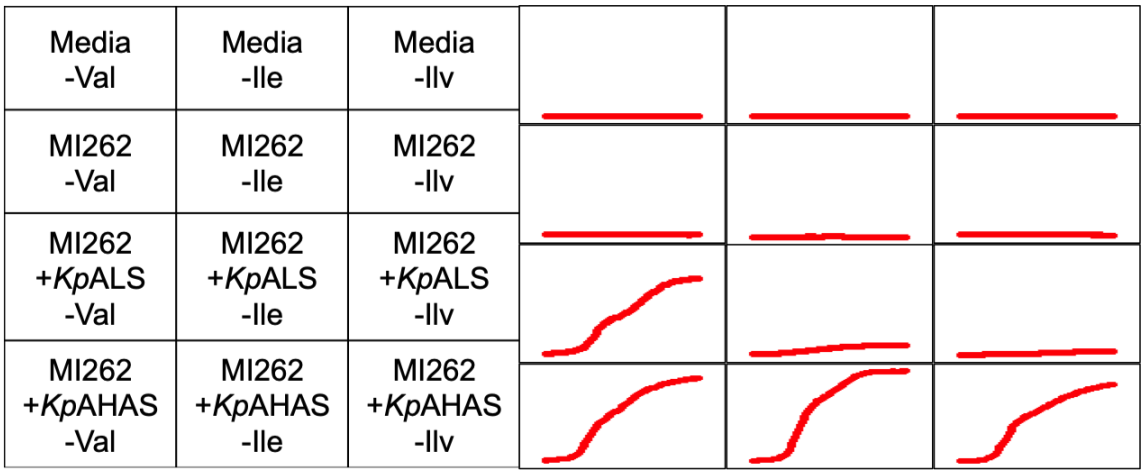

Figure 5.8: Growth of MI262 cells transformed with vectors containing *Kp*ALS and *Kp*AHAS.

5.3 Mutagenesis of *Kp*ALS to promote growth complementation

5.3.1 Identification of candidate residues for mutagenesis

The results from the previous section provide evidence that (i) the growth complementation assay is a suitable screen for AHAS activity and (ii) the lack of growth complementation by *Kp*ALS stems directly from its inability to support isoleucine biosynthesis. Knowing that acetohydroxybutyrate is the product of the carboligation of a pyruvate donor and a α-ketobutyrate acceptor, and that KpALS can use pyruvate as an acceptor, the question then becomes, "can mutagenesis be used to modify *Kp*ALS to use α-ketobutyrate as an acceptor?"

The active site of *Kp*ALS was examined for clues as to which residues could have an influence on substrate specificity. The structure of *Kp*ALS soaked with pyruvate (described in Chapter 3), contains ALThDP, the reaction intermediate formed just before product release. This is significant as it can provide insight on which residues are in close proximity to the intermediate. Focus was placed on the methyl groups, particularly that of the acceptor substrate (orange, Figure 5.9), as the other atoms in the reaction intermediate (*i.e.* the oxo and carboxyl moieties) likely exhibit a similar conformation during acetohydroxybutyrate formation. During formation of acetohydroxybutyrate, this methyl group is replaced by the larger ethyl group.

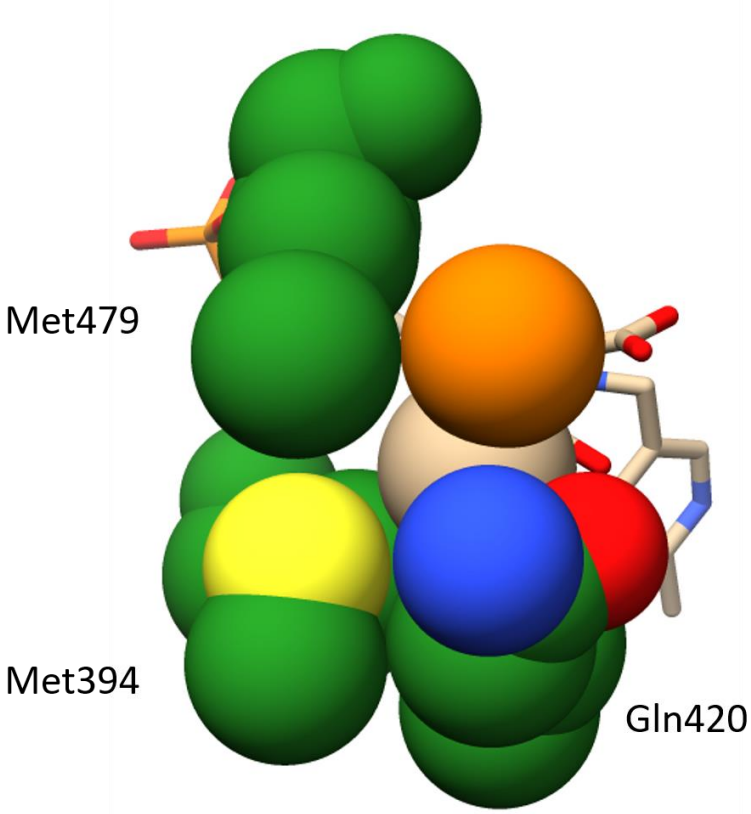

Figure 5.9: Active site residues (green) near the donor and acceptor methyl groups of ALThDP (tan and orange, respectively).

As seen in Figure 5.9, the active site in *Kp*ALS appears too tight to accommodate an ethyl group in this position. The three residues surrounding the methyl groups of ALThDP were identified as Met394, Gln420, and Met479. These three residues appear to surround both methyl groups, and it is clear that a larger acceptor substrate such as α-ketobutyrate would be subject to significant steric interference. As such, all three residues were considered as candidates for mutagenesis studies in an attempt to open the active site to accommodate α-ketobutyrate. Additionally, another residue, Gln483 was considered due to its proposed involvement in positioning of the acceptor substrate (46), as discussed in Chapter 3.

Of the residues identified for mutagenesis, only Met479 is conserved in *Kp*AHAS. Met394 is replaced by valine, Gln420 by glycine residue and a tryptophan residue is found in a spatially similar position to Gln483.

5.3.2 Generation and functional testing of active site variants

The first variants of *Kp*ALS to be tested, M394V and Q420A, were generated using site-directed mutagenesis. These variants were chosen as they would potentially mimic the active site of AHAS at each position. For Q420A, alanine was chosen over glycine to ensure that the protein backbone structure was affected as little as possible by the change. Sequences of primers used in the preparation of the *Kp*ALS variants are presented in Table 5.3. All variants were generated using the methods described in section 2.6.3 using the pBAD*Kp*ALS plasmid as a template.

Table 5.3: List of primers used for mutagenesis of pBAD*Kp*ALS.

Primer Name	Sequence
M394V For	5’-CCGTGGACgTGGGaAGCTTCCATATCTGGATTGCCCGCTACC-3’
M394V Rev	5’-GGTAGCGGGCAATCCAGATATGGAAGCTtCCCACGtCCACGG-3’
Q420A For	5’-GTGATGATCTCCAACGGCCAGgcGACcATGGGCGTCGCCCTGCCCTG-3’
Q420A Rev	5’-CAGGGCAGGGCGACGCCCATgGTCgcCTGGCCGTTGGAGATCATCAC-3’
Q420 SSM For	5’-CTCCAACGGCCAGnnkACcATGGGCGTCGCCCTGC-3’
Q420 SSM Rev	5’-GCAGGGCGACGCCCATgGTknnCTGGCCGTTGGAG-3’
M479A/Q483A For	5’-GGCTACAACgcGGTCGCTATCgcGGAAGAGAAAAAATATCAGaGaCTGTCCGGCGTCGAG-3’
M479A/Q483A Rev	5’-TTCTCTTCCgcGATAGCGACCgcGTTGTAGCCGTTATCGACCCAGATAAGATGCAGCACG-3’

Bases in lowercase indicate mismatch with the template DNA.
Primers were designed to include an extra silent mutation to introduce or remove a restriction site for quick screening following PCR

The first *Kp*ALS variant to be tested was M394V. Growth complementation studies were performed with cells transformed with this variant in media lacking valine (-Val), isoleucine (-Ile), and both valine and isoleucine (-Ilv). The variant was seen to exhibit patterns similar to that of the wild-type enzyme in that growth was only observed in media lacking valine, *i.e.* absence of isoleucine in the media resulted in no cell growth. However, one major difference was observed. The M394V variant was only able to complement growth in media containing at least 0.2% arabinose. This indicated that, while the variant was still active, it is possibly less active than the wild-type enzyme.

The second variant to be tested was Q420A. This variant was tested in all media conditions, and again, growth was only observed in media lacking valine. Taken together, testing of the M394V and Q420A variants indicate that simply swapping residues to mimic the active site of another enzyme does not always give the expected results indicating the necessity of a broader approach. Such a lesson has been learned previously in this laboratory while attempting to engineer the active site of another ThDP-dependent enzyme, benzoylformate decarboxylase (47).

One such approach would be to use saturation mutagenesis to simultaneously introduce multiple different residues into a given position. This technique has shown positive results in a variety of cases from inverting stereospecificity to altering the substrate profile of an enzyme (47-50). Further, in addition to using saturation mutagenesis, introducing mutations at multiple sites, either iteratively or simultaneously, would be more likely provide a *Kp*ALS variant able to support growth in media without isoleucine.

Although Met394 and Met479 were also identified as mutagenesis candidates based on proximity to the acetolactyl moiety (Figure 5.8), it was noted that Met479 is conserved in AHAS, and Met394 is expected to contribute more to the specificity of the donor rather than the acceptor substrate (Figure 5.8). Although the possibility cannot be ruled out, mutation of these residues was considered less likely to promote use of α-ketobutyrate as an acceptor substrate. Consequently, Gln420 was chosen as the first target for saturation mutagenesis as it was predicted to be the largest single contributor to the substrate specificity in *Kp*ALS. To examine this, degenerate primers were designed to introduce mutations at this position.

Site-saturation mutagenesis was performed as outlined in Section 2.6.3. One of the pitfalls of this technique is the screening burden following mutagenesis particularly if a completely random (NNN) library is used. As such, the degenerate primers (Table 5.3) were designed using

an NNK library. This library permits the screening required to ensure 95% coverage of all the possible amino acids at the position of interest to be completed using a single 96-well plate (51).

Following mutagenesis, it was discovered that MI262 cells showed poor transformation efficiency when transformed using the PCR mixture. To alleviate this, the PCR mixture was instead transformed into TOP10 cells and plated on agar containing ampicillin. Resulting colonies were then collected, mixed and grown in a 3 mL culture, before the plasmid DNA was extracted for transformation into MI262 cells. Using this methodology, the transformation proved to be much more efficient, providing significantly more colonies that obtained if the PCR mixture was directly transformed into MI262 cells.

The colonies of MI262 cells transformed with site-saturation mutants of Q420X were individually picked and tested for growth in (-Val) and (-Ile) media. As with the previously tested variants, growth was only observed in media lacking valine. Further mutagenesis was performed to create double variants M394V/Q420X and M479A/Q483A, all yielding the same results, *i.e.*, no growth was observed in media lacking isoleucine.

5.4 Summary and Conclusions

Conferring specific herbicide resistance to plants through expression of an enzyme resistant to inhibition by that herbicide has seen great commercial success (22). While this is an attractive option to control unwanted growth in crop production, identification of a suitable target enzyme is not trivial. The work described in this chapter demonstrates this quite well. Initially, it was shown that *Kp*ALS was not inhibited by the sulfonylurea herbicide, chlorsulfuron (Figure 5.3), and comparison of the sulfonylurea binding site in AHAS, with the homologous site in *Kp*ALS indicated that important residues were lacking in the latter. Given that X-ray structures have shown imidazolinone herbicides to bind in a similar manner (7), it may be expected that *Kp*ALS would be resistant to both classes of herbicides. Consequently, an appropriately modified *Kp*ALS would appear to be a strong candidate to confer herbicide resistance to a target plant.

Using AHAS knockout strains of *E. coli* it was determined that wild-type *Kp*ALS was not able support growth in the absence of isoleucine, but was able to compensate for the absence of valine. This was not surprising as it has been shown (Chapter 3) that ALS catalyzes the formation of the valine precursor, acetolactate, but not acetohydroxybutyrate which is required for the biosynthesis of isoleucine.

While acetolactate is formed from two molecules of pyruvate, acetohydroxybutyrate is formed from one molecule of pyruvate and one molecule of a marginally larger substrate, α-ketobutyrate (Figure 1.13). Remarkably, it appears that *Kp*ALS is able to effectively discriminate between pyruvate and α-ketobutyrate based on the presence of a single methyl group. The residues in *Kp*ALS most likely to contribute to this specificity were identified as Met394, Gln420, Met479, and Gln483. In an attempt to open the active site to accommodate the larger substrate these residues were subjected to site-directed mutagenesis, and, in the case of Gln420, site-saturation mutagenesis. Unfortunately, none of these attempts produced a *Kp*ALS variant able to support growth in isoleucine deficient minimal media.

With the benefit of hindsight, and some experiments described in Chapter 3, it is perhaps not surprising the growth complementation experiments were not successful. But that does not necessarily mean the mutagenesis was not a success as it should be recognized that inability to support cell growth does not necessarily indicate a total inability to use α-ketobutyrate as an acceptor substrate. Over 30 years ago it was established that cellular levels of α-ketobutyrate are nearly 100-fold lower than those of pyruvate (52,53). This presents a sizeable challenge; *Kp*ALS likely cannot be engineered to simply utilize α-ketobutyrate, it must to be engineered to have a strong preference for it as the acceptor substrate. If this does not happen, *in vivo* pyruvate will out-compete α-ketobutyrate.

As shown in Chapter 3, wild-type *Kp*ALS shows a ~10-fold preference for pyruvate as an acceptor substrate. When that is considered in conjunction with the cellular levels of pyruvate and α-ketobutyrate, a rough calculation suggests that, *in vivo*, *Kp*ALS will likely form ~1000-fold more acetolactate than acetohydroxybutyrate. On the other hand, *Kp*AHAS showed a ~70-fold preference for α-ketobutyrate so, under the same conditions *Kp*AHAS will form acetolactate and acetohydroxybutyrate in roughly equal amounts.

Continuing in that vein, to engineer *Kp*ALS so as to catalyze the formation of these products in a ratio equivalent to that catalyzed by *Kp*AHAS, a ~700-fold increase in preference for α-ketobutyrate will be required. To make things more difficult, *Kp*ALS has a K_m value for pyruvate at least 2-fold higher than that of *Kp*AHAS, making the latter better equipped to cope with low intracellular levels. While it is not impossible that *Kp*ALS could ultimately achieve the specificity required, there certainly can be no guarantee that it will. Given the magnitude of the task, it may

prove easier to develop an herbicide-resistant AHAS rather than engineering the active site of *Kp*ALS.

References

1. Chaleff, R. S., and Mauvais, C. J. (1984) Acetolactate synthase is the site of action of two sulfonylurea herbicides in higher plants. *Science* **224**, 1443-1445
2. LaRossa, R. A., and Schloss, J. V. (1984) The sulfonylurea herbicide sulfometuron methyl is an extremely potent and selective inhibitor of acetolactate synthase in *Salmonella typhimurium*. *J. Biol. Chem.* **259**, 8753-8757
3. Shaner, D. L., Anderson, P. C., and Stidham, M. A. (1984) Imidazolinones: potent inhibitors of acetohydroxyacid synthase. *Plant Physiol.* **76**, 545-546
4. Schloss, J. V., Ciskanik, L. M., and Van Dyk, D. E. (1988) Origin of the herbicide binding site of acetolactate synthase. *Nature* **331**, 360-362
5. Pang, S. S., Guddat, L. W., and Duggleby, R. G. (2003) Molecular basis of sulfonylurea herbicide inhibition of acetohydroxyacid synthase. *J. Biol. Chem.* **278**, 7639-7644
6. McCourt, J. A., Pang, S. S., Guddat, L. W., and Duggleby, R. G. (2005) Elucidating the specificity of binding of sulfonylurea herbicides to acetohydroxyacid synthase. *Biochemistry* **44**, 2330-2338
7. McCourt, J. A., Pang, S. S., King-Scott, J., Guddat, L. W., and Duggleby, R. G. (2006) Herbicide-binding sites revealed in the structure of plant acetohydroxyacid synthase. *Proc. Natl. Acad. Sci. U. S. A.* **103**, 569-573
8. (2017) China sulfonylurea herbicides market trends, forecast, and analysis. Report Sellers
9. Duggleby, R. G., and Pang, S. S. (2000) Acetohydroxyacid Synthase. *J. Biochem. Mol. Biol.* **33**, 1-36
10. Seino, S. (2012) Cell signalling in insulin secretion: the molecular targets of ATP, cAMP and sulfonylurea. *Diabetologia* **55**, 2096-2108
11. Amorim Franco, T. M., and Blanchard, J. S. (2017) Bacterial branched-chain amino acid biosynthesis: structures, mechanisms, and drugability. *Biochemistry* **56**, 5849-5865
12. Hutson, S. (2001) Structure and function of branched chain aminotransferases. *Prog. Nucleic Acid Res. Mol. Biol.* **70**, 175-206

13. Battaglin, W. A., Furlong, E. T., Burkhardt, M. R., and Peter, C. J. (2000) Occurrence of sulfonylurea, sulfonamide, imidazolinone, and other herbicides in rivers, reservoirs and ground water in the Midwestern United States, 1998. *Sci. Total Environ.* **248**, 123-133
14. Forlani, G., Mantelli, M., Branzoni, M., Nielsen, E., and Favilli, F. (1995) Differential sensitivity of plant-associated bacteria to sulfonylurea and imidazolinone herbicides. *Plant Soil* **176**, 243-253
15. Boldt, T. S., and Jacobsen, C. S. (1998) Different toxic effects of the sulfonylurea herbicides metsulfuron methyl, chlorsulfuron and thifensulfuron methyl on fluorescent pseudomonads isolated from an agricultural soil. *FEMS Microbiol. Lett.* **161**, 29-35
16. Obrigawitch, T. T., Cook, G., and Wetherington, J. (1998) Assessment of effects on non-target plants from sulfonylurea herbicides using field approaches. *Pestic. Sci.* **52**, 199-217
17. Dale, P. J., Clarke, B., and Fontes, E. M. G. (2002) Potential for the environmental impact of transgenic crops. *Nature Biotechnol.* **20**, 567
18. Kraehmer, H., Laber, B., Rosinger, C., and Schulz, A. (2014) Herbicides as weed control agents: state of the art: I. Weed control research and safener technology: the path to modern agriculture. *Plant Physiol.* **166**, 1119-1131
19. Kraehmer, H., van Almsick, A., Beffa, R., Dietrich, H., Eckes, P., Hacker, E., Hain, R., Strek, H. J., Stuebler, H., and Willms, L. (2014) Herbicides as weed control agents: state of the art: II. Recent achievements. *Plant Physiol.* **166**, 1132-1148
20. Schütte, G., Eckerstorfer, M., Rastelli, V., Reichenbecher, W., Restrepo-Vassalli, S., Ruohonen-Lehto, M., Saucy, A.-G. W., and Mertens, M. (2017) Herbicide resistance and biodiversity: agronomic and environmental aspects of genetically modified herbicide-resistant plants. *Environ. Sci. Eur.* **29**, 5-5
21. Schönbrunn, E., Eschenburg, S., Shuttleworth, W. A., Schloss, J. V., Amrhein, N., Evans, J. N., and Kabsch, W. (2001) Interaction of the herbicide glyphosate with its target enzyme 5-enolpyruvylshikimate 3-phosphate synthase in atomic detail. *Proc. Natl. Acad. Sci. U. S. A.* **98**, 1376-1380
22. Funke, T., Han, H., Healy-Fried, M. L., Fischer, M., and Schönbrunn, E. (2006) Molecular basis for the herbicide resistance of Roundup Ready crops. *Proc. Natl. Acad. Sci. U. S. A.* **103**, 13010-13015

23. Garcia, M. D., Nouwens, A., Lonhienne, T. G., and Guddat, L. W. (2017) Comprehensive understanding of acetohydroxyacid synthase inhibition by different herbicide families. *Proc. Natl. Acad. Sci. U. S. A.* **114**, E1091-E1100
24. Kelley, L. A., Mezulis, S., Yates, C. M., Wass, M. N., and Sternberg, M. J. E. (2015) The Phyre2 web portal for protein modeling, prediction and analysis. *Nat. Protoc.* **10**, 845
25. Pettersen, E. F., Goddard, T. D., Huang, C. C., Couch, G. S., Greenblatt, D. M., Meng, E. C., and Ferrin, T. E. (2004) UCSF Chimera - A visualization system for exploratory research and analysis. *J. Comput. Chem.* **25**, 1605-1612
26. Brown, H. M. (1990) Mode of action, crop selectivity, and soil relations of the sulfonylurea herbicides. *Pestic. Sci.* **29**, 263-281
27. Duggleby, R. G., Pang, S. S., Yu, H., and Guddat, L. W. (2003) Systematic characterization of mutations in yeast acetohydroxyacid synthase. *Eur. J. Biochem.* **270**, 2895-2904
28. Chang, A. K., and Duggleby, R. G. (1997) Expression, purification and characterization of Arabidopsis thaliana acetohydroxyacid synthase. *Biochem. J.* **327 (Pt 1)**, 161-169
29. Lonhienne, T., Garcia, M. D., Pierens, G., Mobli, M., Nouwens, A., and Guddat, L. W. (2018) Structural insights into the mechanism of inhibition of AHAS by herbicides. *Proc. Natl. Acad. Sci. U. S. A.* **115**, E1945-E1954
30. Tittmann, K., Schroder, K., Golbik, R., McCourt, J., Kaplun, A., Duggleby, R. G., Barak, Z., Chipman, D. M., and Hubner, G. (2004) Electron transfer in acetohydroxy acid synthase as a side reaction of catalysis. Implications for the reactivity and partitioning of the carbanion/enamine form of (alpha-hydroxyethyl)thiamin diphosphate in a "nonredox" flavoenzyme. *Biochemistry* **43**, 8652-8661
31. Garcia, M. D., Chua, S. M. H., Low, Y. S., Lee, Y. T., Agnew-Francis, K., Wang, J. G., Nouwens, A., Lonhienne, T., Williams, C. M., Fraser, J. A., and Guddat, L. W. (2018) Commercial AHAS-inhibiting herbicides are promising drug leads for the treatment of human fungal pathogenic infections. *Proc. Natl. Acad. Sci. U. S. A.* **115**, E9649-E9658
32. Störmer, F. C. (1968) The pH 6 acetolactate-forming enzyme from *Aerobacter aerogenes*. II. Evidence that it is not a flavoprotein. *J. Biol. Chem.* **243**, 3740-3741
33. Størmer, F. C., and Umbarger, H. E. (1964) The requirement for flavine adenine dinucleotide in the formation of acetolactate by *Salmonella typhimurium* extracts. *Biochem. Biophys. Res. Commun.* **17**, 587-592

34. Lonhienne, T., Garcia, M. D., Noble, C., Harmer, J., Fraser, J. A., Williams, C. M., and Guddat, L. W. (2017) High resolution crystal structures of the acetohydroxyacid synthase-pyruvate complex provide new insights into its catalytic mechanism. *ChemistrySelect* **2**, 11981-11988

35. Tittmann, K., Golbik, R., Uhlemann, K., Khailova, L., Schneider, G., Patel, M., Jordan, F., Chipman, D. M., Duggleby, R. G., and Hübner, G. (2003) NMR analysis of covalent intermediates in thiamin diphosphate enzymes. *Biochemistry* **42**, 7885-7891

36. Tittmann, K., Vyazmensky, M., Hübner, G., Barak, Z. e., and Chipman, D. M. (2005) The carboligation reaction of acetohydroxyacid synthase II: Steady-state intermediate distributions in wild type and mutants by NMR. *Proc. Natl. Acad. Sci. U. S. A.* **102**, 553-558

37. Störmer, F. C. (1968) The pH 6 acetolactate-forming enzyme from *Aerobacter aerogenes*. I. Kinetic studies. *J. Biol. Chem.* **243**, 3735-3739

38. Holtzclaw, W. D., and Chapman, L. F. (1975) Degradative acetolactate synthase of *Bacillus subtilis*: purification and properties. *J Bacteriol* **121**, 917-922

39. Gollop, N., Damri, B., Chipman, D. M., and Barak, Z. (1990) Physiological implications of the substrate specificities of acetohydroxy acid synthases from varied organisms. *J. Bacteriol.* **172**, 3444-3449

40. Sommer, B., von Moeller, H., Haack, M., Qoura, F., Langner, C., Bourenkov, G., Garbe, D., Loll, B., and Bruck, T. (2015) Detailed structure-function correlations of *Bacillus subtilis* acetolactate synthase. *ChemBioChem* **16**, 110-118

41. Sikdar, M. S. I., and Kim, J. S. (2010) Expression of a gene encoding acetolactate synthase from rice complements two *ilv*H mutants in *Escherichia coli*. *Aust. J. Crop Sci.* **4**, 430-436

42. De Felice, M., Guardiola, J., Malorni, M. C., Klopotowski, T., and Iaccarino, M. (1974) Regulation of the pool size of valine in *Escherichia coli* K-12. *J. Bacteriol.* **120**, 1058-1067

43. Guardiola, J., De Felice, M., and Iaccarino, M. (1974) Mutant of *Escherichia coli* K-12 missing acetolactate synthase activity. *J. Bacteriol.* **120**, 536-538

44. Lawther, R. P., Calhoun, D. H., Gray, J., Adams, C. W., Hauser, C. A., and Hatfield, G. W. (1982) DNA sequence fine-structure analysis of *ilv*G (*Ilv*G+) mutations of *Escherichia coli* K-12. *J. Bacteriol.* **149**, 294-298

45. Guzman, L. M., Belin, D., Carson, M. J., and Beckwith, J. (1995) Tight regulation, modulation, and high-level expression by vectors containing the arabinose PBAD promoter. *J. Bacteriol.* **177**, 4121-4130

46. Pang, S. S., Duggleby, R. G., Schowen, R. L., and Guddat, L. W. (2004) The crystal structures of *Klebsiella pneumoniae* acetolactate synthase with enzyme-bound cofactor and with an unusual intermediate. *J. Biol. Chem.* **279**, 2242-2253

47. Yep, A., Kenyon, G. L., and McLeish, M. J. (2008) Saturation mutagenesis of putative catalytic residues of benzoylformate decarboxylase provides a challenge to the accepted mechanism. *Proc. Natl. Acad. Sci. U. S. A.* **105**, 5733-5738

48. Yep, A., and McLeish, M. J. (2009) Engineering the substrate binding site of benzoylformate decarboxylase. *Biochemistry* **48**, 8387-8395

49. Reetz, M. T., Prasad, S., Carballeira, J. D., Gumulya, Y., and Bocola, M. (2010) Iterative saturation mutagenesis accelerates laboratory evolution of enzyme stereoselectivity: Rigorous comparison with traditional methods. *J. Am. Chem. Soc.* **132**, 9144-9152

50. Andrews, F. H., and McLeish, M. J. (2013) Using saturation mutagenesis to explore reaction mechanism and substrate specificity in thiamin diphosphate-dependent enzymes. *FEBS J.* **280**, 6395–6411

51. Arnold, F. H., and Georgiou, G. (2003) *Directed evolution library creation*, Humana Press Inc., Totowa, NJ

52. Lowry, O. H., Carter, J., Ward, J. B., and Glaser, L. (1971) The Effect of Carbon and Nitrogen Sources on the Level of Metabolic Intermediates in *Escherichia coli*. *J. Biol. Chem.* **246**, 6511-6521

53. Daniel, J., Dondon, L., and Danchin, A. (1983) 2-ketobutyrate: A putative alarmone of *Escherichia coli*. *Mol. Gen. Genet.* **190**, 452-458